Butterfly visual pigments

Vanhoutte, Kürt Johan André

BUTTERFLY VISUAL PIGMENTS:
MOLECULAR CLONING AND OPTICAL REFLECTIONS

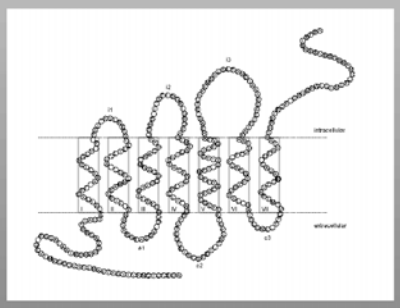

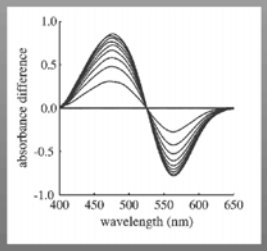

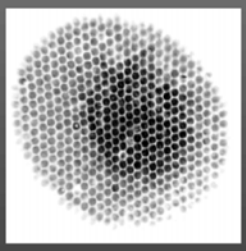

KURT VANHOUTTE

RIJKSUNIVERSITEIT GRONINGEN

Butterfly visual pigments: molecular cloning and optical reflections

Proefschrift

ter verkrijging van het doctoraat in de
Wiskunde en Natuurwetenschappen
aan de Rijksuniversiteit Groningen
op gezag van de
Rector Magnificus, dr. F. Zwarts,
in het openbaar te verdedigen op
vrijdag 19 september 2003
om 16.00 uur

door

Kürt Johan André Vanhoutte

geboren op 23 september 1975
te Waregem (België)

Promotor:	Prof. dr. D.G. Stavenga
Beoordelingscommissie:	Prof. dr. K. Arikawa Prof. dr. W.J. de Grip Prof. dr. A.C. Kooijman

ISBN 90-367-1861-9

aan Joyce

Cover: 2D topology of the amino acid sequence of the UV absorbing opsin derived from cDNA sequences obtained from the satyrine butterfly *Bicyclus anynana* (see Chapter 2).

Absorbance difference spectra representing the fast conversion of green rhodopsin into the metarhodopsin state while illuminating with intense white light after prolonged dark adaptation (see Chapter 4).

Photograph of corneal reflections after bleaching green visual pigment in the nymphalid butterfly *Polygonia c-album* (see Chapter 5).

Contents

Chapter 1: General Introduction 1

Chapter 2: Opsin cDNA sequences of a UV and green rhodopsin of the satyrine butterfly *Bicyclus anynana* 15

Chapter 3: Modeling visual pigment processes in butterfly rhabdoms 27

Chapter 4: Visual pigment absorption spectra of the nymphalid butterfly *Polygonia c-album* derived from *in vivo* reflection measurements 41

Chapter 5: Analyzing the reflections from single ommatidia in the butterfly compound eye with Voronoi diagrams 63

Chapter 6: *In vivo* microspectrophotometry of single butterfly ommatidia in dorsal and ventral eye regions 75

Chapter 7: Summary and General Discussion 87

References 97

Nederlandse samenvatting 107

Nawoord 111

Chapter 1

General Introduction

1. Theme of the thesis 2
2. Structural organization of the butterfly compound eye 2
2.1. Ommatidial architecture 2
2.2. Retinal ommatidial organization: regionalization and heterogeneity 6
3. Visual pigment cycle and phototransduction 8
4. Filtering components determine the photoreceptor's spectral sensitivity 11
5. Visual ecology: color vision in Lepidoptera 12
6. Outline of the thesis 12

1. Theme of the thesis

The visual sense enables animals to recognize and discriminate objects in the outside world. In line with Darwinian evolutionary theory one may argue that the visual functions of any species are optimized to enhance its ecological fitness. In this respect, it is well-known that flower-visitors, like bees and butterflies, have developed highly evolved color vision. In the past, most studies on insect color vision have used the honeybee as a model animal (Menzel and Backhaus, 1989; Menzel et al., 1991). Recently, multidisciplinary studies in moths and butterflies have made important strides in the elucidation of their color vision systems (e.g. Nilsson et al., 1983; Arikawa, 1999; Kelber et al., 2003).

This thesis aims to contribute further insight into the spectral properties of butterfly photoreceptors, by using tools from molecular biology and *in vivo* microspectrophotometry, with a specific focus on the visual pigments.

2. Structural organization of the butterfly compound eye

2.1. Ommatidial architecture

Compound eyes, characteristic of arthropods, are the principal visual components analyzing the optical information from the environment. They are composed of structural units called ommatidia (see Fig. 1.1). An ommatidium is a set of cells, tens of micrometer in width and several hundred micrometer long, which is capped by the dioptrical apparatus, consisting of a light-focussing corneal lens and a crystalline cone. The eyes of flies and butterflies fall into the group of apposition eyes (Exner, 1891), where photoreceptors receive light via the lens of their own ommatidium, as opposed to superposition eyes, where multiple lenses project light on the photoreceptors.

The set of photoreceptor cells of an ommatidium is called a retinula (i.e., a small retina). The photoreceptors have a special structure, the rhabdomere, consisting of evaginations of the apical cell membrane, the microvilli, each ca 1-2 μm in length and 50 nm in width (Suzuki et al., 1993). The assembly of rhabdomeres of a retinula is called the rhabdom. In flies, the rhabdomeres are spatially separate and therefore the rhabdom is said to be open. In butterflies, the rhabdomeres are so closely apposed that they act together as an optical waveguide, and they therefore form a so-called fused rhabdom. The butterfly retinula exists of 9 photoreceptor cells. Surrounding each retinula is a sheath of primary and secondary pigment cells containing

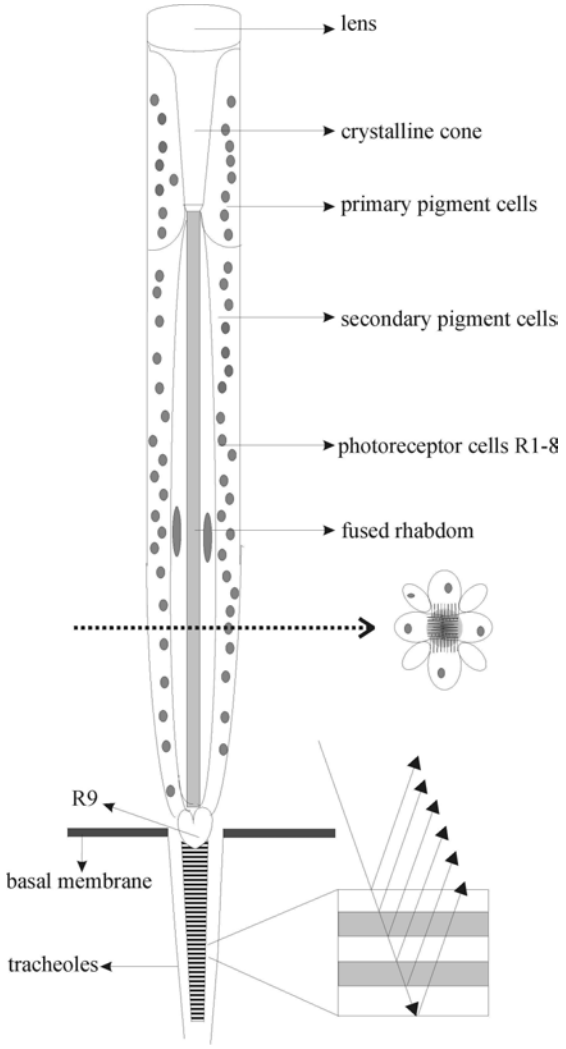

Fig. 1.1: Ommatidial architecture of the butterfly compound eye. Each ommatidium is a bundle of cells, tens of micrometers in width and several hundred micrometers long, which is capped by the dioptrical apparatus, a light focussing corneal lens and a crystalline cone. Proximal to each cone is the retinula, i.e. the set of photoreceptor cells of an ommatidium. A butterfly ommatidium contains 9 photoreceptor cells. Pupil granules inside the photoreceptor cells migrate towards the rhabdom at high illumination intensities. Depending on the type of photoreceptor, so-called short or long axon fibers convey the photoreceptor signal through the basal membrane towards the lamina and medulla. Surrounding each retinula is a sheath of primary and secondary pigment cells containing optically dense pigment granules. These pigments effectively block out off-axis stray light. Tracheoles, air sacks made up of tracheolar cells, penetrate the basement membrane and supply the retinal cells with oxygen. They form multilayered structures on the bottom of the ommatidia which reflect light due to quarter wavelength interference on layers, with alternating layers of cytoplasm and air.

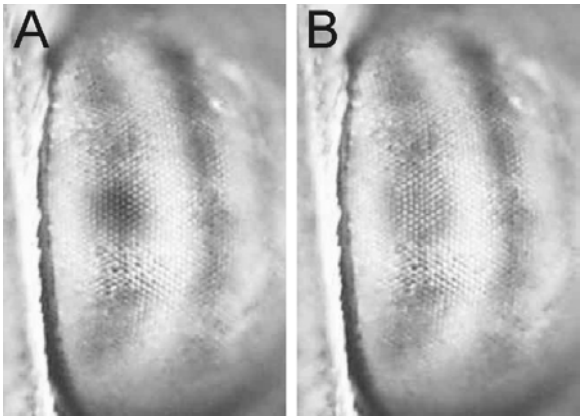

Fig. 1.2: The eye shine in the dorsal eye region of the satyrine butterfly *Bicyclus safitza*. **A.** In the light-adapted state the eye shine is literally hidden in the dark by the migration of pupillary granules which absorb the light flux entering illuminated ommatidia. The dark spot, called the principal pseudopupil, corresponds with the illuminated ommatidia viewing into the microscope objective. **B.** In the dark-adapted state one can see a bright colorful eye shine upon white light illumination, due to light reflected at the tapetum, proximally to the rhabdom. Note: the whitish vertical stripes, which are due to a light-colored screening pigment, are typical for satyrines (from Stavenga, 2002a).

granules of dense black-brown pigment (diameter ~ 0.5 μm). This pigment effectively blocks out off-axis stray light. Tracheoles, air sacks created by tracheolar cells, penetrate the tracheoles, air sacks created by tracheolar cells, penetrate the basement membrane and supply the retinula cells with oxygen (Ribi, 1979a,b). The tracheoles also function as a light-reflecting structure, the tapetum, at the basal membrane, proximal to the rhabdom. The colored eye shine observed with an epi-illumination microscope, using white light, is due to quarter wavelength interference at the multilayered tracheolar plates (Land, 1972). In our optical investigations we analysed the reflected light during white light illumination of the ommatidia looking into the aperture of the objective (see Fig. 1.2) At the center of the eye, the light beams seem to converge into a single spot, a phenomenon called the deep pseudopupil (DPP) image (see Fig. 1.3). In the fused rhabdoms of the two butterfly species *Pieris* and *Papilio*, the distal two third is taken up by rhabdomeres of the photoreceptors R1-4, and the proximal one third is formed by photoreceptors R5-8 (Arikawa, 1999; Qiu et al., 2002). On the basal side, the microvilli of only one photoreceptor cell, R9, participate in the rhabdom. The rhabdom acts as an optical waveguide due to the higher refraction index of the rhabdom medium with respect to the surroundings. The small dimensions of the lightguide, typical diameter 1-2 μm, necessitates waveguide theory to describe the intensity distributions within the lightguide (van Hateren, 1989). The rhabdomeric microvilli contain light-

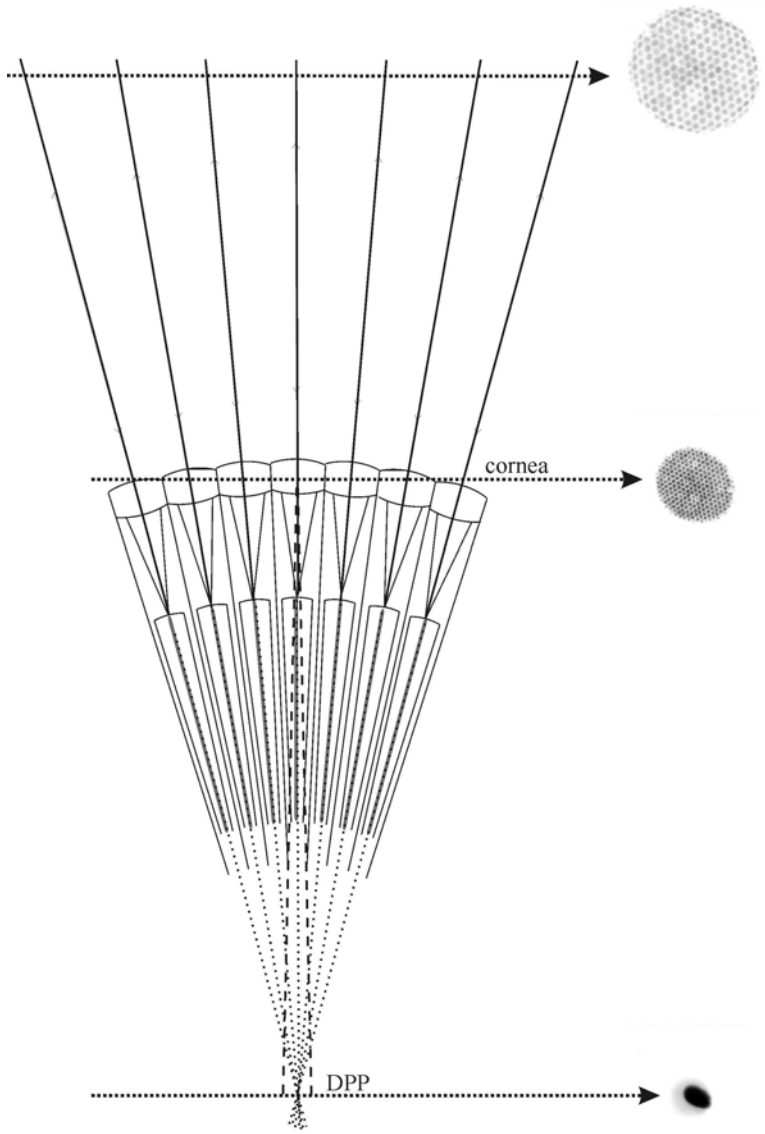

Fig. 1.3: Schematic diagram of the radiation pattern in the eye of the satyrine butterfly *Bicyclus anynana* illustrated with inverted gray pictures at three different levels (dotted arrows). The incident light is reflected on the tapetum and leaves the eye via the same pathway. The light beams seem to emerge from the centre of the eye, a phenomenon called the deep pseudopupil image (DPP). The image is the superimposed enlarged virtual image of the distal rhabdom endings (illustrated in the central ommatidium). The diverging light beams are distinctly visible at a level above the cornea. From the distance of the light beams at different levels the value of the interommatidial angle can be deduced.

absorbing visual pigment molecules, the rhodopsins, as well as the components of the biochemical machinery which transduces the light signal into an electrical response. The light-induced influx of ions, primarily Ca^{++}, triggers the migration of pupillary pigment granules at high illumination intensities (see Fig. 1.2). The name 'pupil' refers to its function, which is similar to that of the human pupil, namely to control the light flux propagating in the fused rhabdom. The photoreceptor signal is conveyed to the optical ganglia, the lamina and medulla, by axons going through the basal membrane, called the short and the long axon fibers, depending on the type of photoreceptor.

2.2. Retinal ommatidial organization: regionalization and heterogeneity

Investigations of the eyes of flies demonstrated heterogeneous types of ommatidia based on different expression of opsins in the R7 and R8 photoreceptor cells (Salcedo et al., 1999). The ommatidia of butterfly eyes are also not uniform: there is a clear variation in their constitutive components, the rhodopsins and screening pigments inside the photoreceptors, the shape of the fused rhabdom or eventually the presence of UV absorbing substances. Based on these differences, several classes of ommatidia can be recognized, randomly distributed over the eye, but mostly with a marked dorso-ventral regionalization. A few rows of ommatidia in the dorsal region form a small special region, the dorsal rim area (Labhart and Meyer, 1999).

The heterogeneous ommatidial organization in butterflies was first extensively demonstrated in the Japanese yellow swallowtail, *Papilio xuthus*. The compound eye of *Papilio* is furnished with at least five types of spectral receptors (UV, violet, blue, green, red), indicating that the animal may have pentachromatic color vision (Arikawa et al., 1987). By combining molecular biological, histological and electrophysiological experiments, three classes of ommatidia were identified, two of which having red screening pigment inside the photoreceptor cells and the third type having a yellow pigment. The ommatidia distribute rather randomly over the eye (Arikawa and Stavenga, 1997). Nevertheless, the spectral receptors appear in a fixed pattern in the three classes of ommatidia. Papilionids are unique among the butterflies however, as they lack a reflecting tapetum underneath the ommatidia.

In butterfly species with a reflecting tapetum, reflection measurements also reveal heterogeneous ommatidia, with spectrally different reflections. This is clear from single facet recordings (see Chapter 6 for a large data-set), as well as from digital images taken with a tele-microscopic set-up (Stavenga, 2002b). These measurements revealed that butterfly eyes frequently show a clear dorso-ventral regionalization: the dorsal eye region is mostly homogeneous and

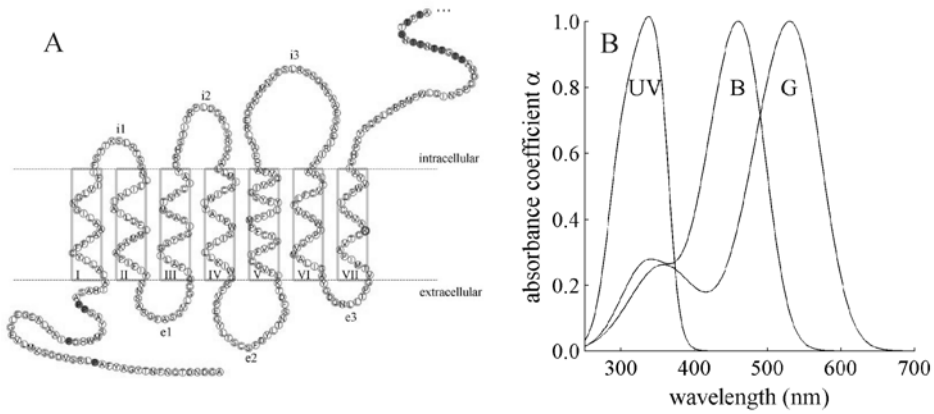

Fig. 1.4: Visual pigment structure and spectral absorbance**. A.** 2D topological structure typical for visual pigments. The 377 amino acid residues shown here in circles together constitute the primary structure derived from the cDNA sequence of the UV opsin cloned in *Bicyclus anynana*. Seven transmembrane regions, the rectangular areas I-VII, define α-helices spanning the lipid membrane. The helices are interconnected by the intracellular (i1-i3) and extracellular (e1-e3) loops. The seventh helix contains a lysine residue where the chromophore, 11-cis-3-OH-retinal, can be covalently attached. Other structural features of the ca 38 kDa apoprotein include a G-protein binding site (HEA-motif) at the C-terminal site of TM region 5 and proline residues (filled circles) at the extracellular N-terminal, which are probably involved in structural stabilization and membrane insertion (Gärtner, 2000). Intracellularly at the COOH-terminal tail there are serine-threonine residues (filled circles), probably phosphorylation sites, which may be involved in inactivation of a photoconverted visual pigment molecule. **B.** Spectral absorbance coefficients described by templates (Govardovskii, 2000) of three prevalent classes of rhodopsins peaking in the UV at 340 nm, in the blue at 480 nm and in the green at 530 nm.

ventrally there are mostly two spectrally different types of ommatidia. In some cases the dorsal eye region is very small (like in *Pieris rapae*) or the eye appears completely homogeneous (e.g. in *Polygonia* and *Inachis io*).

Different ommatidial classes were also identified in detailed anatomical studies. In the ventral eye region of the small white, *Pieris rapae*, two different types of red screening pigment appear to be expressed, giving rise to two different spectral types of ommatidia as seen by microspectrophotometry (Chapter 6). Based on the shape of the rhabdom three anatomically different types of ommatidia were found (Qiu et al., 2002).

In the nymphalid butterfly *Vanessa cardui* and the moth *Manduca sexta* the ommatidial expression pattern of three cloned opsins, belonging to ultraviolet (UV), blue (B) or green (G) absorbing rhodopsins, respectively, was elucidated (Briscoe et al., 2002; White et al., 2003). In both *Manduca* and *Vanessa*, the green rhodopsins are expressed in all ommatidia over the whole eye, in at least 6 photoreceptor cells. The short-wavelength (UV/B) absorbing rhodopsins are expressed in different combinations in the dorso-ventral (dv)

oriented photoreceptors in three types of ommatidia, i.e. UV-UV, UV-B and B-B. The UV-rhodopsin is predominantly present in the dorsal region; the blue rhodopsin is more frequent in ventral areas.

We have investigated the visual pigments in the satyrine *Bicyclus anynana* into considerable detail. In the next chapter we report on two cloned partial cDNA sequences of the green and UV-opsins. Optical visual pigment studies, similar to those described for *Polygonia c-album* in Chapter 4, together with electrophysiological spectral sensitivity studies in *Bicyclus safitza* and *Bicyclus anynana*, revealed a predominant distribution of the green rhodopsin

over the whole eye. Also the UV-rhodopsin could be optically demonstrated (Vanhoutte and Stavenga, unpublished data). The expression of a blue rhodopsin was not substantiated, neither by cloning or by electrophysiologal and optical investigations in dorsal eye regions. More dedicated optical/electrophysiological studies and *in situ hybridisation* of the cloned opsins are necessary to clarify this issue. No red absorbing visual pigment, like reported in *Papilio* (Kitamoto et al., 1998), was found in *Bicyclus*. Alltogether the data at present do indicate rhodopsin expression profiles in *Bicyclus* similar to those reported for *Vanessa cardui* (Briscoe et al., 2003) and *Manduca sexta* (White et al., 2003).

3. Visual pigment cycle and phototransduction

Vision starts with the absorption of light quanta by the visual pigment molecules. Visual pigments are members of the G-protein binding family, composed of a protein moiety and a chromophore. The chromophore of the visual pigment of flies and butterflies, 11-cis-3-OH-retinal, is derived from the alcohol retinol, vitamin A, an essential nutrient present in e.g. carrot and liver. The protein moiety is generally composed of ca 380 amino-acids, structured in seven transmembrane helices (see Fig. 1.4A). Light absorption by a rhodopsin molecule triggers a conformational change of the chromophore from the cis to the all-trans configuration, yielding the metarhodopsin state. The rhodopsins of butterflies typically absorb in the UV, blue (B) or green (G) wavelength range (see Fig. 1.4B). The green rhodopsins, with an absorption peak above 500 nm, are photoconverted into a metarhodopsin, which absorbs in the blue, typically around 490 nm. The metarhodopsin in the activated state transduces the visual signal into an electrical response (rev. Hardie, 2001). The principal characteristics of the biochemical phototransduction cascade, occurring after absorption of a light quantum by a visual pigment molecule and its subsequent conversion into metarhodopsin, involves binding of a heterotrimeric G-protein

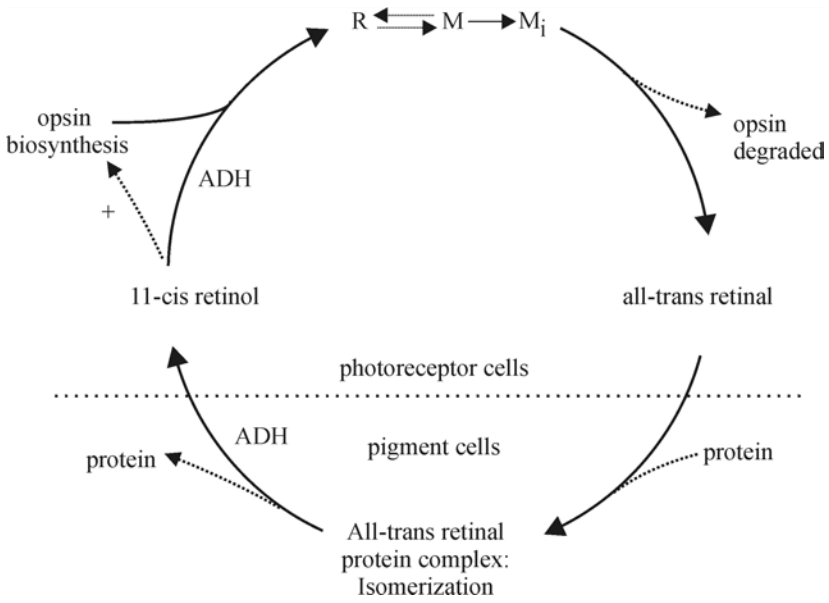

Fig. 1.5: Schematic flow-chart of visual pigment renewal and the cycle of the chromophore in flies (adapted from Schwemer, 1993; Hamdorf et al., 1989). The visual pigment of invertebrates is thermostable: rhodopsin and metarhodopsin can be interconverted by photon absorption, essentially changing the conformation of the chromophore, from the all-trans to the 11-cis configuration. Selective metarhodopsin degradation results in degradation of the protein moiety. The all-trans chromophore is recycled. After transportation to (presumably) the primary pigment cells the all-trans chromophore is isomerized to the 11-cis retinal configuration by a soluble photoisomerase, in flies a (blue) light-dependent enzyme (Schwemer, 1984). After alcohol dehydrogenase (ADH) activity, which may originate from a corresponding enzyme or the isomerase itself, the chromophore is redirected to the photoreceptor cells as retinol. The 11-cis retinol in flies stimulates opsin biosynthesis (Schwemer, 1993). Finally, the photoreceptor ADH converts retinol to a functional retinal, which is (presumably) bound to opsin during its biosynthesis. Transport of retinal requires retinoid carrier molecules to translocate the hydrophobic chromophore between photoreceptor cells and primary pigment cells.

by the metarhodopsin, which after some delay triggers nucleotide exchange (GTP for GDP) and subsequently results in release of the G_α-subunit which remains active until the bound GTP is hydrolysed. G_α activates a phosholipase C, which then can cleaves the membrane lipid phosphatidylinositol biphosphate (PIP_2) into the soluble component inositol 1,4,5-triphosphate (IP_3) and the membrane-bound diacylglycerol (DAG). The latter may be further metabolized into poly-unsaturated fatty acids (PUFAs), like arachidonic acid. The PUFAs cause the opening of ion-channels in the microvilli, resulting in Ca^{++}-influx (Chyb et al., 1999). The phototransduction process is inactivated by negative feedback, a two-step process. First, rhodopsin is phosphorylated by G-protein-coupled receptor kinases, thereby increasing the affinity for arrestin

binding on the activated metarhodopsin (Dolph et al., 1993). There is a delay of 30-50 milliseconds between absorption of a photon and the electrical response, the quantum bump. The very fast phototransduction process obviously requires a spatially close interaction of the phototransduction components. The very small dimensions of the microvilli (Postma et al., 2000) and anchoring proteins, like INAD, ensure fast and reliable phototransduction (Hardie, 2001). The phototransduction process is a highly dynamic and regulated system. The light-induced increase of Ca^{++}-ions in the photoreceptors, which drives the migration of pigment granules towards the rhabdom. The migrating pigment hence acts as a light-controlling pupil, because the granules absorb light and therefore reduce the light flux propagating in the rhabdom. Illumination of a dark-adapted eye thus results in a rapid fading of the reflected light. In the investigation of visual pigments one therefore needs to apply proper time protocols to circumvent the contribution of pupillary pigments (see also Chapter 4).

To maintain steady levels of receptor sensitivity, the rhodopsin content in the microvilli has to be kept at high levels. Rhodopsin may be regenerated by two pathways: photoregeneration and biosynthesis or rhodopsin renewal (see Fig. 1.5). Photoregeneration is likely an important regeneration mechanism in flies and butterflies. The inactivated arrestin-bound metarhodopsin is a short-living stable complex in the dark, but can re-isomerize to phosphorylated rhodopsin (p-R) upon photon absorption, thereby releasing arrestin and exposing the p-R to Ca^{++}-dependent *rdgC* phosphatases (Byk et al., 1993). In blowflies it has been hypothesised that red screening pigments, which surrounds the photoreceptor cells, selectively transmit red stray light to convert the predominant metarhodopsin (λ_{max} = 580 nm) in R1-6 cells (Stavenga, 1995). In butterflies red light may convert all green rhodopsin molecules into metarhodopsin, thus turning the animal functionally blind under continuous red illumination. Several butterfly eyes do contain red screening pigments, but they probably serve another role: shifting the spectral sensitivity (Chapter 7, Stavenga 2002a).

Renewal of rhodopsin via the visual pigment regeneration cycle is the second, long-term regeneration pathway (Fig. 1.4). After inactivation, the metarhodopsin may be degraded into its chromophore (all-trans-retinal) and protein moiety, which is further broken down (Bernard, 1983). The all-trans retinal is recycled by binding to retinal-binding proteins, which transport the chromophore to the primary pigment cells. Like in vertebrates, after isomerisation to the 11-cis retinal conformation, the chromophore is redirected to the photoreceptor cells. In flies, the isomerization process depends on UV/blue light (Schwemer 1984, 1993; Hamdorf et al., 1989).

Though the exact regulation is unclear, the amount of 11-cis retinal has been shown to be critical in regulating opsin transcription (Paulsen and Schwemer, 1983). Important posttranslational modifications are the transient glycosylation (Huber et al., 1990) and incorporation of the recycled chromophore, attached to the lysine residue. The newly synthesized rhodopsin may be directed to the rhabdomere in membranic vesicles.

4. Filtering components often modify the photoreceptor's sensitivity spectrum

The sensitivity spectrum of a photoreceptor is its normalized light sensitivity to different wavelengths. Typically the spectral sensitivity is measured by determining at several wavelengths the photon flux that elicits a certain physiological criterion response. The sensitivity spectrum is therefore sometimes also called the action spectrum. The sensitivity spectrum is under certain conditions well-approximated by the normalized absorptance spectrum of the visual pigment (Goldsmith and Bernard, 1974).

All butterfly visual pigments are likely to have the same chromophore, 3-OH-retinal, attached to the lysine in the 7th helix, where polar groups interact with the chromophore π-system. The absorption spectrum is therefore thought to be mainly determined by the amino-acids surrounding the chromophore. To study the characteristics of visual pigments, various *in vivo* and *in vitro* studies have been performed. Heterologous in vitro expression was unsuccessful in yeast, bacteria (no glycosylation), insect cells (baculovirus) and mammalian cells (SFV). Visual pigment was at least successfully expressed *in vivo* in transgenic *Drosophila* flies (Salcedo et al., 1999; Mollereau et al., 2000). Transgenic animals are therefore useful to investigate the visual pigment absorbance spectra.

Inside the photoreceptors, or in accessory pigment cells, sometimes colored substances are present, which filter the incident light, as was first noticed in flies. The role of red screening pigments has been intensely disputed (Goldsmith, 1965), but it has become clear that the primary function of screening pigments in accessory pigment cells is to block stray-light. In butterflies, e.g. in *Pieris* and *Papilio*, modelling microspectrophotometric recordings and anatomical studies suggests that red screening pigments, which act as long-pass filters, shift the spectral sensitivity of the photoreceptors towards longer wavelengths (Qiu et al., 2002; Stavenga, 2002b; Chapter 6). This corroborates behavioural evidence that color discrimination in the red is well developed in this species (Kolb and Scherer, 1982; Scherer and Kolb, 1987). It has been hypothesized that this red sensitivity may be well enhanced,

especially in the proximal receptors, when a tapetum exists which reflects in the long-wavelength range (Stavenga, 2002a).

5. Visual ecology: color vision in Lepidoptera

Photoreceptors signal the incident light intensity by the number of quanta absorbed by the visual pigment. However, a single photoreceptor can impossibly distinguish between wavelengths: color vision requires at least two photoreceptors with different sensitivity spectra.

The Lepidoptera, one of the four large insect orders, are subdivided in the night living moth species, which form the majority, and the day-light living butterflies. Color oriented behavior, most studied in the day-light living species, is important for territoriality, conspecific mate-finding, (larval) food plant choice and oviposition (Bernard and Remington, 1991; Kolb and Scherer, 1982; Scherer and Kolb, 1987; Kelber, 1999a). Also night living moth species have color vision capacities (Kelber et al., 2003). As this color oriented behaviour is not equally important for males and females, one expects sex differences in the color system, as has been reported for Lycaenidae (Bernard and Remington, 1991).

Like in bees, trichromatic color vision with UV, B and G absorbing opsins seems to be common in butterflies. In the investigated species, i.e. *Heliconius sp.* (Hsu et al., 2001), *Vanessa cardui* (Briscoe et al., 2003) and *Bicyclus anynana* (Vanhoutte et al., 2002) no more than 3 different opsins were found. *Papilio xuthus* and *P. glaucus* are exceptional as they have multiple long-wavelength absorbing opsins (Kitamoto et al., 1998; Briscoe, 1998). They curiously lack the reflecting tapeta.

6. Outline of the thesis

This thesis aims to contribute to the understanding of the photoreceptor basis of insect color vision, especially of butterflies. There are three basic levels of description throughout the thesis. The most basic description is the *primary structure* of the visual pigment (Chapter 2). Second, we explore visual pigment photochemistry in a group of *homogeneous* ommatidia (Chapter 4, 5) or in a single ommatidium. The third level is that of a *heterogeneous* population of ommatidia (Chapter 6). The study of visual pigment photochemistry relies on a theoretical frame-work (Chapter 3) and the development of new tools (Chapter 5) to interpret and record light, reflected on the tapeta.

In summary, the main scope of this thesis is to further develop the quantitative description of visual pigments at different structural levels. In addition, we will encounter throughout the thesis the integrated functionality of

the visual pigment with other team players in the ommatidia, e.g. the pupil, screening pigments and tapeta.

In **Chapter 1** we introduce the general topics of this thesis.

In **Chapter 2** we describe the cloning of cDNA sequences of visual pigments in *Bicyclus anynana*. The cDNA's of an ultraviolet (UV) and a long-wavelength (green) absorbing rhodopsin were partially identified. The UV sequence, encoding 377 amino acids, is 76 to 79% identical to the UV opsin sequences of the papilionids *Papilio glaucus* and *Papilio xuthus* and the moth *Manduca sexta.* A dendrogram derived from aligning the amino acid sequences reveals an equidistant position of *Bicyclus* between *Papilio* and *Manduca*. The sequence of the green opsin cDNA fragment, which encodes 242 amino acids, represents 6 of the 7 transmembrane regions. At the amino acid level, this fragment is more than 80% identical to the corresponding long-wavelength (LW) opsin sequences of *Dryas*, *Heliconius*, *Papilio* (rhodopsin 2) and *Manduca*. Whereas three long-wavelength absorbing rhodopsins were identified in the papilionid butterflies, only one green opsin was found in *Bicyclus anynana*.

In **Chapter 3** we present a photochemical formalism to model visual pigment processes in the butterfly eye when measured by reflection microspectrophotometry. We analyse how the rhodopsin conversion occurs. As a first step we use a realistic model which can explain the optical densities and fractional rhodopsin concentation after white light illumination and during dark adaptation. We have tuned our parameter set to the experiments performed in *Polygonia* (Chapter 4). This suggested a compartmental model were UV, blue and green rhodopsins are expressed in a 1:1:6 ratio. This configuration is an average ommatidial composition, in accordance with our optical recordings which reflect the integrated absorption characteristics of a large population of ommatidia.

In **Chapter 4** we investigate visual pigment absorbance in the eye of *Polygonia c-album,* a butterfly with a uniform, homogeneous eye shine. We demonstrate how the spectral and kinetic properties of the visual pigments, especially the green rhodopsins, can be assessed. In general, the development of the automated fast digital acquisition of spectral data and images has allowed us to monitor and visualize dynamic phenomena in the butterfly eye.

In **Chapter 5** we describe an image analysis technique based on Voronoi diagrams to analyze reflections from single ommatidia of the butterfly compound eye. This is a useful tool evolved from our efforts to make fast quantitative interpretations of images of the colored eye shine. We illustrate the 'Voronoi-tool' in preliminary studies on bleaching visual pigments in *Polygonia* and the pupil activation in the satyrine *Pararge aegeria*.

In **Chapter 6** we investigate homogeneous and heterogeneous eye regions of butterfly species representative for the (sub-)families of Nymphalinae, Satyrinae, Lycaenidae and Pieridae. We measured therefore single facet reflection spectra from a large data-set (20 butterfly species). These data allow us to map the regionalization and heterogeneity based on the colorful eye shine, whereby we discuss an emerging classification. The spectra also provide a quantitative measure of the cut-on/off reflection wavelengths of the tapeta and indicate the possible presence of long-pass, red screening pigments.

Chapter 7 provides a summary and general discussion, emphasizing how the spectral properties of visual pigments (Chapters 4-5), together with additional filtering components like screening pigments and tapeta (Chapter 6) account for a realistic description of light absorption in a fused rhabdom. The optical tools developed here to assess the spectral properties together with classical experimental techniques like electrophysiology and molecular biology (Chapter 2) provide an excellent experimental framework to describe and integrate the physical parameters in a quantitative model (Chapter 3). Eventually, on a case by case basis, this may allow us to understand recorded photoreceptor sensitivities. Likely this will finally enhance our understanding of how the assembly of photoreceptor sensitivities is processed to provide color vision.

Chapter 2

Opsin cDNA sequences of a UV and green rhodopsin of the satyrine butterfly *Bicyclus anynana*[†]

1. Introduction **16**
2. Materials and methods **16**
2.1. mRNA extraction and cDNA synthesis 16
2.2. PCR and 3´ and 5´ RACE 17
2.3. Analysis of nucleotide and amino acid sequences 18
3. Results **18**
3.1. Partial isolation of a UV opsin cDNA of *Bicyclus anynana* 18
3.2. Partial isolation of an LW opsin cDNA of *Bicyclus anynana* 18
3.3. Phylogenetic analysis of the obtained opsin sequences 21
4. Discussion **22**
4.1. Identification of an ultraviolet and a long-wavelength absorbing rhodopsin of *Bicyclus anynana* 22
4.2. Phylogenetic classification and sequence comparison with other insect opsins 26
4.3. Perspectives 26
Accession numbers **26**

[†] This chapter has been published in Insect Bioch.Mol.Biol. *32*:1383-1390

1. Introduction

Many insect species, notably butterflies, have the capacity of processing spectral information from their environment (e.g. Kinoshita et al., 1999; Arikawa, 1999; Briscoe and Chittka, 2001). Research on butterfly vision recently has focussed on the visual pigments in the photoreceptor cells, i.e., the rhodopsins. Light absorption by a rhodopsin molecule triggers the phototransduction process, which converts the absorbed light into a change in the photoreceptor membrane potential. The absorption spectrum of the rhodopsin therefore shapes the sensitivity spectrum of the photoreceptor cell. The absorption spectrum is determined by the interaction of the chromophore (a retinaldehyde) and the protein moiety, the opsin (review Gärtner, 2000).
Insect compound eyes generally contain a number of different rhodopsins with peak wavelengths ranging from the ultraviolet up to the red: ca 350-600 nm (reviews Stavenga and Schwemer, 1984; Briscoe and Chittka, 2001). For example, the honeybee, *Apis mellifera,* has three types of photoreceptor cells, with peak sensitivity in the ultraviolet (UV), blue and green, respectively (Menzel and Backhaus, 1989), corresponding to three types of rhodopsin (Townson et al., 1998). The fruitfly *Drosophila* has 6 rhodopsins, 5 of which are expressed in the photoreceptor cells of the compound eye (Salcedo et al., 1999; Gärtner, 2000; Minke and Hardie, 2000). The Japanese yellow swallowtail, *Papilio xuthus*, has 5 different rhodopsins expressed in the retina (Arikawa et al., 1997; Kitamoto et al., 1998, 2000). In another papilionid, *Papilio glaucus,* 6 different opsins have been identified (Briscoe, 1998).

We study the visual pigments of the satyrine butterfly *Bicyclus anynana*, a bush brown. Here we describe the isolation of (partial) UV and LW opsin cDNAs from *B. anynana,* in 3′ and 5′ RACE reactions with degenerate primers, designed from consensus invertebrate opsin sequences. The obtained sequences are compared with other cloned insect opsins. Phylogenetic analyses using the UV and LW opsin amino acid sequences demonstrate the high homology between sequences of *Papilio*, *Manduca* and *Bicyclus*.

2. Materials and methods

2.1. mRNA extraction and cDNA synthesis

mRNA was isolated from the eyes of 10 butterflies, *Bicyclus anynana*, obtained from a culture maintained by the Institute of Evolutionary Sciences, University of Leiden. The animals were first frozen in liquid nitrogen. The eyes then were dissected, held in phosphate buffer solution (PBS) and stored in 96% ethanol at –80 ^{o}C until further use. After dissection and homogenization, mRNA was

extracted from *Bicyclus anynana* eyes using the mRNA extraction kit (Pharmacia) under RNAse-free conditions. Next, cDNA was generated using the SMART-cDNA synthesis kit (Clontech).

2.2. PCR and 3´ and 5´ RACE

Bicyclus anynana cDNA was subjected to PCR amplification, using degenerate oligonucleotides based on homologous regions of invertebrate opsins (see Table 2.1). The obtained PCR fragments were purified (QIA quick Gel Extraction Kit, Qiagen) and subcloned in the pCRII plasmid (pCRII-TOPO, Invitrogen). After plasmid isolation (Wizard® Plus Minipreps DNA Purification System, Promega), the inserts were sequenced using M13 primers (Base-Clear, Leiden, the Netherlands).

Based on the obtained sequences, gene-specific primers were designed and used in combination with the anchor primers at the 3´- and 5´-terminus (Universal Primers, Clontech) in 3´and 5´ RACE- reactions. The PCR conditions were: 1 min at 94 ^{o}C, 30 cycles of 1 min at 45-58 ^{o}C depending on the predicted optimal annealing temperature of the primer, and 2 min at 72 ^{o}C. 3´ and 5´ RACE products were subcloned and sequenced as described above.

Primer	Source	Class	Size	Sequence(5'->3')
BDF	NDP	All	24	GCBDTBTYBGAYYTBHTRATGATG
BrDF	B98	All	19	GANCARGCNAARAARATGA
BuvR	NGSP	UV	23	CTATGAGCGCCATCACTCCGTAG
BuvF	NGSP	UV	23	AGCGGTTACATGCAAGGCAGTAG
MPuvF1	K00	UV	25	GCGAATTCTGYTTYYTNTTYGTNGC
HLuvR	K00	UV/S	28	CGGGATCCTANAYCCANGGRTCDATRCA
HLuvmF1	K00	SW	28	GCGAATTCGAYGAYGARHAYACNAARGT
BblDR	K00	SW	18	YGGYARKATRGTGAAHGG
BlwF	NGSP	LW	23	CTGGCTAAGGTGGCTCTAATGAC
BlwR	NGSP	LW	23	GTCATTAGAGCCACCTTAGCCAG
BlwNF	NGSP	LW	18	CGAGACCATGACGATCAG
BlwNR	NGSP	LW	20	TCTGATGACCTGAGAGAAGC
F5	K98	LW	29	GCGAATTCCGSGANCARGCMAARARRWT
R8	K98	LW	26	CGGGATCCDAYRSMRTANACRAWNGG

Table 2.1: Degenerate and gene specific primers used in the PCR reactions. The class of opsins against which primers are directed are indicated. Positions of homologue sequences on the *Bicyclus* opsins are indicated in Figs. 2.1 and 2.2. The abbreviations used are: NDP (new degenerate primer), NGSP (new gene specific primer), B98 (Briscoe, 1998), K00 (Kitamoto, 2000).

2.3. Analysis of nucleotide and amino acid sequences

Cloned sequences were further analysed by searching in the GenBank database for homologue opsin sequences (http://www.ncbi.nlm.nih.gov/blast). Multiple alignments of the *Bicyclus* partial sequences against other insect opsins were calculated with ClustalW software (www.ebi.ac.uk/clustalw). Using the neighbour-joining method, phylogenetic trees were derived from visually inspected opsin amino-acid (AA) alignments (PHYLIP 3.5c). Trees were displayed with TreeView1.6 (© Roderick D.M. Page).

3. Results

3.1. Partial isolation of a UV opsin cDNA of Bicyclus anynana

PCR using degenerate UV opsin primers MPuvF1 and HLuvR (Table 2.1) produced a predominant product of 162 bp, which was purified and cloned (Fig. 2.1). BLAST analysis of the obtained sequences (2 clones, single stranded sequencing) revealed a high degree of homology between the obtained sequence and UV opsin cDNA sequences of other invertebrates, indicating that we obtained a fragment of *Bicyclus anynana* UV opsin.

A fragment that extended the obtained UV opsin cDNA with 569 bp at the 5´- end was generated by PCR using the primers BDF and BuvR (Table 2.1, Fig. 2.1). With 3´-and 5´ RACE, using primers PDF or BuvF and BuvR (Table 2.1), a total of 1431 bp of UV opsin cDNA were cloned and sequenced (Fig. 2.1).

One clone of each primer combination was single-stranded sequenced. All these clones contain overlapping open reading frames of 377 amino acids in total. As summarized in Table 2.2, a BLAST search identified highest pairwise basepair identities of the *Bicyclus* UV opsin with (UV) opsin sequences of *Manduca sexta* (Chase et al., 1997), *Papilio xuthus* (Kitamoto et al., 2000), *Papilio glaucus* (Briscoe, 1998) and *Bombyx mori* (Shimizu et al., 1998).

3.2. Partial isolation of an LW opsin cDNA of Bicyclus anynana

A PCR-fragment of 265 bp was amplified with the degenerate primers F5 and R8 (Table 2.1, Fig. 2.2) and cloned. Out of 15 clones, 9 fragments were identified as a long-wavelength (LW) fragment in a BLAST search, possessing a high pairwise similarity with LW opsins. Another degenerate forward primer, PDF (Table 2.1), in combination with the degenerate reverse primer R8 (Table 2.1) picked up the same LW opsin fragment (Fig. 2.2, one clone, single

stranded sequencing). Both primer combinations also amplified an 18S rRNA partial fragment. We extended the opsin fragment in the 5´ direction with 460 bp with a reverse directed gene-specific primer BlwR (1 clone, single stranded sequencing) and the degenerate forward primer BDF (Table 2.1, Fig. 2.2). The 3´ and 5´ RACE reactions with the gene-specific primers BlwR and BlwF and the nested primers BlwNR and BlwNF did not amplify opsin cDNA (Table 2.1, Fig. 2.2). The obtained total of 725 basepairs translates into 242 amino acids.

Table 2.3 summarizes the result of a BLAST search in the GenBank database of the 725 basepairs of opsin cDNA sequence. Best matches were the long-wavelength opsins of *Heliconius erato* and *Heliconius melpomene* (Hsu et al., 2001), *Papilio xuthus* rhodopsin 2 (Kitamoto et al., 2000), *Papilio glaucus* rhodopsin 2 (Briscoe, 1998) and *Manduca sexta* (Chase et al., 1997). It appears that the obtained fragment of 242 amino acids forms a major part of the LW opsin, namely 6 of the 7 transmembrane regions.

Best match	Identities (% identities)	Significance (bits/ e-value)	Accession Number
Manduca sexta UV opsin, complete cds	189/228 (82%)	143/ 4e-31	L78081
Papilio xuthus UV opsin, complete cds	278/350 (79%) 49/54 (90%)	123/ 4e-25 67.9/ 2e-08	AB028218
Papilio glaucus UV opsin, complete cds	66/77 (85%) 39/44 (88%)	65.9/ 8e-08 48.1/ 0.019	AF077191
Bombyx mori mRNA, partial cds	84/102 (82%)	60.0/ 5e-06	AB047925

Table 2.2: Best matches of the *Bicyclus anynana* UV cDNA sequence in a BLAST search against partial and complete cDNA sequences (cds) in the GenBank database and percentage of nucleotide identities.

Best match	Identities (% identities)	Significance (bits/e-value)	Accession number
Heliconius erato opsin, partial cds	535/651 (82%)	371/ 1e-100	AF126750
Papilio xuthus Rhodopsin 2, complete cds	464/578 (80%)	242/ 3e-61	AB007424
Heliconius melpomene opsin, partial cds	231/273 (84%)	200/ 4e-51	AF126751
Papilio glaucus Rh2 opsin, complete cds	529/674 (78%)	188/ 4e-45	AF077190
Manduca sexta LW opsin, complete cds	169/198 (85%)	163/ 2e-37	L78080

Table 2.3: Best matches of the *Bicyclus anynana* LW cDNA opsin in a BLAST search against partial and complete cDNA sequences (cds) in the GenBank database and percentage of nucleotide identities.

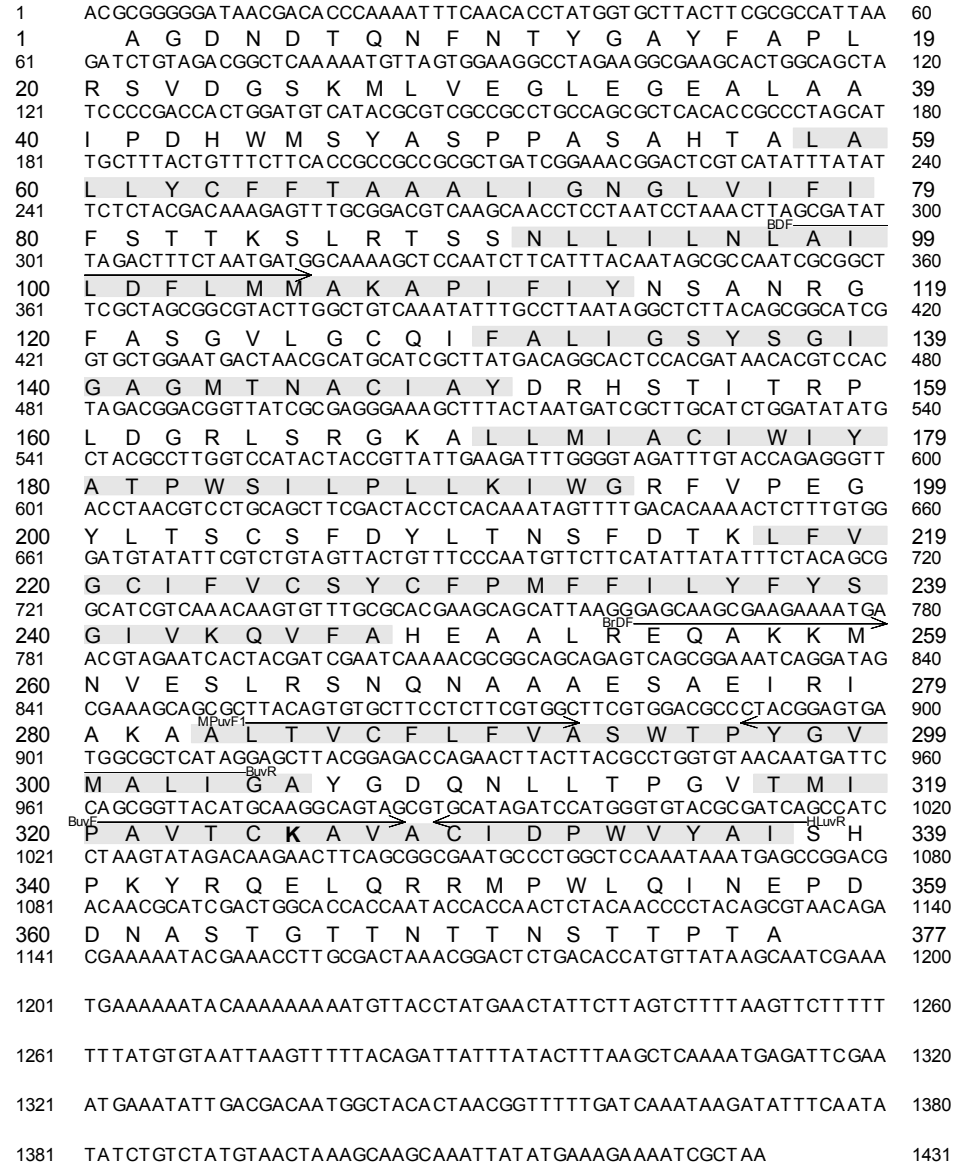

Fig. 2.1: cDNA sequence of the UV-opsin (1431 bp) and translated coding region centered under the corresponding cDNA codons. Arrows indicate the position of the homologue nucleotide sequences of the primers. Primers are identified at the start of the arrow (Table 2.1). Arrows to the right and to the left are forward and reverse directed, respectively. The transmembrane regions are shaded in gray. The lysine chromophore binding site at position 325 is drawn in bold.

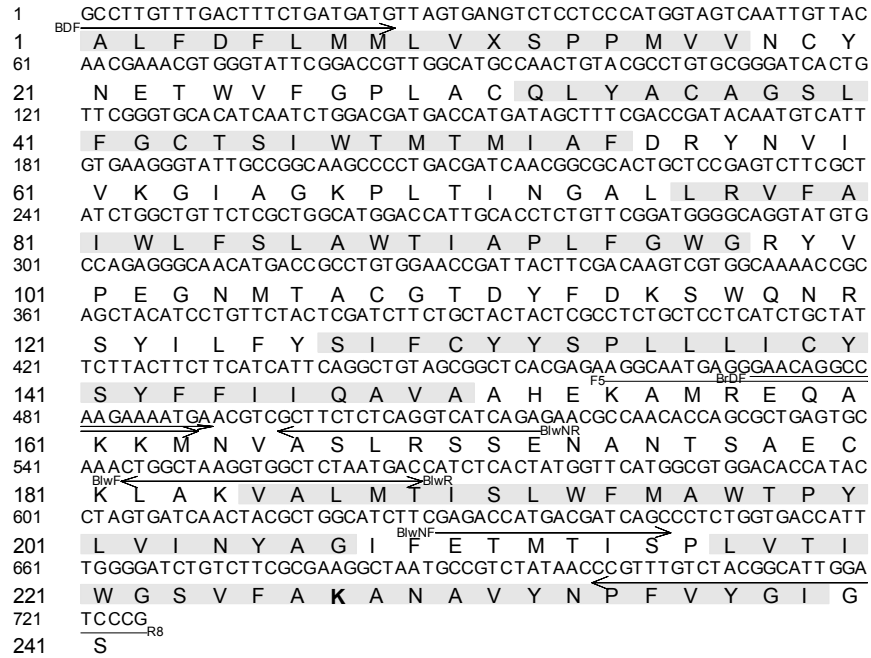

Fig. 2.2: cDNA sequence of the LW-opsin (725 bp) and translated coding region centered under the corresponding cDNA codons. Arrows indicate the position of the homologue nucleotide sequences of the primers. Primers are identified at the start of the arrow (Table 2.1). Arrows to the right and to the left are forward and reverse directed respectively. Transmembrane regions II, III, IV, V, VI and VII are shaded in gray. The lysine chromophore binding site at position 227 is drawn in bold.

3.3. Phylogenetic analysis of the obtained opsin sequences

Multiple ClustalW alignments of both the cDNA sequence and the translated amino acid sequence of the *Bicylus* UV opsin with the complete sequences of all known invertebrate UV opsins were performed (Fig. 2.3). The similarity score between the species, indicating the degree of similarity at each amino acid position, shows the degree of conservation of a specific amino acid in the UV opsins. Interestingly, the lysine amino acid in the HEK (histidine-glutamine-lysine) motif, involved in G-protein binding and identified in all invertebrate rhodopsins at the C-terminal side of transmembrane region V (Gärtner, 2000), appears to be specifically replaced by an alanine residue in all butterfly and moth UV opsin sequences. The *Bicyclus anynana* opsin shares more than 75% identical amino acids with other moth and butterfly species (Table 2.4).

	BicanUV	ManseUV	PapxuUV	PapglUV	CamabUV	CatboUV	ApimeUV	DromeUV3	DromeUV4
BicanUV	**100**	-	-	-	-	-	-	-	-
ManseUV	**79**	100	-	-	-	-	-	-	-
PapxuUV	**77**	74	100	-	-	-	-	-	-
PapglUV	**76**	75	95	100	-	-	-	-	-
CamabUV	**59**	59	58	58	100	-	-	-	-
CatboUV	**59**	61	58	58	88	100	-	-	-
ApimeUV	**60**	61	60	59	84	85	100	-	-
DromeUV3	**56**	55	55	54	61	60	62	100	-
DromeUV4	**54**	55	52	51	56	56	56	69	100

Table 2.4: Pairwise amino acid identities in percentage of all known invertebrate UV absorbing pigments (see Fig. 2.3).

A phylogenetic tree based on these alignments demonstrates that *Papilio*, *Manduca* and *Bicyclus* diverged about equally from a common ancestor (Fig. 2.4). UV opsins from the honeybee *Apis mellifera* and the ants *Cataglyphis bombycina* and *Camponotus abdominalis* form a third group seperated from the opsins of *Drosophila* and the moth and butterflies.

To compare partial sequences of 25 known invertebrate LW opsin sequences, we aligned 215 amino-acid long homologue sequences, including the transmembrane regions 3, 4, 5 and 6. A rootless tree (Fig. 2.5) shows that the *Bicyclus* LW opsin has diverged from the same branch as the *Manduca sexta* LW opsin, the *Papilio* rhodopsin 2 LW opsin and the *Heliconius* LW opsins. *Bicyclus* is most closely related to the *Heliconius* species, with more than 85% pairwise identities.

4. Discussion

4.1. Identification of an ultraviolet and a long-wavelength absorbing rhodopsin of Bicyclus anynana

We cloned the opsin of a UV absorbing rhodopsin of the bush brown *Bicyclus anynana*, except for a small region at the 5′ end. Based on amino acid alignments an estimated 5 amino acids of the coding region have so far eluded identification. The (predicted) lack of 5 N-terminal amino

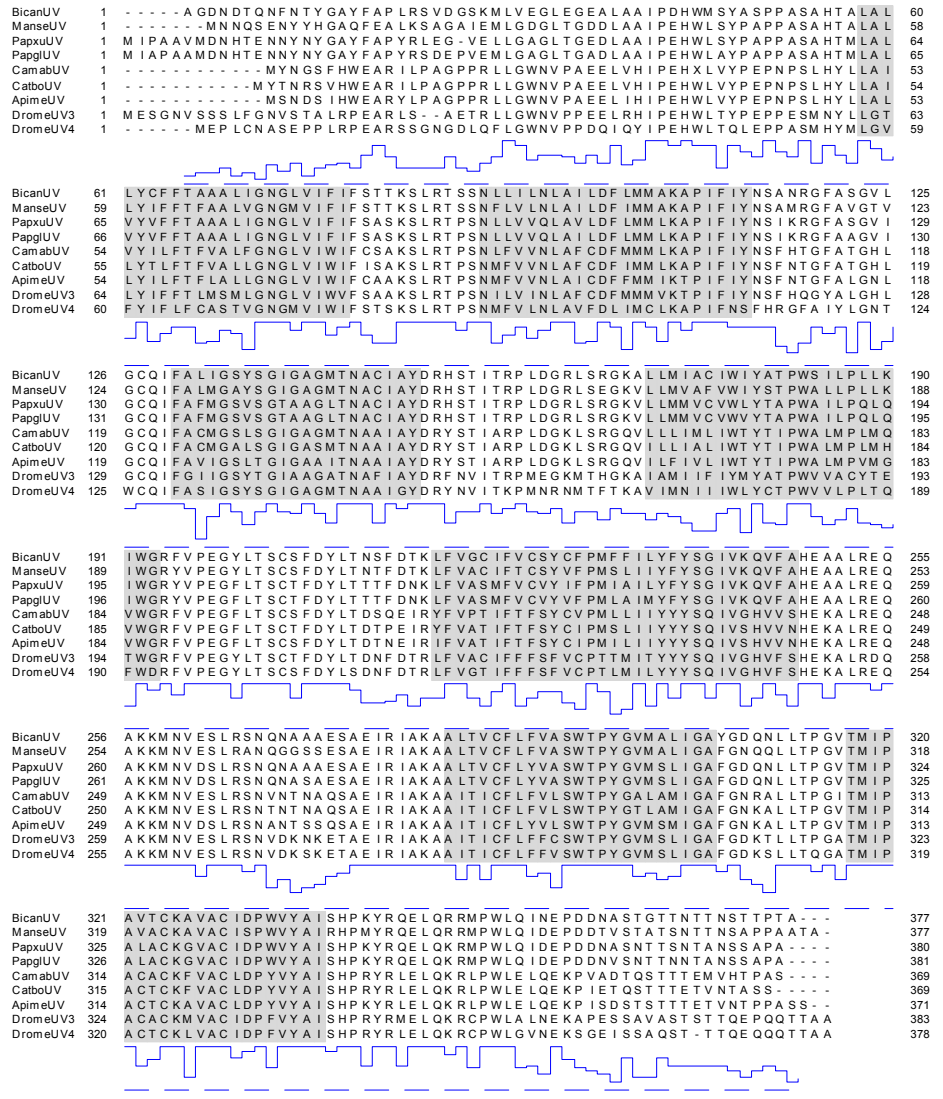

Fig. 2.3: Clustal W (1.81) multiple sequence alignment of the *Bicyclus anynana* UV-opsin (BicanUV) with the UV opsin sequences of *Manduca sexta* (ManseUV, L78081), *Papilio xuthus* (PapxuUV, AB028218), *Papilio glaucus* (PapglUV, AF077191), *Cataglyphis bombycina* (CatboUV, AF042787), *Camponotus abdominalis* (Catab, AF042788), *Apis mellifera* (ApimeUV, AF004169) and *Drosophila melanogaster* (DromeUV3, M17718; DromeUV4, M17719). Putative transmembrane regions are indicated in gray. The degree of conservation at each amino acid position is indicated by an intersimilarity score, going from no similarities (dashed baseline) to 100% identity.

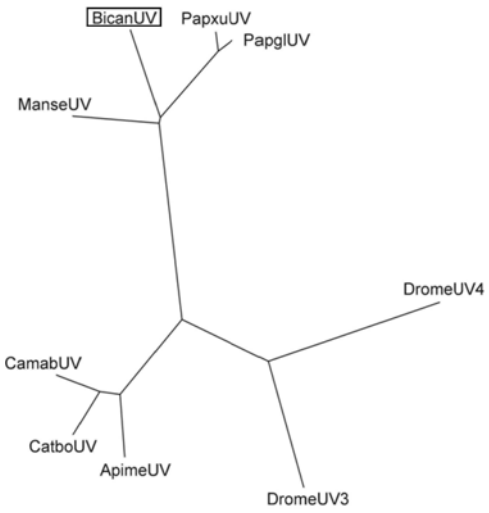

Fig. 2.4: Phylogenetic rootless trees (PHYLIP) based on Clustal W (1.81) multiple amino acid sequence alignment of the UV-opsin (BicanUV) with the complete UV opsin cDNA sequences of *Manduca sexta* (ManseUV), *P. xuthus* (PapxuUV), *Papilio glaucus* (PapglUV), *Cataglyphis bombycina* (CatboUV), *Camponotus abdominalis* (Catab), *Apis mellifera* (ApimeUV) and *Drosophila melanogaster* (DromeUV3, DromeUV4). Accession numbers are given in Fig. 2.3.

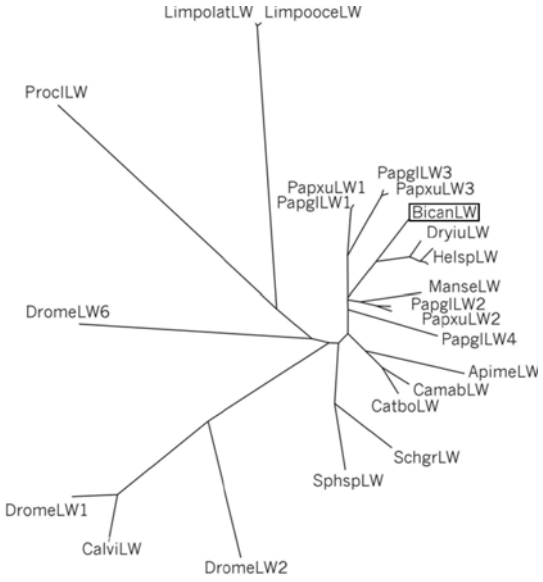

Fig. 2.5: Phylogenetic trees (PHYLIP) based on Clustal W (1.81) multiple sequence amino acid alignment of the *Bicyclus anynana* LW-opsin (BicanLW) with the corresponding homologue sequences of *Apis mellifera* (ApimeLW, U26026), *Calliphora vicina* (CalviLW, M58334), *Cataglyphis bombycina* (CatboLW,U32501), *Camponotus abdominalis* (CamabLW, U32502) , *Drosophila melanogaster* (DromeLW1/2,6, K02315, M12896, Z86118), *Dryas iulia* (DryiuLW, AF126757), 7 *Heliconius sp.* (HelspLW, AF126757, AF126750/1/2/3/4/5/6), *Limulus polyphemus* (lateral eye, L03781 and ocelli, L03792), *Manduca sexta* (ManseLW, L78080), *Papilio xuthus* (PapxuLW, AB007423/4/5), *Papilio glaucus* (PapglLW1/2/3/4, AF077189/90, AF067080, AF077193), *Procambarus clarkii* (ProclLW, S53494), *Schistocerca gregaria* (SchgrLW, X80071), *Sphrodomantis sp*. (SphspLW, X71665).

acids might be due to premature termination of reverse transcription during first strand cDNA synthesis.

It seems likely, based on the phylogenetic relationship and the proven spectral sensitivities in other butterflies (e.g. Struwe, 1971; Eguchi et al., 1982; Arikawa et al., 1987; Shimohigashi and Tominaga, 1991; Bernard and Remington, 1991; Kinoshita et al., 1997; rev. Briscoe and Chittka, 2001) that at least 3 rhodopsins are expressed. However, several attempts to isolate the expected short-wavelength (SW), blue- absorbing rhodopsin with degenerate primers remained so far unsuccessful. Possibly the SW-opsin has a relatively low expression level compared to the other opsins or it is more divergent.

We have identified a partial LW opsin cDNA sequence of 725 basepairs in *Bicyclus anynana*, encoding a sequence of 242 amino acids. Three different combinations of primer sets were used (see Materials and methods, section 3.2); all amplified overlapping partial sequences of the same LW opsin. The sequence is highly similar to the sequences of the LW opsins of *Heliconius erato* and *Manduca sexta.* Whereas the papilionids *Papilio glaucus* and *Papilio xuthus* possess three different long-wavelength (LW) opsins (Briscoe,1998; Kitamoto et al.,1998), only one LW opsin was amplified in 7 *Heliconius* species (Hsu et al., 2001). Studies on the nymphalid *Vanessa cardui* also revealed the expression of only one long-wavelength absorbing pigment (Briscoe and Szeto, unpublished). Presumably also only one LW opsin exists in *Bicyclus anynana*.

Indirect evidence arguing for the presence of an LW (green) rhodopsin comes from *in vivo* microspectrophotometry (unpublished results). The eyes of *Bicyclus,* like many other butterflies, have a clear dorsal-ventral regionalization, which can be visualized *in vivo* by epi-illumination microscopy, due to the presence of a reflecting tapetum proximal to the rhabdom (Stavenga et al., 2001). The reflection color from the ommatidia in the dorsal area of *Bicyclus anynana* is homogeneous: all ommatidia reflect in the yellow-green. In the ventral area, in addition to the yellow-green reflecting type, red-reflecting ommatidia exist (Stavenga, 2002b). Reflection spectra obtained by *in vivo* microspectrophotometry in the dorsal area indicate the expression of an LW opsin, i.e. the calculated difference spectra could be well described with a long-wavelength absorbing rhodopsin and a blue-absorbing metarhodopsin, with a peak wavelength at 560 nm and 490 nm, respectively (unpublished data).

4.2. Phylogenetic classification and sequence comparison with other insect opsins

BLAST analysis indicates that the *Bicyclus* UV opsin is most similar to the UV opsin of the butterfly *Papilio* and the moth *Manduca*. ClustalW alignments of the amino acid sequence of the UV rhodopsin indicate an equidistant phylogenetic relationship between the butterflies and the moth. A search in the ribosomal database bank (http://rdp.cme.msu.edu) showed that *Bicyclus* and *Galleria mellonella*, the greater wax moth, have a very similar partial 18S rRNA fragment, corroborating the close relationship of *Bicyclus* with moths. The LW opsins of *Bicyclus anynana* and *Manduca sexta* have a high similarity with the rhodopsin 2 of the papilionids. In *Papilio*, rhodopsin 2 is distributed equally over the eye and seems to have high expression levels compared to the other opsins (Kitamoto et al., 2000). Up till now 3 butterfly species, *Heliconius*, *Dryas* and *Bicyclus,* all have favoured the expression of a single *Papilio* rhodopsin 2-like type of opsin.

4.3. Perspectives

Color vision is mediated by the collaboration of photoreceptor cells with different sensitivity spectra. The latter spectra are predominantly determined by the rhodopsin absorption spectra. In butterflies, spectral tuning by screening pigments or by the reflecting tapeta may contribute to improve color vision. A description of the ommatidia in terms of co-expression of rhodopsins, tapeta and screening pigments will be crucial for understanding the design principles underlying butterfly vision and the behavioural consequences, e.g. mate recognition, predator avoidance, food search and oviposition (Kelber, 1999a; Gärtner, 2000; Briscoe and Chittka, 2001).

From a developmental point of view it will be interesting to investigate how the expression of a limited set of color units is genetically programmed. The possibility to make transgenic butterflies (Tamura et al., 2000) and the tools developed in *Drosophila* genetic research to screen for morphological eye mutants (Pichaud and Desplan, 2001) opens new pathways for investigating the expression and functionality of color units in accessible species like *Bicyclus anynana*. The identification of the cDNA of an ultraviolet absorbing and a long-wavelength absorbing opsin in this butterfly may be a helpful step in reaching that goal.

Accession numbers: The GenBank accession numbers for the sequences reported in this chapter are AF484248 (UV opsin) and AF484249 (LW opsin).

Chapter 3

Modeling visual pigment processes in butterfly rhabdoms

1. Introduction 28
2. Materials and methods 29
2.1. Photochemistry of invertebrate visual pigments 29
2.2. Absorbance and difference spectra derived from butterfly eye shine reflectances 33
3. Results 35
4. Discussion 38

1. Introduction

The eyes of animals detect incident photons, because the light quanta are absorbed by the visual pigment molecules of the photoreceptor cells. The absorbed incident light causes conversion of the visual pigments which subsequently triggers the phototransduction machinery and results in an electrically coded visual signal. Spectrally selective light absorption by the visual pigments thus determines a crucial characteristic of the eye's sensory quality, namely the spectral light sensitivity of the individual photoreceptors.

Quantitative measurements of light absorption by photoreceptors are in general quite difficult, and therefore a useful approach is to investigate the light absorption by the visual pigments via modelling (Warrant and Nilsson, 1998; Stavenga et al., 2000b). The aim of this chapter is to present a formalism which provides insight into the light-induced visual pigment conversions in butterfly eyes.

The visual pigments of the eyes of invertebrates are concentrated in special subcompartments of the photoreceptors, the rhabdomeres. In the compound eyes of butterflies, sets of nine photoreceptors are grouped in special units, the ommatidia. Each ommatidium has a dioptrical system consisting of a facet lens and a crystalline cone. Light from the environment, entering a facet lens more or less axially, then is channeled into the fused rhabdom, which is the joint structure consisting of the rhabdomeres of the photoreceptors of an ommatidium. The rhabdom acts as a dielectric, optical waveguide, in which light is efficiently propagated in specific light patterns, the waveguide modes. Part of the light in a mode propagates inside the rhabdom boundary. This fraction can be absorbed by the visual pigments of the various rhabdomeres. The light fraction travelling outside the rhabdom boundary can be absorbed by pigment granules existing in the photoreceptor soma, when these granules are sufficiently close to the rhabdom. The latter type of photoreceptor pigment is called the pupillary pigment, as it controls the light flux not unlike the pupil of the human eye.

The ommatidia of butterfly eyes are anatomically very similar to that of other insects with fused-rhabdom apposition eyes, like bees or locusts, but their unique feature is the presence of a light-reflecting tapetum located very precisely proximal to the rhabdom in each ommatidium. Light which has propagated the complete length of a rhabdom, and hence has not been absorbed, then is reflected by the tapetum and thus is sent at a return route. Part of the reflected light escapes absorption also at the way back, and then leaves the eye. This reflected light is called the butterfly eye shine. The eye shine depends on many factors, e.g. the absorption spectra of the visual pigments and

their concentrations, the reflectance spectrum of the tapetum, the rhabdom waveguide properties, and of course the spectrum of the incident light. A suitable model hence has to account for these factors.

2. Materials and methods

2.1. Photochemistry of invertebrate visual pigments

The following section presents a computational example, inspired by the experiments of Chapter 4. In that chapter three visual pigments, a UV, blue and green rhodopsin, were identified to exist in the homogeneous eye of the comma *Polygonia c-album*. Their peak wavelengths were estimated to be 345, 440 and 532 nm, the peak wavelengths of their metarhodopsins 480, 485 and 493 nm, and their isosbestic wavelengths 376, 378 and 525 nm, respectively. Fig. 3.1 presents the spectra of these three visual pigments.

Invertebrate visual pigment molecules can exist in two thermostable states, rhodopsin and metarhodopsin. These states are photo-interconvertible, i.e., absorption of a photon can convert a rhodopsin into metarhodopsin molecule, and vice versa. The conversion kinetics is described by a first order reaction:

$$\mathrm{R} \underset{k_{\mathrm{M}}}{\overset{k_{\mathrm{R}}}{\rightleftarrows}} \mathrm{M} \tag{1}$$

The absorption spectra of both states can be phenomenologically described by visual pigment templates, the most recent of which is that derived by Govardovskii et al. (2000). The characteristic absorption bands of a visual pigment template, primarily the α-band and β-band, are described by exponential functions. The normalized α-band is described by

$$S_\alpha = \left\{\exp\left[A(a-x)\right] + \exp\left[B(b-x)\right] + \exp\left[C(c-x)\right] + D\right\}^{-1} \tag{2}$$

with $x = \lambda_{\max}/\lambda$, and where $\lambda_{\max}$ is the peak wavelength of the α-band.
The optimal set of parameters for visual pigments with a chromophore derived from vitamin A1 were deduced from a set of experimental spectra (with $\lambda_{\max}$ in nm):

$A = 69.7,\ \mathrm{a} = 0.8795 + 0.0459 \exp\left[-\left(\lambda_{\max} - 300\right)^2 / 11940\right]$

$B = 28,\ b = 0.922,\ C = -14.9,\ c = 1.104,\ D = 0.674$

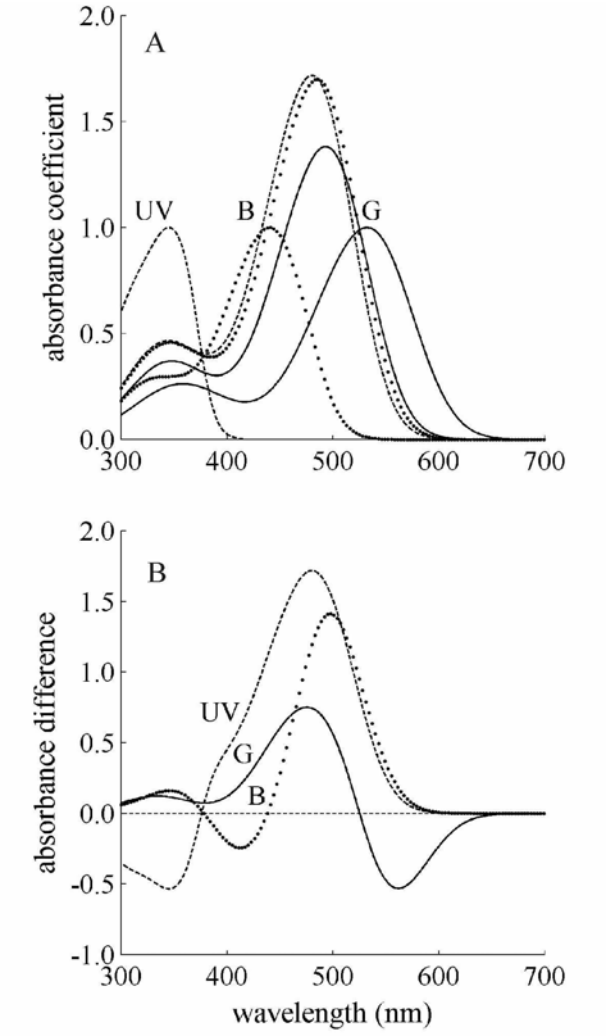

Fig. 3.1: A. Absorption spectra of the visual pigments of the comma, *Polygonia c-album* of the UV, blue and green rhodopsin, with peak wavelengths of the rhodopsin state 345, 440 and 532 nm, and of their metarhodopsins with peak wavelengths 480, 485 and 493 nm, respectively. **B.** Difference spectra of the three visual pigments in Fig. 3.1A.

In addition a Gaussian function for the β-band was derived

$$S_\beta = A_\beta \exp\left\{-\left[\left(\lambda - \lambda_{m\beta}\right)/d\right]^2\right\} \tag{3}$$

where A_β is the amplitude of the β-band relative to that of the α-band, $\lambda_{m\beta}$ the position of the β-peak, and d a bandwith parameter, with optimal parameter values (with λ_{max} in nm):
$A_\beta = 0.26$, $\lambda_{m\beta} = 189 + 0.315\ \lambda_{max}$, $d = -40.5 + 0.195\ \lambda_{max}$

When the total concentration of visual pigment, C_0, is constant, it is useful to express the concentrations of rhodopsin and metarhodopsin as fractions of C_0, i.e. $C_R = f_R C_0$ and $C_M = f_M C_0$, so that at time t:

$$f_R(t) + f_M(t) = 1 \tag{4}$$

When the visual pigment molecules are irradiated with broad-band light the fractional change in rhodopsin concentration can be described as

$$\frac{df_R}{dt} = -k_R f_R + k_M f_M \tag{5}$$

with rate constants

$$k_R = \int I(\lambda)\alpha_R(\lambda)\gamma_R d\lambda \tag{6a}$$

and

$$k_M = \int I(\lambda)\alpha_M(\lambda)\gamma_M d\lambda \tag{6b}$$

in which the light intensity, $I(\lambda)$, depends on the location in the rhabdom, $\alpha_R(\lambda)$ and $\alpha_M(\lambda)$ are the molecular absorption coefficients, and γ_R and γ_M the quantum efficiencies for photoconversion of R into M and of M into R, respectively. The products of the latter two quantities are also called the photosensitivities: $K_R(\lambda) = \alpha_R(\lambda)\gamma_R$ and $K_M(\lambda) = \alpha_M(\lambda)\gamma_M$. It follows from integrating Eq. 5 that the fraction f_R at time t is given by

$$f_R(t) = f_{R,\infty} + (f_{R,0} - f_{R,\infty})e^{-(k_R + k_M)t} \tag{7}$$

The fraction of rhodopsin in the photosteady state, i.e. in equilibrium ($t = \infty$), $f_{R,\infty}$, equals:

$$f_{R,\infty} = \frac{k_M}{k_R + k_M} \tag{8}$$

With an incident light intensity $I_0(\lambda)$ at the rhabdom tip, and assuming that light is propagated in only one waveguide mode, the intensity of the propagating light flux at a distance z from the rhabdom entrance is described by a modified Lambert-Beer law:

$$I(\lambda, z) = I_0(\lambda) e^{-\int_0^z \kappa_{eff}(\lambda, z)dz} \tag{9}$$

where κ_{eff}, the effective absorption coefficient of the rhabdom medium:

$$\kappa_{eff} = \eta\kappa_i + (1-\eta)\kappa_o \tag{10}$$

is the weighted absorption coefficient of the inside and outside media, with η the fraction of the light flux propagating by the mode within the rhabdom and κ_i the absorption coefficient of the rhabdom medium with the visual pigments and κ_o that of the surrounding medium (which can contain screening pigment granules).

The rhabdom transmittance is the fraction of light that travels the rhabdom length one-way without having been absorbed:

$$T(\lambda, z) = \frac{I(\lambda, z)}{I_0(\lambda)} = e^{-\int_0^L \kappa_{eff}(\lambda, z)dz} = e^{-\bar{\kappa}_{eff} L} \tag{11}$$

where $\bar{\kappa}_{eff}$ is the average effective absorption coefficient. The light flux that reaches the tapetum is reflected with an efficiency given by the reflectance $M(\lambda)$. The reflected light travels the reverse way, so that the light intensity available for photoconversion at location z equals:

$$I(\lambda,z) = I_0(\lambda)\left[e^{-\int_0^z \bar{\kappa}_{eff}(\lambda,z)dz} + M(\lambda)T(\lambda,z)e^{-\int_{L-z}^{L} \bar{\kappa}_{eff}(\lambda,z)dz} \right] \quad (12)$$

This quantity implemented in Eq. 12 determines the rate of visual pigment conversion. However, visual pigment conversion results in a change in the effective absorption coefficient, which causes a change in the spectrum of the local light intensities. Visual pigment conversions induced by broad-band illuminations hence can be only elucidated by numerical computations. This was executed by a programme written in MATLAB, incorporating the formulae above.

2.2. Absorbance and difference spectra derived from butterfly rhabdom reflectances

Light-induced photochemical changes in the visual pigment composition can be measured in completely intact living butterflies by epi-illumination microspectrophotometry, utilizing the eye shine. The fraction of the light flux which enters a butterfly rhabdom and, after being reflected at the tapetum and having travelled twice the length, L, of the rhabdom returns at the rhabdom entrance is called the rhabdom reflectance (Stavenga et al., 1977):

$$R = MT^2 \quad (13)$$

A generally used quantity, derived from the transmittance, is the absorbance, also called the optical density, which is defined as the negative decadic logarithm of the transmittance: $A = -\log_{10}(T)$. We can similarly define the absorbance of the butterfly rhabdom by taking the negative logarithm of the reflectance, Eq. 13, yielding:

$$A = -\log_{10}(R) = 0.87\kappa L - \log_{10}(M) \quad (14)$$

where $\kappa = \bar{\kappa}_{eff}$.

A simplified case is that where the waveguide properties can be neglected ($\eta = 1$ in Eq. 10). A light-induced conversion of the visual pigment causes a change in the reflectance, and the difference in absorbance between the new and the initial situation then is:

$$\Delta A = 0.87(\kappa_2 - \kappa_1)L \tag{15}$$

where κ_1 and κ_2 are the rhabdom's absorption coefficients in the two conditions.

The advantage of the absorbance difference is that it cancels many unknowns, specifically the tapetal reflectance, but also the possible effect of other absorbing pigments, which are not changed by the illumination. More importantly, the absorbance difference can be calculated even when only the reflection is known without knowledge of the incident light flux $I_0(\lambda)$. The latter quantity, as well as other time-invariant, wavelength-dependent factors, e.g. the transmittance of the measuring optics and spectral characteristics of the microspectrophotometer, is also divided out when calculating the absorbance difference.

The light absorption by the rhabdomeres of all contributing photoreceptors determine the rhabdom absorption coefficient, κ. When all rhabdomeres have the same type of visual pigment, with concentration of the rhodopsin and metarhodopsin molecules being C_R and C_M, then

$$\kappa = \alpha_R C_R + \alpha_M C_M \tag{16}$$

When photoconversion changes the initial concentrations $C_{R,1}$ and $C_{M,1}$ into $C_{R,2}$ and $C_{M,2}$, respectively, the absorbance difference is:

$$\Delta A = 0.87\{[C_{R,2} - C_{R,1}]\alpha_R + [C_{M,2} - C_{M,1}]\alpha_M\}L \tag{17}$$

or, when $f_R = 1 - f_M$ is the average rhodopsin fraction in the rhabdom and the fractions in the initial situation, $f_{R,1}$ and $f_{M,1}$, are changed into $f_{R,2}$ and $f_{M,2}$, respectively, the absorbance difference is:

$$\Delta A = 0.87C_0[f_{R,2} - f_{R,1}](\alpha_R - \alpha_M)L \tag{18}$$

Eq. 18 can be simplified by choosing an initial situation where $f_{R,1} = 1$. Calculation of difference spectra for a new state where $f_R = f_{R,2}$ then yields:

$$\Delta A = 0.87C_0[1 - f_R](\alpha_R - \alpha_M)L = 0.87C_0 f_M(\alpha_R - \alpha_M)L \tag{19}$$

Eqs 18 and 19 show that difference spectra are proportional to the difference between the molecular absorbance coefficients of R and M. This of course only

holds when the rhabdom contains no more than one visual pigment type. When more than one type of visual pigment is present, the right hand term of Eq. 18 has to be extended with terms for the additional number of visual pigments.

3. Results

A simplified computational model was developed that consists of a rhabdom containing equally sized rhabdomeres of eight photoreceptors over its total length. A rhabdom is considered with length L = 450 μm (a typical rhabdom length of Nymphalinae; see Briscoe et al., 2003), which is filled with the visual pigments of Fig. 3.1. The reflectance coefficient of the tapetal mirror proximal to the rhabdom is taken to be spectrally flat with magnitude M = 0.8. The peak molecular absorbance coefficients of all rhodopsins were assumed to be the same: $\alpha_R(\lambda_{max})$ =1.56·10^{-8} μm^2 (Dartnall, 1972). With a visual pigment concentration C_0 = 3.2·10^5 μm^{-3} a peak-absorbance coefficient κ_{max} = 0.005μm^{-1} results. The quantum efficiencies for photoconversion were assumed to be equal: $\gamma_R = \gamma_M$ = 2/3 (Dartnall, 1972; Hamdorf, 1979). Two cases are compared to illustrate the photochemical events occurring due to illumination with broad-band light. In the first case (Fig. 3.2A,C,E), all eight photoreceptors are green receptors, i.e., contain the same type of green absorbing rhodopsin. In the second case (Fig. 3.2B,D,F), the rhabdom contains 1 ultraviolet receptor (UV), 1 blue receptor (B), and 6 green receptors (G). Initially all visual pigment molecules are assumed to be in the rhodopsin state. Illumination with light containing the same number of photons at all wavelengths then causes conversion of part of the molecules into the metarhodopsin state. The conversion speed depends on intensity (Eqs 6-9), and thus will decrease at locations further into the rhabdom, because the absorbing visual pigments result in a decreasing intensity with increasing depth in the rhabdom (cf Eq. 9).

The resulting local light intensity spectra at depths z = 0, 150, 300 and 450 μm are presented in Fig. 3.2A, relative to the incident light intensity, taken to be 5·10^6 photons s^{-1} μm^{-2}. Because the local intensities are due to the sum of the light fluxes from distal to proximal and *vice versa*, the (summed) relative intensity is the same at all wavelengths when absorbing visual pigment is totally absent: 1+ M = 1.8 (indicated by the dashed horizontal line on top of Fig. 3.2A,B). This value holds throughout the rhabdom at wavelengths λ > 650 nm, where visual pigment absorption becomes negligible, but smaller relative intensity values are reached where significant visual pigment absorption occurs at short and middle wavelengths.

At time t = 0 all visual pigment molecules exist in the rhodopsin state, but later on light absorption causes rhodopsin to convert into metarhodopsin, resulting in

an absorption increase, i.e. a decrease in relative light intensity at $\lambda < \lambda_{iso}$, the isosbestic wavelength, and an absorption decrease, i.e., a relative intensity increase at $\lambda > \lambda_{iso}$. The light-induced visual pigment conversions cause changes in the absorbance, shown as log reflectance at seven time points in Fig. 3.2C,D. The spectra of Fig. 3.2C are proportional to the difference spectrum of the molecular absorbance coefficients of the green rhodopsin and metarhodopsin, $\alpha_M - \alpha_R$ (Eq. 19). The proportionality factor is the change in rhodopsin fraction, $f_M = f_{R,2} - f_{R,1}$, where the index 1 refers to the initial (full rhodopsin) situation: $f_{R,1} = 1$. Normalizing the spectra of the different time points (Fig. 3.2B) to the final, steady state therefore yields horizontal lines (Fig. 3.2E). The situation is slightly more complex when three visual pigments populate the rhabdom. The expression for the absorbance difference (Eq. 19) then consists of three terms, one for each visual pigment type. Due to the large majority of the green visual pigment, the difference spectra of Fig. 3.2D appear very similar to those of Fig. 3.2C. Normalization to the final, steady state yields approximately horizontal lines, but anomalous behaviour occurs near the green visual pigment's isosbestic wavelength. We will see in Chapter 4 that this aberrant phenomenon is indeed encountered experimentally.

Fig. 3.3A,B gives the rhodopsin fractions at four locations in the rhabdom, separated by 150 μm. The photochemical processes of rhodopsin to metarhodopsin conversion occurs fastest at the rhabdom tip, which is of course due to the fact that the light intensity is extreme there. The processes are slowed down when the distance to the entrance, z, increases, due to the decrease in light intensity caused by the absorbing visual pigment molecules. In the steady state, reached in the examples of Fig. 3.2 after about 2 s, the fraction of green rhodopsin is about 0.6 at virtually all locations throughout the rhabdom. Apparently, the broadness of the filtered light spectra underlies the invariance of the equilibrium state. In the steady state of the three visual pigment case (Fig. 3.3B), slightly higher UV- and blue-rhodopsin fractions exist, which also more vary with location. It will be clear that the creation of a substantial metarhodopsin fraction of the UV- and blue visual pigments causes the anomalous peaks in Fig. 3.2F.

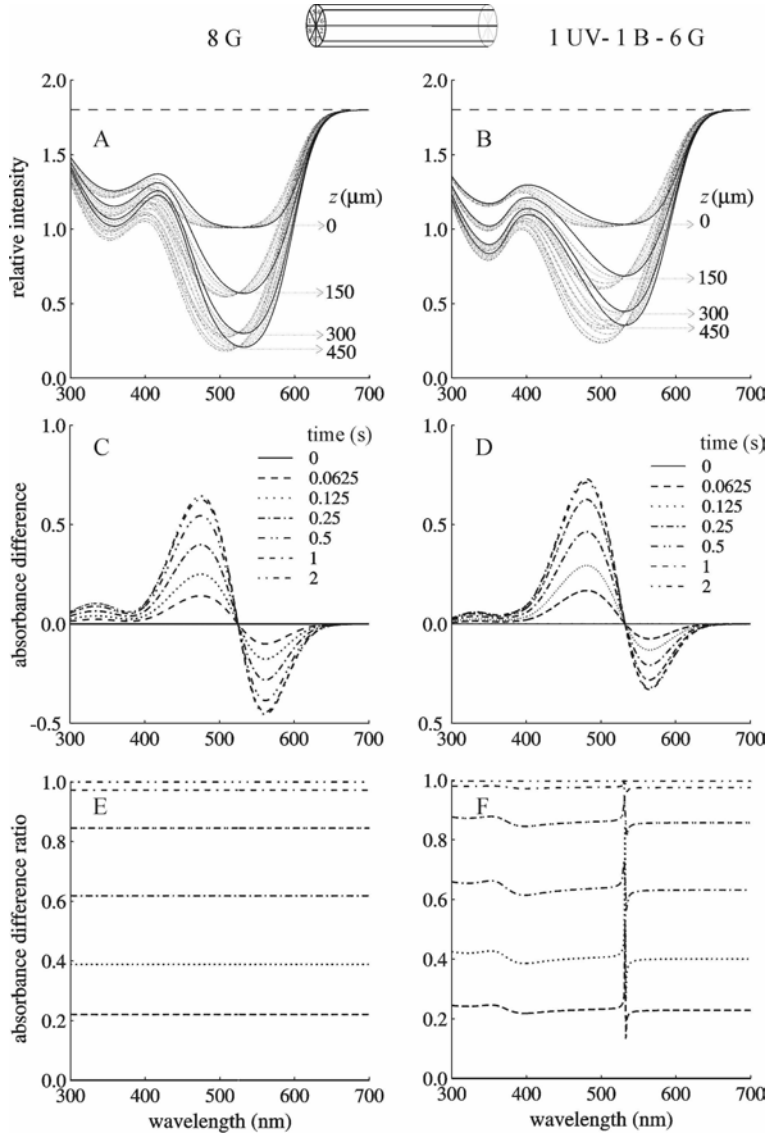

Fig. 3.2: Relative intensities and photochemical processes in two model butterfly rhabdoms, consisting of eight photoreceptors, in the first case (**A**, **C**, **E**) all containing the same type of green absorbing rhodopsin, equally sharing the rhabdom volume and in the second case (**B**, **D**, **F**) the rhabdom contains 1 ultraviolet receptor (UV), 1 blue receptor (B), and 6 green receptors (G). **A-B**. The resulting local light intensity spectra relative to the incident light intensity ($5 \cdot 10^6$ photons s^{-1} μm^{-2}) at depths z = 0, 150, 300 and 450 µm. **C-D.** The light-induced visual pigment conversions cause absorbance changes, shown as log reflectance at seven time points. **E-F.** Normalizing the spectra of the different times to the final, steady state yields horizontal lines (**C**). Aberrant phenomena occur around the isosbestic point in the three pigment case (**D**).

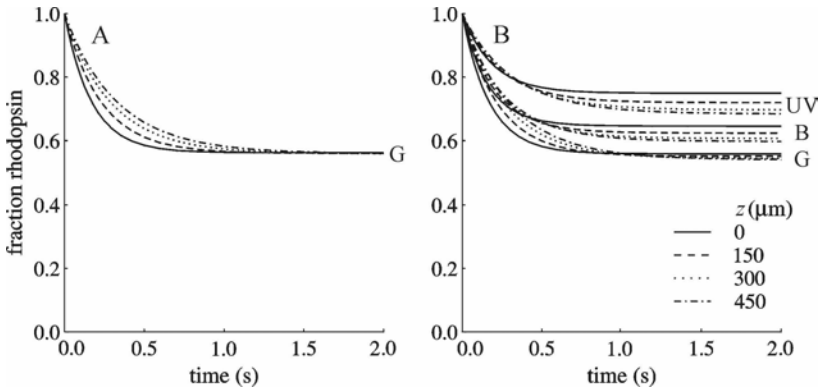

Fig. 3.3: Rhodopsin fractions at four depth locations in the rhabdom after illuminating a rhabdom with eight green receptors (**A**, see Fig. 3.2 **A,C,E**) or with three visual pigments, 1 ultraviolet, 1 blue and 6 green receptors (**B**, see Fig.3.2 **B, D,F**).

4. Discussion

Butterfly visual pigments can be investigated in vivo by epi-illumination microspectrophotometry (Stavenga,1979; Bernard, 1983). Butterflies offer a special advantage for experimental studies on the visual pigments because a reflecting mirror, the tapetum, is built-in in each butterfly ommatidium. A slight drawback is that the reflectance spectrum of the tapetum is generally unknown, which forms a complicating factor in the spectral analyses. Measuring difference spectra overcomes this problem and furthermore is done relatively straightforwardly on photochemical steady states, especially when using monochromatic light (Stavenga et al., 2000b), but photoconversions with broad-band illumination, as occurs in natural circumstances, are complicated because the butterfly rhabdom is a long cylinder, containing several visual pigment types, usually three (Briscoe and Chittka, 2001).

The model presented above is helpful for gaining understanding of the photochemical processes induced by broad-band white light. The choice to study a rhabdom with eight photoreceptors, R1-8 (1 UV, 1 blue and 6 green receptors), is related to the recent findings that the majority of butterfly photoreceptors contain rhodopsins peaking in the green (e.g. Kinoshita et al.,1997; Briscoe et al., 2003; White et al., 2003). In nymphalids eight rhabdomeres occupy more or less equally the rhabdom volume. There is a ninth photoreceptor, R9, which is neglected here, because its short rhabdomere is restricted to the very proximal part of the rhabdom, and therefore the optical contribution of R9 will be minor.

Starting with an initial 100% rhodopsin population, it appears that bright white light causes conversion to a steady state with a final rhodopsin fraction of ca 0.6, virtually independent of location (Fig. 3.3A,B). The conversion speed changes also quite unconsiderably over the rhabdom (Fig. 3.3A,B), i.e. for the green visual pigment no more than a factor two, and even less for the UV and blue visual pigments, indicating that light sensitivity is virtually unhampered by self-screening, i.e. the phenomenon of diminishing light in proximal rhabdom layers due to light filtering by the distal layers.

A standard procedure in photochemical studies is the calculation of absorbance difference spectra, because then constant factors are factored out. Because visual pigments are photochromic substances, photochemical changes result in proportional difference spectra. This property is illustrated in Fig. 3.2E, but Fig. 3.2F shows that it breaks down with mixtures of different photochromic materials: near isosbestic points strong anomalies can arise.

The developed model is only roughly approximating the real situation of butterfly rhabdoms. Incident light is focused into the rhabdom, there exciting waveguide modes propagating light fluxes with wavelength-depending intensities. Also, the distribution of the light fluxes over the allowed waveguide modes depends on wavelength. Although these spectral dependencies are not strong, they have been fully neglected in the modelling. The maximum absorbance coefficient of the visual pigments is assumed to be 0.005 μm^{-1}, well in the middle of known values of insect photoreceptors (Warrant and Nilsson, 1998), but whether this value is accurate for butterflies is unsettled. Furthermore, the reflectance spectrum of the tapetum has been assumed to be wavelength independent and no less than 0.8. The assumption of a flat tapetal spectrum is probably correct up to a certain cut-off value, being well above 600 nm for many nymphalid tapeta (see Chapter 6), and therefore the assumption is quite acceptable, because most visual pigment absorptions are minor to negligible in the red. The value of 0.8 is little more than a wild guess, based on the assumption that the tapetum is a functional component of the butterfly visual system. A reflectance lower than 0.6 will mean that the light reflected by the tapetum has little importance for the light sensitivity of R1-8 photoreceptors. A reflectance value of 1.0 will be in practice out of reach. Possibly therefore a value 0.8 is realized.

The computational results are based on a formalism which assumes that the concentration of visual pigment molecules stays constant. However, in the dark, visual pigment molecules which exist in the metarhodopsin state are rapidly degraded and new rhodopsin molecules are reconstituted in the rhabdomeric membrane (Bernard, 1983). The total visual pigment concentration, C_0, then may not be constant, and therefore Eq. 16 must then be

used together with the proper time course of the changes in rhodopsin and metarhodopsin.

In the main part of the eye of pierids red screening pigments strongly affect the light flux in the rhabdom, thus obscuring the wavelength range where photochemical changes could be measured. Modelling visual pigment processes in rhabdoms surrounded by screening pigments forms a challenge for the future.

Chapter 4

Visual pigment absorption spectra of the nymphalid butterfly *Polygonia c-album* derived from *in vivo* reflection measurements

1. Introduction 42
2. Methods 43
2.1. Animal and preparation. 43
2.2. Optical set-up. 44
2.3. Experimental protocol: 3 variations on a photochemical theme 46
2.4. Spectrophotometric analysis. 47
3. Results 49
3.1. Photochemical conversion of the green rhodopsin 49
3.2. Bleaching green metarhodopsin 51
3.3. Regeneration of the green rhodopsin 54
3.4. Photochemical conversion of a UV metarhodopsin 54
4. Discussion 57
4.1. White light-induced conversion of a green-absorbing rhodopsin 57
4.2. Regeneration and degradation of the green visual pigment 57
4.3. Bleaching green visual pigment and tapetum reflectance spectra 58
4.4. Derivation of the UV and blue visual pigments 59
Appendix 60

1. Introduction

A unique feature of butterfly eyes is their colorful eye shine (Exner, 1891; Miller and Bernard, 1968;Goldsmith and Bernard, 1974; Ribi, 1980). In the past decades, combined anatomical, optical and physiological studies have yielded considerable insight into the origin and optical mechanisms underlying this intriguing phenomenon. First, at the level of individual ommatidia, light is focussed by a lens on the rhabdom, a cylindrical structure consisting of microvilli contributed by 9 photoreceptor cells, which contain the visual pigment molecules. Light is travelling along this light guide so realizing a high chance of light absorption by the visual pigments. At the proximal end of the ommatidia, light which has not been absorbed is reflected at a multilayered structure, created by intricately folded tracheoles. After a second passage through the rhabdom, part of the light leaves the eye, giving rise to colorful reflections. The color of the eye shine is attributed to the integrated action of the interference filter properties of the tapetum and the selective spectral absorption by visual pigments (Stavenga, 2002a), in several occasions enhanced by colored screening pigments, which surround the rhabdom (Arikawa et al., 1999a; Qiu et al., 2002). An investigator, illuminating the eye of a dark-adapted butterfly in an epi-illumination microscope, sees a rapidly fading eye shine: pupillary pigments inside the photoreceptor cells migrate towards the rhabdom upon light adaptation (Stavenga et al., 1977), effectively decreasing the propagating light flux.

Recent research, applying molecular biology and electrophysiology, has shown that butterfly ommatidia are heterogeneous in the composition of their cellular components, especially in the visual pigments, tapeta and screening pigments. It appears that the eyes contain a few classes of randomly distributed ommatidia, with often a marked dorso-ventral regionalization (Stavenga et al., 2001; Qiu et al., 2002;). The eye has usually specialized regions and the optical resolution of the eye is not uniform (Stavenga et al., 2001; Rutowski and Warrant, 2002).

The main challenge of the present research is to understand the basic principles of eye design evolved in lepidopterans in relation to their ecology (Bernard and Remington, 1991; Arikawa and Stavenga, 1997; Kelber, 1999a). This requires a description of the heterogeneity, together with a quantitative treatment of the individual ommatidial components and their integrated action. Powerful experimental approaches, applied so far to a restriced number of butterfly species, have been the recording of reflection spectra from individual facets (see Chapter 6) or from a group of ommatidia by micro-spectrophotometry (Bernard and Remington, 1991) or with a digital camera

(Stavenga, 2002a,b; Chapter 5). The distinct advantage of non-invasively probing the living butterfly *in vivo* has urged us to extend the analysis of reflectance spectra in more quantitative detail. To explore the individual characteristics of the major ommatidial components the visual pigments and the tapetum, we have recorded reflection spectra with a high spectral (0.3 nm) and temporal resolution (10 ms integration time). In this chapter we explore a few procedures to determine the spectral properties of the visual pigments and the underlying tapetum. We have calculated absorbance difference spectra (see Chapter 3) from measured reflection spectra during photochemical conversions of the visual pigments, as well as during long-term dark processes, due to metarhodopsin degradation and rhodopsin regeneration.

The present study on the comma, *Polygonia c-album*, is the first of a series of comparative studies performed on the eyes of different butterflies. The eye of *Polygonia* has been selected because of its homogeneous red-orange eye shine, extending far into the red (halfwidth cut-off value at 700 nm), indicating a strongly homogeneous population of ommatidia (Stavenga, 2002a).

2. Methods

2.1. Animal and preparation.

The investigated butterfly, *Polygonia c-album*, was captured in Groningen, the Netherlands. The butterfly was mounted in a plastic tube and positioned on the goniometer of a microspectrophotometric set-up. The head and thorax were sealed to the plastic tube with wax, to avoid eye movements. The animal was fed with a sugar solution before the experiment.

The set-up, described in the next section, is a modified epi-illumination microscope which allows observation of the eye shine of butterfly eyes. When a dark-adapted eye is observed with the microscope focused at the level of the eye's cornea, i.e. the facet lenses, one sees a bright shine in those ommatidia which have a visual field within the aperture of the microscope, due to the reflecting tapetum (Fig. 4.1A). The number of shining facets thus depends on the numerical aperture of the microscope objective. The assembly of shining facets is called the luminous corneal pseudopupil (Franceschini and Kirschfeld, 1971; Stavenga, 1979). The eye shine merges into a single bright spot when the microscope is focused at the level of the center of curvature of the eye (Fig. 4.1B). This spot is called the luminous deep pseudopupil (see Chapter 1, Fig. 1.3).

The eye shine vanishes within a few seconds of illumination, because pigment granules existing in the somas of the photoreceptors migrate

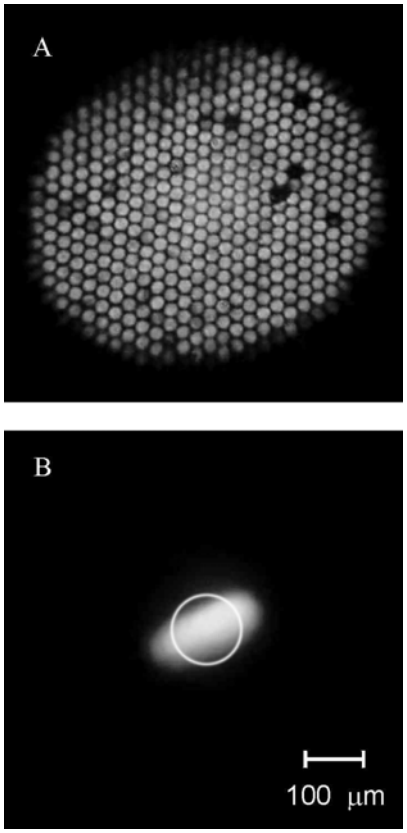

Fig. 4.1: A. Magnified image of the cornea obtained with the epi-illumination set-up of Fig. 4.2. The eye shine, being light reflected from the tapeta in the individual ommatidia, has a nearly homogeneous orange-yellow color. Black dots are bad reflecting facets (or dust pieces). Nearly 400 facets, with an average diameter of 25 μm, contribute to the eye shine at the corneal level. It is also called the luminous corneal pseudopupil (Stavenga, 1979). As the objective acceptance angle is 35° and the cross-section of the corneal pseudopupil is made up of 23 ommatidia, the interommatidial angle is ca 1.5°. **B.** Focusing the photomicroscope at the level of the center of curvature of the eye yields the luminous deep pseudopupil (DPP). Its shape is slightly oval, due to the somewhat ellipsoidal shape of the eye. The tip of the optical fiber of the spectrophotometer (solid circle) is positioned in the magnified image of the DPP (see Fig. 4.2, D2) in the microspectrophotometrical experiments.

towards the rhabdom and there absorb the light flux propagated in the boundary wave. Obviously, this pupil mechanism can strongly disturb the study of the visual pigments, the theme of this chapter. This disturbance can be largely avoided by an appropriate protocol, which allows enough time to temporarily retract the pigment granules from the lightguide.
The photochemical measurements of the present chapter were performed at the level of the deep pseudopupil. Our improved time-resolution allows us to measure *in vivo* instantaneous photochemical conversions of the green visual pigment of butterflies.

2.2. Optical set-up.

Reflection spectra were recorded with the optical set-up described by Stavenga (2002b), which was slightly modified for the present experiments (Fig. 4.2).

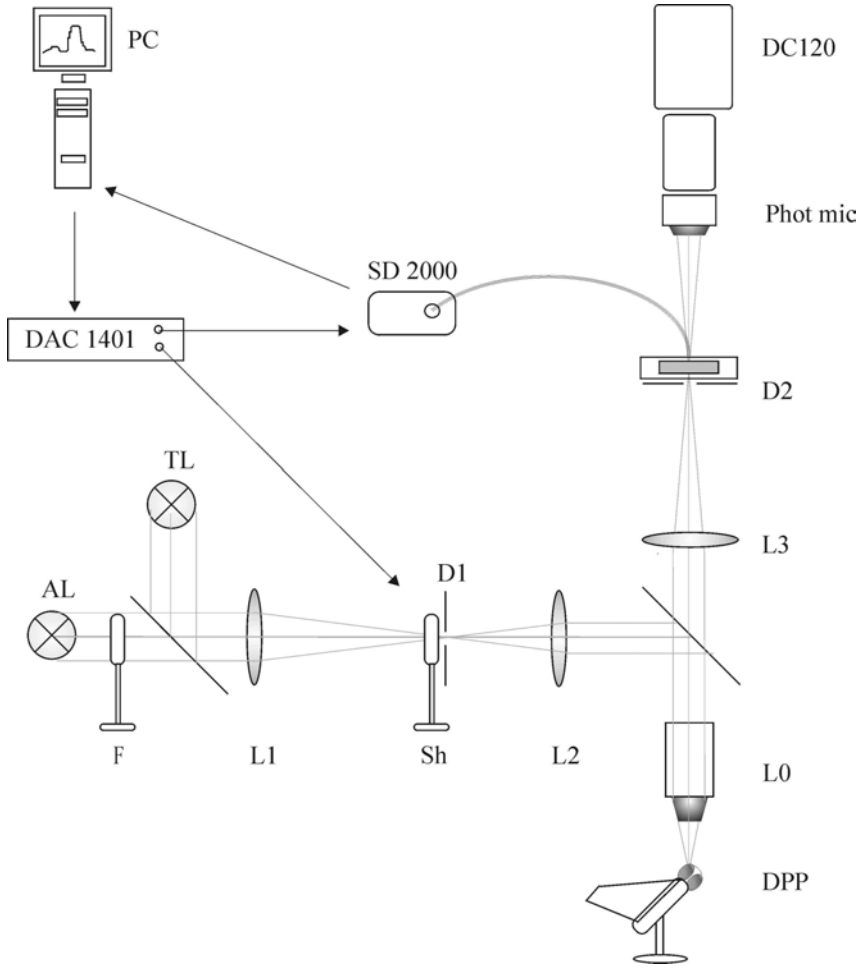

Fig. 4.2: The optical set-up used to record reflectance spectra (adapted from Stavenga, 2002). Central to the set-up is the spectrometer (Avantes, SD2000), which can be triggered to start data-acquisition by a signal from the 1401 DAC (Cambridge Electronics Design). Data-acquisition and opening of the shutters (Sh) in the light path are triggered simultaneously by TTL pulses of DAC's of the CED 1401 under control of Signal2 software (Cambridge Electronic Design) on a Pentium computer (PC). Signals from the DAC and flow of spectral information to the PC are indicated with solid arrows. A half-mirror placed at 45° transmits light from both the test (TL) and adapting light (AL) source. Density filters or interference filters (F) may be placed in the light beam. A parallel beam enters the microscope objective (L0, Zeiss, 10x, NA 0.3) and is focused on the deep pseudopupil image (DPP), which can be seen in the center of the eye. The telescopic lens pair of objective and L3 images the DPP on the secondary focal plane of L3, where the tip of an optical fiber is positioned. Light entering the fiber is guided to the spectrometer, which has a 2048 element photodiode array spanning a spectral range of 178 nm to 890 nm. In an alternative arrangement, a photomicroscope (Phot mic), equipped with a Photar lens and a digital camera (Kodak, DC120) is used to photographing either the the DPP image or the eye's corneal facet lenses (see Fig. 4.1). Stray light is minimized by diaphragms D1 and D2.

A 50 W halogen lamp and a 100 W mercury lamp were used as a test and adapting light source, respectively. Interference (Schott, DAL, bandwidth ca 15 nm) and long-pass filters (Schott, OG570) in the light beams provided selective spectral irradiation. The halogen light beam was equipped with an additional slightly blue-colored filter (Wratten, Kodak) to enhance the light flux in the blue, where the eye shine generally is weak (Fig. 4.3A). Light was projected on the eye's deep pseudopupil (DPP, Fig. 4.1) by a Zeiss 10x objective (NA 0.3). The microscope images the DPP in the secondary focal plane of lens L3. The reflected light there is captured by a glass fiber (diameter 600 μm) connected to a spectrophotometer (SD2000, Avantes). Its monochromator projects the light on a linear diode array, with high spectral resolution, i.e. 0.3 nm, extending over a wide spectral range (178 to 890 nm).

The irradiance at the level of the focal plane of the microscope objective was measured for each filter with a calibrated photometer (Graseby). Photometer readings at 17 monochromatic wavelengths were transformed in irradiance units: photons s^{-1} nm^{-1} cm^{-2} (Fig. 4.3A).

The data-acquisition, operating in the Labview 6.0 environment (HSD drivers, Avantes), can be externally triggered in combination with the shutters in the light path, which were driven by TTL pulses of DAC's of a CED 1401 interface under control of Signal2 software (Cambridge Electronic Design). Time series of spectra were recorded with a minimum integration time of 10 ms for a single spectrum. The spectra were analyzed off-line in MATLAB5.3.
Single facet reflection spectra were measured with the SD2000 spectrophotometer connected to a conventional epi-illumination microscope (Leitz Ortholux) equipped with a 4x, 0.1 objective and a 100 W xenon arc lamp (Spindler and Hoyer); see also Qiu et al. (2002). The microscope was focused at the level of the cornea, and a circular diaphragm, selecting the reflection from a single facet lens, was positioned at the microscope's image plane.

2.3. Experimental protocol: 3 variations on a photochemical theme

Based on the present knowledge, that (1) intense illumination rapidly creates a photo-steady state, with a rhodopsin-metarhodopsin ratio depending on the spectral content of the illumination (see Methods), (2) metarhodopsin is rather rapidly degraded, in a time course of several minutes at room temperature (Bernard, 1983), and (3) rhodopsin is more slowly reconstituted, i.e. within a few hours (Bernard, 1983), we have applied 3 photochemical protocols to investigate photochemical equilibria, metarhodopsin bleaching, and visual pigment regeneration, respectively.

1. We can change the rhodopsin-metarhodopsin photo-equilibrium by selective illumination. When studying the green rhodopsin we used unfiltered broad-band white light from the halogen lamp. In the case of the UV opsin, we either adapted with red light, by spectrally filtering the mercury lamp with a long pass (LP) filter, OG570, (which has a high transmittance above 570 nm), or the eye was illuminated with monochromatic light in the spectral range 364 nm to 390 nm for a period, sufficient to reach the photosteady state.

2. Intense, long-wavelength light results in a virtually total conversion of the green rhodopsin in its blue-absorbing metarhodopsin state. Because metarhodopsin is degraded, continuous red light therefore should result in a steady, gradual depletion of the green visual pigment. However, continuous light causes closure of the pupil, i.e. the accumulation of pupillary granules near the rhabdom, which not only strongly reduces the converting-light flux, but also obstructs measurement of the state of the visual pigment composition. To circumvent the pupil mechanism, an intense red light flash of 2 s, sufficient to create a photo-steady state, was applied every 5 min during a total period of well over 3.5 hour, and a test beam was applied shortly before the red flash to measure the reflection.

3. While metarhodopsin is selectively degraded rather fast, rhodopsin is regenerated more slowly. To probe this process we used a weak test light (grey filter of density 0.9) from the halogen lamp (Fig. 4.2) lasting 70 ms. Although with an integration time of 10 ms this yields 7 spectra, due to the long rise time and slow closure of the shutter, effectively no more than 4 spectra were usable for averaging. Alternatively, we probed rhodopsin regeneration with a weaker test light (grey filter density 2.5); recording in that case 6 spectra with an integration time of 50 ms.

2.4. Spectrophotometric analysis.

Spectra were analyzed off-line on a Pentium PC. The standard analysis comprises five steps. First, spectral data from the spectrophotometer were stored on the PC as raw reflection spectra. Second, overlapping reflection spectra were averaged and/or smoothed with a Savitzky-Golay polynomial smoothing filter with polynomial order 2 and frame size less than 25 nm (75 data points). Third, the recorded spectral data were converted into relative reflectance spectra by dividing the spectra with a spectrum measured from a white reference reflector (MgO). We normalized the spectra by dividing the relative reflectance spectra by the value of maximal (relative) reflectance. The absolute amplitude of the reflectance was not determined, because the reference is a strong light diffuser and the angular dependence of the diffusion was not

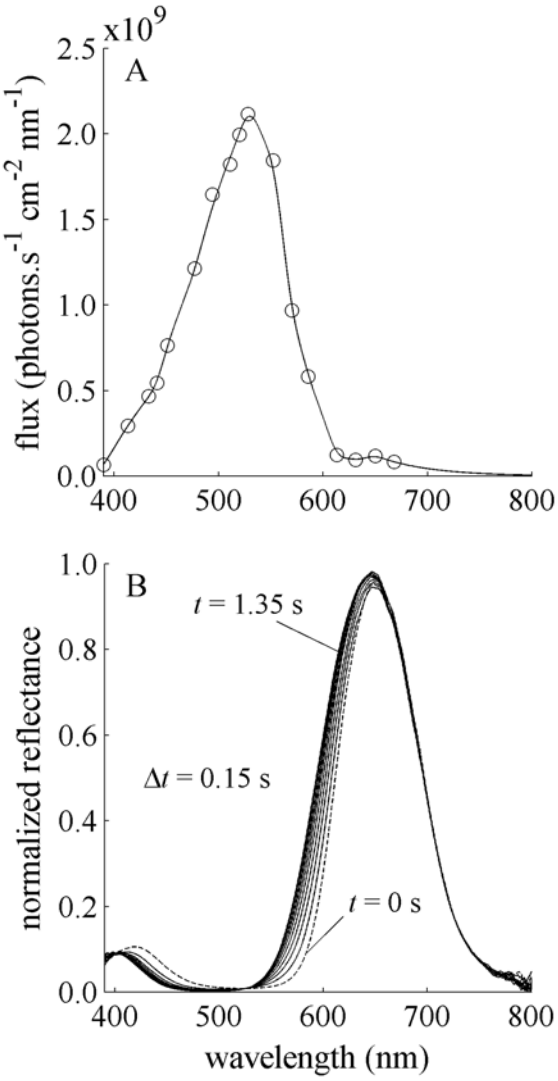

Fig. 4.3: A. Irradiance of the halogen lamp at the DPP. The irradiance (number of photons/s cm^2 nm) was derived from photometer readings at 17 monochromatic interference filters within the spectral range 390 to 668 nm. **B.** During 2 seconds white light illumination, reflection spectra were recorded with an integration time of 10 ms. Here 10 reflectance spectra, normalized to the peak value of the last spectrum, are plotted with a time interval of 0.15 s, including the first spectrum after dark regeneration (dashed line). Spectra are averages over 30 ms, i.e. of 3 successive spectra, except for the first spectrum, which was the average over the first 20 ms.

calibrated. Fourth, difference spectra were calculated as the decadic logarithm of a certain selected spectrum, taken at a fixed time-point, divided by reflectance spectra, taken at specified time-intervals. Usually, the reference spectrum was that obtained after dark regeneration, where one may assume to have a condition with 100% rhodopsin. Fifth, the time course of the absorbance changes was calculated. Mean values of the normalized spectra then indicated the relative fractional concentration change in time (see Chapter 3).

3. Results

3.1. Photochemical conversion of the green rhodopsin.

A comma, *Polygonia c-album*, was dark adapted for a prolonged time, and then reflection spectra were recorded during 2 seconds white light illumination, using an integration time of 10 ms (Fig. 4.3B). The illumination causes a reflection increase in the long-wavelength region, above 525 nm, and a reflection decrease below that wavelength. The light-induced changes are more clearly seen in the logarithm of the reflection spectra (Fig. 4.4A). Fig. 4.4B shows the absorbance difference spectra, where the first spectrum after dark regeneration (dashed in Fig. 4.4A) was taken as a reference. The spectral changes accompanying the conversion can be readily interpreted by assuming that the visual pigment, from the initial 100% rhodopsin fraction, is partly shifted to a photo-equilibrium where a considerable fraction of the visual pigment is in the metarhodopsin state. The rhodopsin and metarhodopsin absorb predominantly in the green and blue, respectively, resulting in a light-induced absorption decrease at wavelengths above 525 nm, i.e., the isosbestic point, and an absorption increase between 400 and 525 nm. The time course of the conversion is well approximated by a first order exponential with a time constant of 413 ms and 507 ms depending on the spectral interval of averaging, respectively 440-500 nm and 540-600 nm (Fig. 4.5). The average time constant is 460 ms.

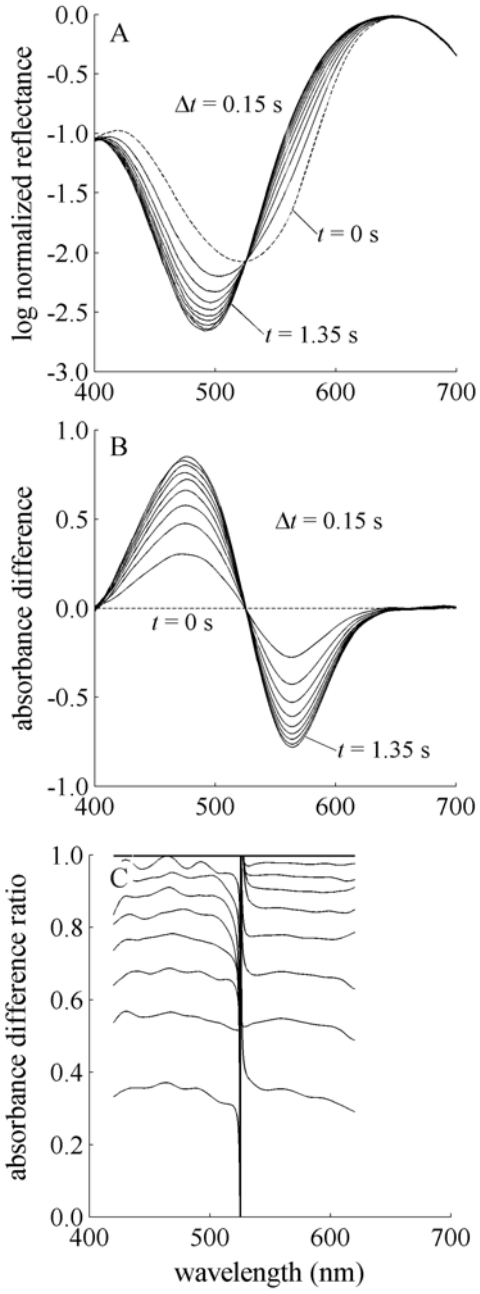

Fig. 4.4: A. The logarithm of the reflectance spectra of Fig. 4.3B show the direction of the reflection changes in time when metarhodopsin is created. **B.** Difference spectra in time with the first dark spectrum used as a reference (dashed line, t = 0 s). During white illumination, green visual pigment, initially 100% rhodopsin, is partly converted to metarhodopsin. Therefore the absorption increases between 400 and 525 nm, the isosbestic point. **C.** Absorbance difference ratio of the spectra given in **B** divided by the last spectrum (t = 1.35 s). The spectra become noisy below 420 nm and above 620 nm due to the small absorbance differences and therefore were omitted from Fig. 4.4C.

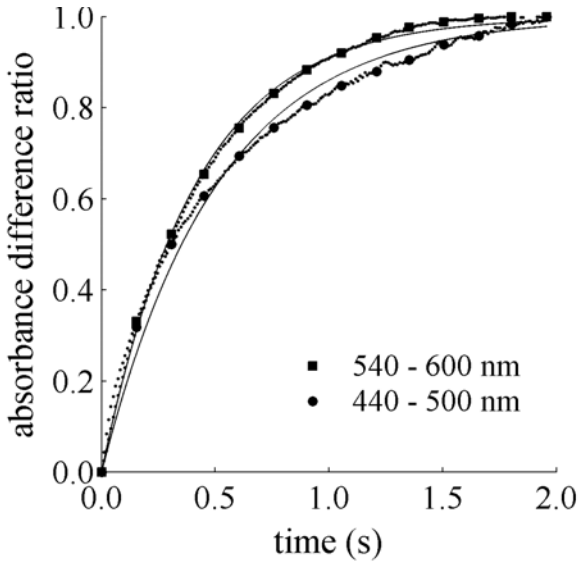

Fig. 4.5: Conversion of 100% rhodopsin (R) to a new equilibrium fraction of metarhodopsin (M). In an infinitesimal layer with bidirectional R-M conversion, the absorbance difference is proportional to the fraction of metarhodopsin created over time (see Chapter 3, Eq. 19). The proportionality constant, the mean of the absorbance difference ratio (see Fig. 4.4C), is plotted for every difference spectrum (dots, Δt = 10 ms) over the spectral interval 440-500 nm (●, Δt = 150ms) and 540-600 nm (■, Δt = 150ms) i.e. below and above the isobestic wavelength, 525 nm. The conversion can be approximated with a first order exponential time course with a time constant of 413 (●) and 507 ms (■), respectively.

3.2. Bleaching green metarhodopsin

Following the adaptation to bright white light (Figs. 4.3B, 4.4), the green visual pigment was depleted from the rhabdom. We used a bleaching protocol slightly modified from that described by Bernard (1983). During a total period of 215 min, we applied each 5 min a 2 s red flash. Before applying the red flash the reflection was measured with a short test light pulse (see Materials and methods, section 2.3, protocol 3). Absorbance difference spectra were calculated by using the spectrum resulting after the 215 min measurement period as the reference spectrum (Fig. 4.6A). The spectra reveal that the red flashes converted the green-absorbing rhodopsin into the blue-absorbing metarhodopsin, which then gradually vanished. The metarhodopsin absorbs maximally at 492 ± 1 nm (Fig. 4.6A). When we neglect an initial period of 15 min after the first red light pulse, the time course of the bleaching process can be well approximated by an exponential function with a time constant of 56 min (Fig. 4.6B). The deviation of the initial part indicates a very rapid reconstitution of rhodopsin during the first 15 min. Reconstitution clearly cannot keep up with degeneration, as the metarhodopsin degenerates at a more rapid pace. However the bleaching was not complete, as the reflection still increased very slowly after the 3.5 hour measurement period.

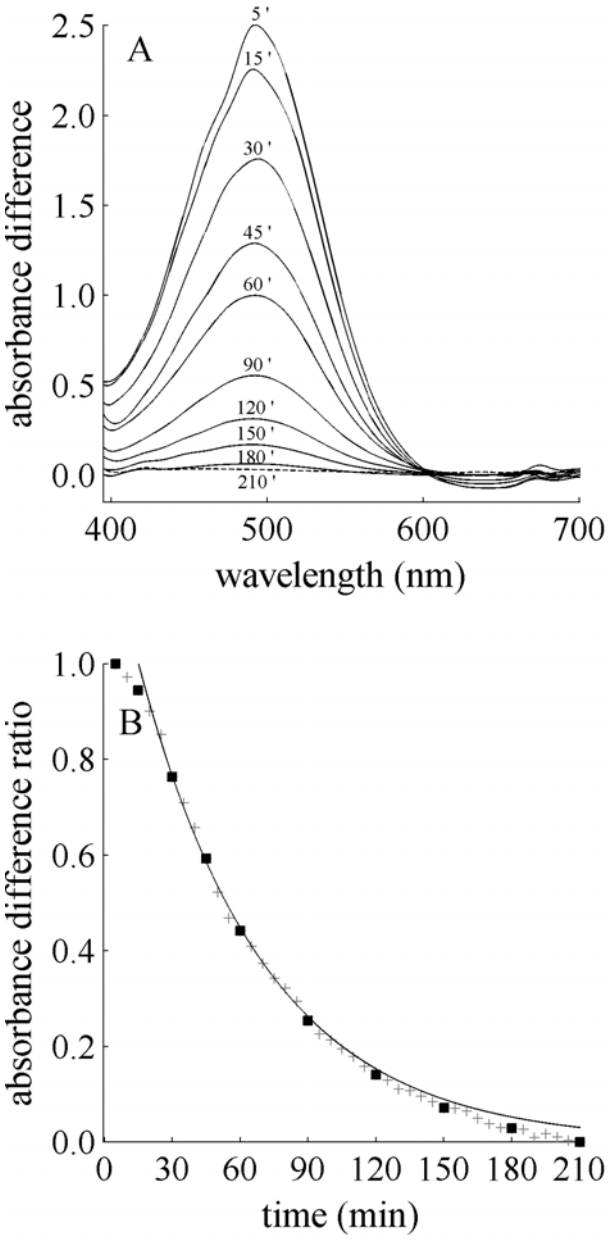

Fig. 4.6: Bleaching green visual pigment. The bleaching protocol was started after the eye was regenerated in the dark overnight. After the eye was white-light adapted, causing partial conversion of the green rhodopsin to metarhodopin (cf. Fig. 4.3-4), each 5 min during 210 min a 2 s red adapting flash light was delivered **A.** Difference spectra calculated from the reflectance spectra. The reflectance spectrum measured after 210 minutes 'bleaching' (dashed line) is taken as the reference spectrum, because of the higher signal to noise ratio, and therefore higher accuracy. The difference spectra show intrinsic bleaching of the green rhodopsin's photoproduct, metarhodopsin, which absorbs maximally at 492 ± 1 nm. Time labels are placed at the peak values. **B.** The time course of bleaching is approximated by calculating the absorbance difference ratio, dividing every difference spectrum over the whole spectral range by the difference spectrum taken 5 min after the first red flash. At times indicated in **B** the mean of the absorbance difference ratio over the spectral interval 440-500 nm is plotted (■) together with intermediate time points (+, Δt = 5 min). The time course of the bleaching protocol can be approximated with a first order exponential, with a time constant of 56 min. Only recordings 15 min after the first red light pulse, were incorporated in the exponential fit.

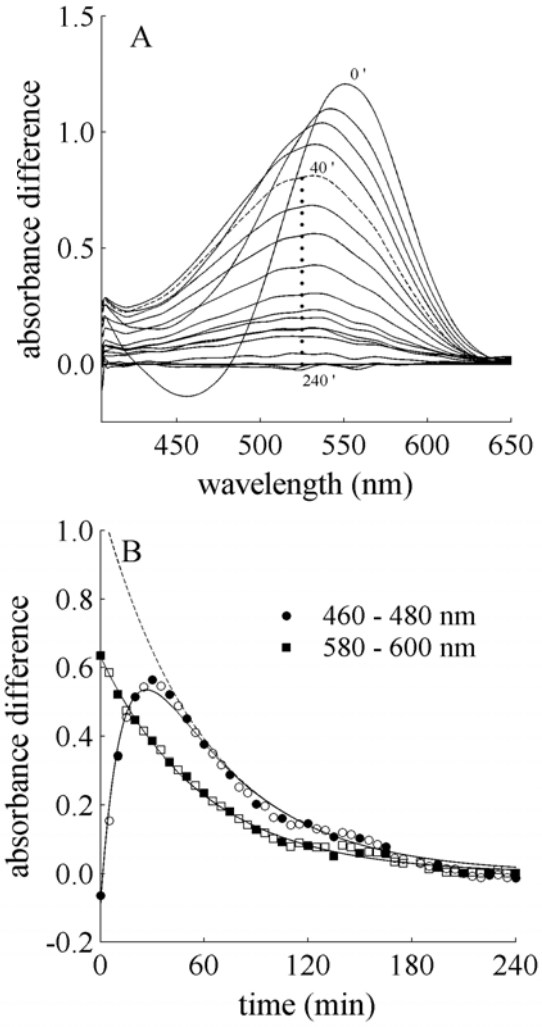

Fig. 4.7: Kinetics of dark regeneration of green visual pigment. After white conversion metarhodopsin is degraded. Every 5 min a spectrum was recorded.
A. Difference spectra with the last dark-adapted spectrum (t = 240 min) as a reference. Here we show 19 spectra, the first hour every 10 min; after 1 hour regeneration in the dark only every 15 min a spectrum is plotted. The peaks of the difference spectra dominated by the regeneration process are centered around 532 ± 2 nm (dotted line). **B**. The time course of regeneration and degradation is approximated by calculating the absorbance difference from corresponding spectra shown in **A**, as the mean of the absorbance difference over the spectral interval 580-600 nm (■), together with intermediate time points (□, Δt = 5 min). From this data the time course of regeneration is approximated with a single exponential function with a time constant of 59 min (solid line fit). The absorbance difference over the spectral interval 460-480 nm for spectra shown in A(●) and the intermediate spectra (○, Δt = 5 min) is approximated with two exponential functions, one for regeneration (time constant of 59 min, dashed line) and one for degradation (time constant of 15 min; see the Appendix).

3.3. Regeneration of the green rhodopsin

In the dark, metarhodopsin is degraded and rhodopsin is reconstituted. From the measurements of the previous sections the visual pigment absorbance spectra and the kinetics of regeneration and degradation cannot be derived straightforwardly (cf. discussion). We therefore studied these processes, especially rhodopsin regeneration, after adapting the eye with bright white light (section 3.1) and after bleaching with red light (section 3.2). After adapting the eye with white light (Fig. 4.3A), the eye shine was probed during 4 hours, by taking every 5 minutes a reflection spectrum. Absorbance difference spectra were calculated from the measured reflection spectra, with the spectrum measured after 240 min in the dark as the reference spectrum (Fig. 4.7A). The difference spectra can then be used to derive the relative fraction of rhodopsin built in. From the absorbance difference ratio we approximated degradation and regeneration with first order exponentials (see Appendix). The time constant of degradation is 15 min. Regeneration has a time constant of 59 min (Fig. 4.7B).

3.4. Photochemical conversion of a UV rhodopsin

After bleaching the green visual pigment (black lines) we investigated whether a blue and/or a UV visual pigment was present. We therefore illuminated the eye with various monochromatic lights in the blue to green wavelength range, but we could not find convincing proof for a photoconvertible blue visual pigment. Subsequently, we applied intense monochromatic 364 nm light for 5 seconds. Because this strongly activated the pupil, we allowed for a three minutes dark-adaptation period, and then recorded reflection spectra during 2 s (integration time 10 ms). The spectra are corrected for the pupil, which is triggered immediately, i.e. pupillary granules migrate to the rhabdom and effectively absorb the boundary waves. White illumination after actinic red light (LP570) does not alter the photochemistry of the UV pigment, and the pupil contribution can be directly measured from these series. After pupil correction, the initial spectra show a distinctly decreased reflection in the blue, between 400 and 500 nm. Illumination with the white test light results in a reflection increase. The 364 nm light apparently had created a blue-absorbing metarhodopsin, which the test light reconverted back into its UV-absorbing rhodopsin (Fig. 4.8A). The reflection spectra measured during the latter conversion process yielded the difference spectra of Fig. 4.8B; the first spectrum was the reference.

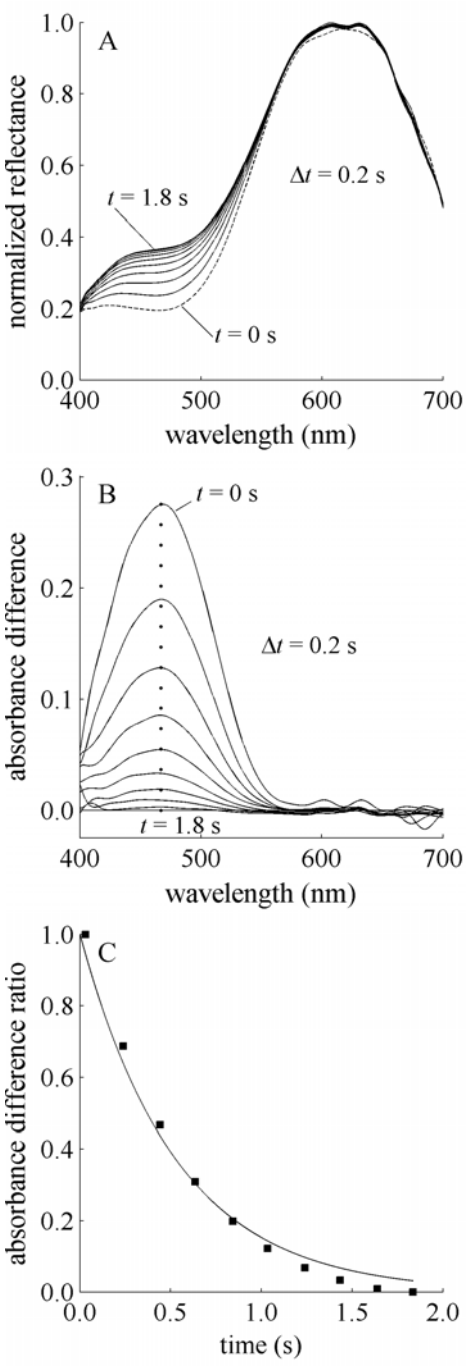

Fig. 4.8: Photochemical conversion of UV metarhodopsin after bleaching the green visual pigment. **A.** The eye is adapted to monochromatic 364 nm flashes. After a dark period of 3 min, necessary for pupil withdrawal, the eye was illuminated for 2 s with white light illumination. Reflection spectra were recorded with an integration time of 10 ms. Here 10 reflectance spectra, normalized to the peak value of the last spectrum, are plotted with a time interval of 200 ms, including the first spectrum after dark regeneration. The white light illumination converts the metarhodopsin form to rhodopsin. Therefore the reflection increases between 400 and 500nm. **B.** The corresponding difference spectra in time where calculated with the final spectrum (t = 1.8 s) as a reference. One clearly sees absorption decreases due to UV metarhodopsin conversion. The difference spectra are nearly proportional, peaking at 467 ± 2 nm (dotted line). **C.** The time course of metarhodopsin conversion is approximated by calculating the absorbance difference ratio, dividing every difference spectrum over the whole spectral range by the first spectrum (t = 0 s, peak absorbance difference 0.27). The mean absorbance difference ratio is calculated from corresponding spectra shown in **B**, as the mean of the absorbance difference ratio over the spectral interval 440-500 nm. The time course is approximated with a first order exponential with a time constant of 499 s.

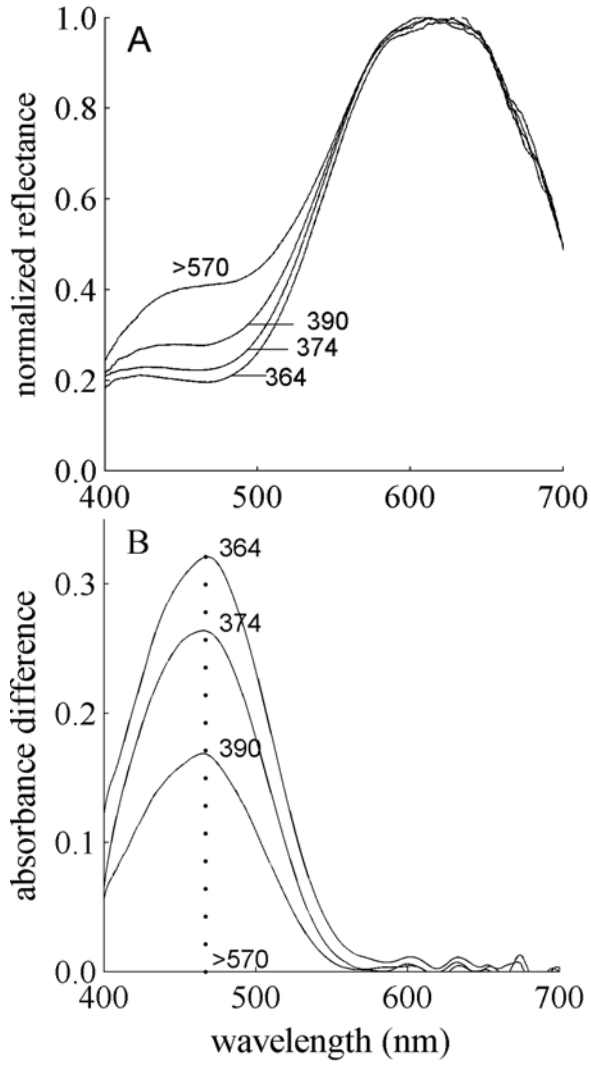

Fig. 4.9: Dark spectra after UV adaptation. **A.** First spectra after 3 minutes dark adaptation following 3 UV actinic monochromatic light flashes, i.e. at 364 nm, 374 nm and 390 nm. The spectra are compared with the spectrum after bleaching with a long pass 570 nm filter (>570). **B.** The corresponding difference spectra are shown. The bleached spectrum after red adaptation is taken as a reference. The peak of the UV difference spectra is 467 ± 2 nm.

Clearly, the reflectance increase, i.e. absorption decrease, in the blue results from conversion of a blue-absorbing metarhodopsin, with wavelength peak at 467 ± 2 nm. Actinic illuminations with monochromatic light flashes with wavelengths 374 nm and 390 nm, respectively, yielded reflection changes similar to that induced by 364 nm light (Fig. 4.9A). The amplitudes of the difference spectra were progressively smaller, however, in accord with conversions of a UV-absorbing metarhodopsin (Fig. 4.9B).

4. Discussion

4.1. White light-induced conversion of a green-absorbing rhodopsin

The classical method of studying visual pigments is via extraction of the visual pigment(s) from the retinal tissue. This approach has been successfully used in the case of moth eyes (Schwemer and Paulsen, 1973). Microspectrophotometry of eye cup preparations provided the possibility to study small samples in situ (Schwemer, 1984). Microspectrophotometry of visual pigments in the eyes of completely intact, living animals is possible in butterflies due to the unique presence of tapeta proximally of the rhabdoms (Stavenga, 1975; Bernard, 1979a,b, 1982). Difference spectra derived from reflection spectra measured *in vivo* then allow the estimation of the spectral characteristics of the rhodopsin and metarhodopsin state.

Here we performed spectrophotometric recordings in a novel telemicroscopic set-up (Stavenga, 2002b). Due to the improved temporal resolution we were able to follow in real time the rhodopsin-metarhodopsin conversions induced by broad-band white light, especially the conversion of the predominant green rhodopsin after a prolonged regeneration time in the dark (Fig. 4.3).

4.2. Regeneration and degradation of the green visual pigment

The regeneration experiments in the comma, *Polygonia c-album,* show that the majority of the visual pigment in the rhabdoms, i.e., ca 75%, is a green-absorbing rhodopsin. It thus confirms the expression pattern of the green pigments, identified in species with a more simple three pigment sytem, e.g. 72% in *Vanessa cardui* (Briscoe et al., 2003) and 71.4% in *Manduca sexta* (White et al., 2003). The kinetics of the regeneration process also corroborates the general picture, as outlined by Bernard (1983). The fast metarhodopsin degradation with a time constant of k_d = 15 min at ca 21 ^oC is comparable to a metarhodopsin decay with k_d = 18 min measured by Bernard (1983) at 23 ^oC in

Vanessa cardui. Like reported by Bernard (1983), rhodopsin regeneration is much slower, with a time constant of k_r = 60 min. Compared to the fly, the kinetics is fast, as there k_d = 3.3 h and k_r = 200 h (Schwemer, 1984).

The molecular mechanism behind the selective metarhodopsin degradation remains to be elucidated. Cytosolic protein degradation is known to occur in lysosomes or in proteolytic complexes called proteasomes after covalent attachment of a chain of ubiquitins on the target proteins. Degradation of metarhodopsin -a membrane protein- may occur by recognition of a specific exposed amino-acid sequence by specialized proteins which may trigger endocytosis and subsequent lysosomal degradation. Arrestins are good candidates, as they specifically bind phosphorylated metarhodopsin. Arrestins can also participate in signalling to downstream effectors (Lefkowitz et al., 1998). A sub-class of arrestins, has been shown to be involved in receptor-mediated endocytosis because of their ability to act as adaptors to facilitate clathrin-mediated endocytosis (Goodman et al., 1996).

The molecular pathways for regeneration in butterflies and their relative importance are unknown. Photoregeneration by conversion of metarhodopsin is favoured by its higher absorption coefficient and the abundance of blue light from the sky. Rhodopsin renewal must also occur to catch up with metarhodopsin degradation. The mechanism likely resembles the regulation in flies. Studies on blowflies have established an important role for the chromophore 11-cis retinol, which activates opsin biosynthesis (Schwemer, 1984). As the chromophore is recycled after degradation, isomerization of the all-trans retinal to the cis-state by a (photo-)isomerase and subsequent redirection of the chromophore to the photoreceptor cells may constitute a positive feed-back mechanism (Chapter 1, Fig. 1.4). In flies, blue light is necessary to activate the photo-isomerase in the primary pigment cells. In butterflies the precise action remains to be elucidated. Likely transport of newly synthesized opsins may occur with motor proteins like Kinesin II or Myosin VIIa, carrying their opsin cargo along the microtubuli and actin filaments with a speed of ~0.2 μm/s (Williams, 2002). The close spatial interaction with the endoplasmatic reticular system at the base of the microvilli may allow fast recovery. Constitutive membrane turn-over provides an additional pathway for pigment renewal.

4.3. Bleaching green visual pigment

In his bleaching protocol for green visual pigments, Bernard (1979a, 1983) used a red flash or a series of red flashes, followed by long dark periods (60 to 90 minutes) where a few sample spectra were taken. In our experiments the

prolonged dark periods lead to substantial incorporation of new rhodopsin, however. In the experiments with the repeated red flashes, any newly created rhodopsin was promptly converted to the metarhodopsin form, which then degraded in the dark, yielding a better spectral separation of the metarhodopsin. The λ_{max} values estimated in the bleaching and regeneration experiments, respectively 492 nm for M and 532 nm for R, are similar to the values of the green pigment of the related nymphalid *Vanessa cardui* (Briscoe et al., 2003).

4.4. Derivation of the UV and blue visual pigments

After bleaching the green visual pigment, we were able to isolate a UV-absorbing pigment. In our set-up, substantial conversion of the UV metarhodopsin, peaking at ca 367 nm, required illumination periods of several seconds because activation of the pupil effectively diminished the photochemical conversion. The optical density of the UV-pigment (see Fig. 4.9B) matches known expression levels in the literature. In *Vanessa cardui* the UV pigment makes up 15% of the total visual pigment content (Briscoe et al., 2003). Histological studies of the UV-opsin in the moth retina of *Manduca sexta* (White et al., 2003) yield similar values (14.3%).

In the latter studies one found that the blue pigment is also scarcely expressed, e.g. *Vanessa cardui* (12%) and the moth *Manduca sexta* (14.3%). In our experiments we could not see clear photochemical conversion in the blue, even after bleaching green visual pigment (see Fig. 4.8). However, the analysis of the difference spectra, demonstrating predominant conversion of green rhodopsin during white light illumination (see Fig. 4.3-6) shows slight anomalous phenomena around the isosbestic point in the normalized difference spectra (data not shown). In the previous chapter we showed that a three pigment model, including a blue rhodopsin, could account for this phenomenon, suggesting the presence of blue rhodopsins in *Polygonia*. Also in a related *Polygonia* species blue spectral receptors were found (Kinoshita, 1997). The peaks of the blue rhodopsin/metarhodopsin are probably very close. In the moth *Deilephila elpenor* the absorbance peak of rhodopsin and metarhodopsin were estimated P440 and M490 respectively (Schwemer and Paulsen, 1973). Therefore, due to the small expression levels of blue visual pigment, and the fast regeneration of green visual pigments, the blue pigment escaped isolation in the photochemical experiments.

Appendix: Derivation of time-constant of rhodopsin regeneration and metarhodopsin degeneration

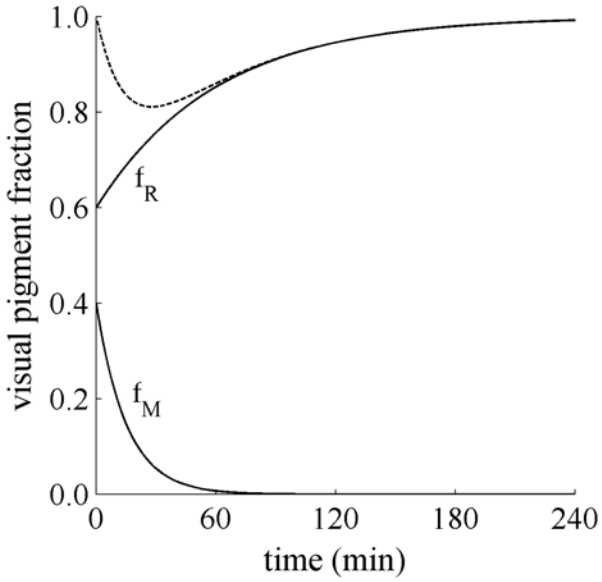

Fig. 4.10: Fractional rhodopsin and metarhodopsin concentrations during dark regeneration and degradation. Here the two processes are described by exponential functions with time constants of 60 and 15 min, respectively. The summed fractional concentration is not constant (dashed line).

The steady state absorbance after *t* min dark regeneration is (Eq. 14):

$$A(t) = 0.87\kappa(t)L - \log M \tag{20}$$

with $\kappa(t) = \alpha_R C_R(t) + \alpha_M C_M(t)$.
The difference spectra at times *t* with respect to time *T* are given by

$$\Delta A(t) = A(T) - A(t) = 0.87\big(\kappa(T) - \kappa(t)\big)L \tag{21}$$

Assuming dark regeneration is complete at time *T*, i.e., $f_R(T) = 1$ and $\kappa(T) = \alpha_R C_R(T) = \alpha_R C_0$ then

$$\Delta A(t) = 0.87 C_0 L\left[\alpha_{\mathrm{R}}\left(1 - f_R(t)\right) - \alpha_{\mathrm{M}} f_{\mathrm{M}}(t)\right] \tag{22}$$

with $f_{\mathrm{R}}(t) = \dfrac{C_{\mathrm{R}}(t)}{C_0}$ and $f_{\mathrm{M}}(t) = \dfrac{C_{\mathrm{M}}(t)}{C_0}$.

The processes of rhodopsin regeneration and metarhodopsin degradation can be described by first order exponentials, with time constants τ_{r} and τ_{d} (Fig. 1):

$$f_{\mathrm{R}}(t) = 1 - (1 - f_{\mathrm{R},0})\mathrm{e}^{-\frac{t}{\tau_{\mathrm{r}}}} = 1 - f_{\mathrm{M},0}\mathrm{e}^{-\frac{t}{\tau_{\mathrm{r}}}} \tag{23}$$

$$f_{\mathrm{M}}(t) = f_{\mathrm{M},0}\mathrm{e}^{-\frac{t}{\tau_{\mathrm{d}}}} \tag{24}$$

The total concentration of visual pigment, the sum of the fractional concentrations f_{R} and f_{M} (dashed line, Fig. 4.10) times C_0, is not constant because of the difference in the time constants. The time course of the difference spectra is finally described by:

$$\Delta A(t) = 0.87 C_0 L f_{\mathrm{M},0}\left\{\alpha_{\mathrm{R}} e^{-\frac{t}{\tau_{\mathrm{r}}}} - \alpha_{\mathrm{M}} e^{-\frac{t}{\tau_{\mathrm{d}}}}\right\} \tag{25}$$

Chapter 5

Analyzing the reflections from single ommatidia in the butterfly compound eye with Voronoi diagrams[†]

1. Introduction 64
2. Materials and Methods..... 65
2.1. Recording single facet reflections with a digital camera 65
2.2. Transforming single facet centers into Voronoi diagrams 66
3. Results..... 68
3.1. Bleaching green visual pigment in a homogeneous eye..... 68
3.2. Pupil activation in a heterogeneous eye 71
4. Discussion 72
4.1. A new method to quantify single facet reflections..... 72
4.2. Simultaneous analysis of individual ommatidia..... 73
4.3. Perspectives..... 74

[†] A modified version of this chapter is submitted to the Journal of Neuroscience Methods

1. Introduction

Observing butterfly eyes with an epi-illumination microscope reveals an often spectacular eye shine, which is due to the reflection of incident light on a multilayer tapetum, created in each ommatidium by tracheoles proximal of the light-guiding rhabdom (Miller and Bernard, 1968). The eye shine phenomenon is highly useful for non-invasive, optical investigations of retinal processes, e.g. the photochemistry of visual pigments (Stavenga, 1975, 1979; Bernard, 1979a,b; Bernard and Remington, 1991; Chapter 4) and the light-dependence and dynamics of the pupil mechanism (Stavenga et al., 1977; Järemo Jonson et al., 1998). The eye shine is especially bright when observed with the microscope focused at the level of the center of curvature of the eye, because of the approximately spherical shape of compound eyes and the appearance there of the so-called deep pseudopupil (Franceschini and Kirschfeld, 1971). The deep pseudopupil is the superimposed image of numerous rhabdoms projected by the corresponding dioptrical systems, and therefore measurements on the deep pseudopupil have an optimal signal to noise ratio. However, because of the superposition, the obtained signal is an average of several ommatidia. Recent research has demonstrated that the ommatidia of butterfly eyes can be highly heterogeneous (Arikawa and Stavenga, 1997; Stavenga, 2002a, 2002b), and this heterogeneity is obscured in deep pseudopupil measurements.

This chapter presents a novel approach to simultaneously study dynamical processes in individual ommatidia of the butterfly eyes. A key element in the presented method is the Voronoi diagram. This mathematical tool defines cells, each of which is an assembly of points closest to a certain lattice point. A Voronoi cell is equivalent to the Wigner-Seitz primitive cell in crystallography, which is easily recognized in the cross-section of a compound eye's facet lens (Stavenga, 1979). Eye shine images obtained at the level of the corneal facet lenses therefore can be analyzed straightforwardly with Voronoi diagrams. To discriminate the individual facets, a morphological image processing (M.I.P.) algorithm is used (Michielsen and De Raedt, 2001). The coordinates of the detected facets are then transformed into a Voronoi diagram, yielding the 'natural' hexagonal topology of the original facet lens lattice. The diagram, superimposed on the image of the corneal facets can then be used to derive information of the underlying ommatidia: spatial dimensions of the facet lattice, reflection intensities and spectral information.

We provide two examples. First, we show the effect of bleaching the green visual pigment in the homogeneous eye of the nymphalid *Polygonia c-album* (see also Chapter 4). Second, we study the intensity range of pupil activation in green and red reflecting ommatidia in the heterogeneous eye of the

satyrine butterfly *Pararge aegeria*. These examples demonstrate that the developed technique may be a powerful tool to characterize the heterogeneity of butterfly eyes.

2. Materials and Methods

2.1. Recording single facet reflections with a digital camera

In our first case study we have studied the ommatidial reflection after bleaching. The green rhodopsins of butterflies have a peak-absorption typically around 530 nm. Upon photon absorption, the rhodopsin converts into a blue-absorbing metarhodopsin, which is rapidly degraded, resulting in a decreasing absorption called bleaching. Bleaching can be achieved *in vivo* with a protocol based on repetitive red light flashes (Bernard, 1979a). Recently, we investigated the photochemistry in the eye of a nymphalid butterfly, *Polygonia c-album* (Chapter 4). To demonstrate the possibility of selective bleaching, and to investigate the ommatidial homogeneity we applied the bleaching protocol to a confined eye region, by illuminating the butterfly eye with intense light provided by a Xenon 150 W lamp of a microspectrophotometric set-up (see Chapter 6), via a microscope objective with a small numerical aperture (4x, NA 0.1, Spindler and Hoyer). Because of the limited field of view of the ommatidia, bleaching of the green visual pigment occurred only locally, i.e., in those ommatidia which had their visual field within the aperture of the illuminating objective. After bleaching we immediately transferred the animal to a set-up (described in Chapter 4), which is equipped with a digital camera (Kodak, DC120) and an objective with a large numerical aperture (10x, NA 0.3, Zeiss). The digital camera was focused on the eye's corneal facet lenses. A halogen lamp served as the light source. The picture was converted in Paint Shop Pro 6 from the standard Kodak format to compressed JPG format with a resolution of 640x480 pixels. The image was further cropped to the region of interest for further processing (section 2.2).

In addition to visual pigment bleaching in the homogeneous eye of *Polygonia c-album*, pupil activation in the satyrine *Pararge aegeria* was analyzed, and specifically in the ventral eye region where the ommatidia are heterogeneous. Two classes of ommatidia, reflecting in the green and red, respectively, stand out (Stavenga, 2002a; Chapter 6). Illumination of a dark adapted butterfly eye with a bright light source activates the pupil mechanism, i.e. the assembly of pigment granules in the photoreceptors. The granules are driven towards the rhabdom and there reduce the light flux by absorbing light from the boundary wave. The applied procedure was as follows. Immediately

after prolonged illumination with monochromatic light (494 nm), the corneal eye shine caused by the halogen lamp was photographed with the digital camera. The halogen illumination was always the same, but the intensity of the monochromatic pre-illumination was varied. Five light intensities (1-5, Fig. 5.9) covering the dynamic range of pupil activation, i.e. about 2 log units, were applied.

2.2. Transforming single facet centers into Voronoi diagrams

The images were preprocessed before calculating the reflectance of the individual ommatidia. Standard M.I.P. algorithms were applied to the image as follows. A morphological unit (a so-called star) is manipulated by operators (open, close, dilate, erode) to enclose the desired objects in the image, i.c. the facets. The order and frequency of these operators are first optimized in a dedicated script language (Michielsen and De Raedt, 2001). The processing results in a binary image with white spots representing the original facets (Kuipers et al., 2002). The centers of gravity of the white clusters represent the individual facets.

Visual comparison of the calculated facets with the eye shine image shows that the algorithm is not completely without flaws; facets are sometimes taken together or overlooked. We therefore manually corrected the calculated facet lattice with a custom-made Matlab-interface, by repositioning clearly displaced facets or adding missing points.

In the third phase of the analysis, we constructed a two- dimensional lattice from the assembly of facet lenses along the two major axes, the H^*-axis and V^*-axis (Stavenga, 1979). We therefore first assigned column (i^*) and row (j^*) indices to each facet, starting with an arbitrarily chosen facet in the middle of the image, which is assigned the index pair (0,0); see Fig. 5.1.

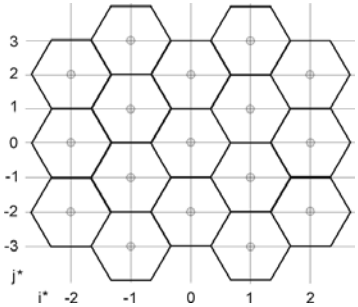

Fig. 5.1: A two-dimensional lattice of facet lenses in the eye of a butterfly, defined by column and row indices *i** and *j**, relative to a central lattice point (0,0), defines a Voronoi diagram, where each cell is the assembly of points closer to a given lattice point than to all other lattice points. The horizontal and vertical axes H* and V* are relative axes, with origin (0,0); see Stavenga (1979).

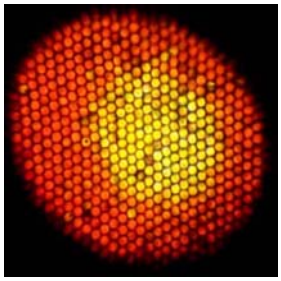

Fig. 5.2: Overview picture of colorful reflections obtained by epi-illumination microscopy on the cornea in the butterfly *Polygonia c-album.* After applying a bleaching protocol, ommatidia reflect yellow due to depletion of green absorbing visual pigment

Next, we fitted second-order polynomial lines to the facets that have the same index values, resulting in horizontal (vertical) lines for facets with the same row (column) index. When the number of fitted points is less than 7, the fit becomes inadequate; we then used a first-order polynomial.
The intersections of the polynomial lines then were taken to indicate the coordinates of the facet lens centers.

Finally, we use the facet lens center coordinates to derive a Voronoi diagram. Given the facet lens centers -the Voronoi vertices- a Matlab routine based on the Delaunay triangulation, is used to derive the Voronoi edges. These line segments define the Voronoi diagram, which appears here as an assembly of connected hexagons. The Voronoi cells –the area bounded by Voronoi edges– are the set of points nearest to the original facet lens centers and are virtually congruent with the facet lens boundaries. The determination of the Voronoi cells, i.e. the individual facets, allows the calculation of the optical characteristics of the facets, e.g. the spatial properties (area, radius), the intensity distribution (average intensities, mode patterns) and the spectral information (color).

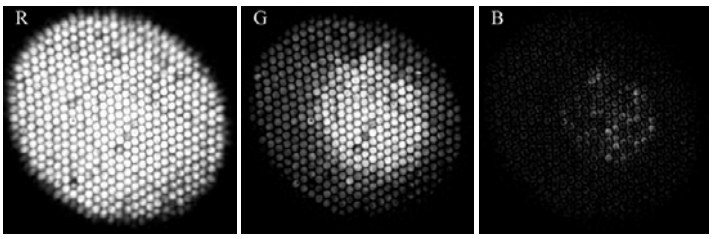

Fig. 5.3: The image is decomposed into RGB pixel intensity values, clearly showing an increased green reflection in the intensely illuminated (bleached) facets.

3. Results

3.1. Bleaching green visual pigment in a homogeneous eye

The eye shine of the comma, *Polygonia*, observed at the level of the corneal facet lenses with a large aperture objective, after it has been intensely illuminated via a small aperture objective, shows bright yellow facets in a central region, surrounded by red facets with lower reflectance (Fig. 5.2). Decomposition of the original digital picture into the RGB pixel intensity values shows that the differences in ommatidial reflectance are very minor in the red (R), quite distinct in the green (G) channel and rather minor in the blue (B), the latter being due to the low blue signal (Fig. 5.3).The green picture was further processed to a binary image with facet center points. Applying the procedure as described in Materials and methods, we used a star of 3 pixels as the basic morphological unit and a threshold intensity value of 180 of the 256 levels (8 bit), yielding 450 facets (Fig. 5.4A).

For clarity, the calculated facet coordinates are plotted as dots on the inverted original image (green pixel intensity). Visual inspection immediately reveals that, although the algorithm performs rather adequately, some incorrect center points appear. We manually corrected these 'failures' with a graphical MATLAB-user-interface (Fig. 5.4B). Subsequently, the corrected center points were used to assign lattice indices to all facet centers. Polynomial lines were fitted in horizontal and vertical directions to yield a retinal lattice (Fig. 5.5).

The intersection points of the polynomial lines define the new facet coordinates. Finally, applying the Voronoi algorithm, line segments surrounding the center points were obtained, yielding hexagons overlapping with the original facet lenses (Fig. 5.6A). The peripheral Voronoi cells are clearly unrealistic, and they were therefore removed, leaving 373 cells for further analysis (Fig. 5.6B). The green reflection value of all points within a cell then was averaged, yielding the average reflection per ommatidium. We choose an intermediate threshold criterion (G = 88) to distinguish between bleached and unbleached ommatidia, overlapping with the yellow and red facets, respectively (Fig. 5.7). The average green reflection values of the unbleached facets are all well below 80, whereas the values of the bleached population exceed the level of 120. The amplitude in both populations, plotted in Fig. 5.8, shows a rather broad distribution, indicating that the ommatidial reflectance is far from constant, neither in the unbleached nor in the bleached state.

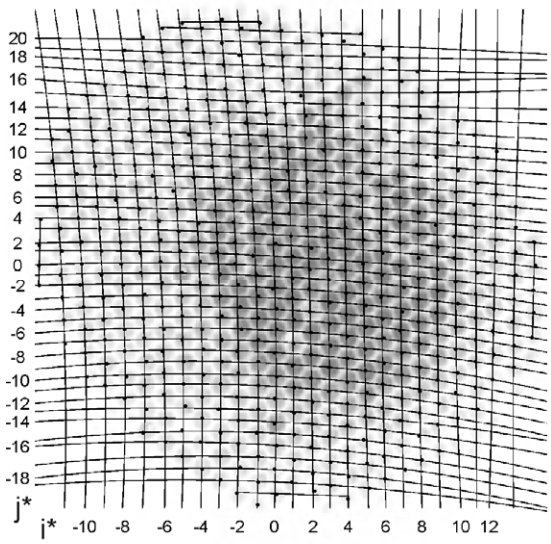

Fig. 5.5: Correction of facet centers on a 2-dimensional lattice. Polynomial lines of the 2nd order are fitted through points with the same vertical or horizontal indices. The intersection of the polynomial lines define the new coordinates.

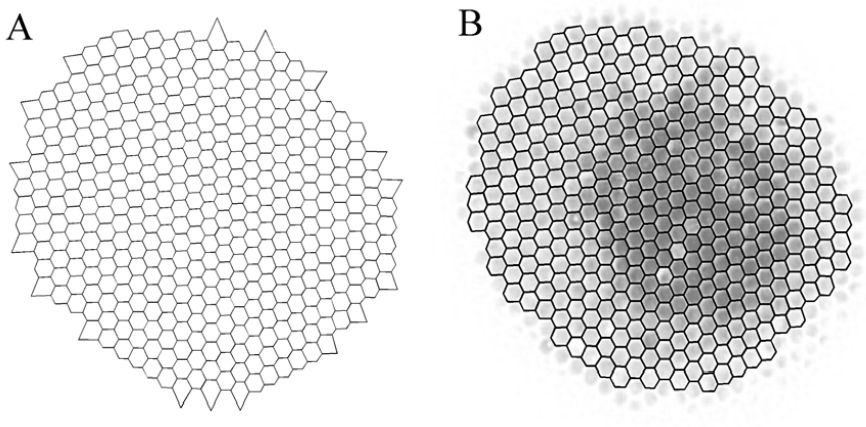

Fig. 5.6: Voronoi cells overlap with corneal facets. **A**.Voronoi line diagram based on 450 visually inspected and corrected facet center coordinates. **B**. Selection of 373 hexagonal patches to quantify single facet reflections.

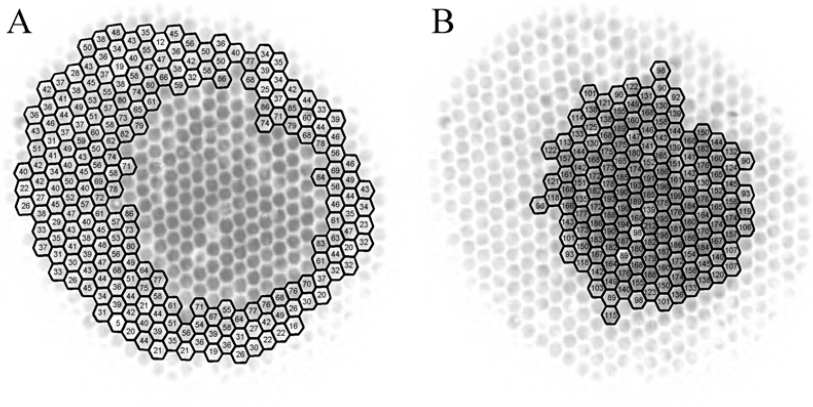

Fig. 5.7: To distinguish between bleached and unbleached ommatidia the mean green intensity value, averaged over a single facet surface area, is calculated, and an appropriate threshold criterion was choosen (G = 88). The individual values are shown in the center of the individual facets. **A.** Most unbleached facets have intensity values well below level 80. **B.** Nearly all bleached facets coincide with green intensity values >120 (see also Fig. 5.8).

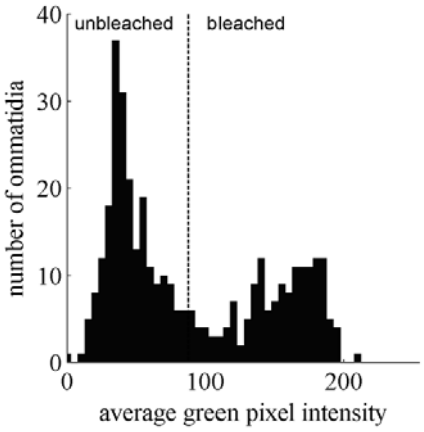

Fig. 5.8: Histogram intensity distribution of bleached and unbleached single facet reflections. Average values for the green pixel intensity are plotted. We chose a threshold criterion (G = 88, dashed line) to distinguish between bleached and unbleached ommatidia. The mean averaged green pixel intensity is resp. 53 and 163 for unbleached vs bleached facets (Table 5.1).

All facets (n = 373)	R	G	B	Σ (RGB)/3
Unbleached (n = 215)	189 ± 19	53 ± 17	8 ± 2	82 ± 11
Bleached (n = 158)	206 ± 12	163 ± 30	21 ± 12	131 ± 12

Table 5.1: The mean reflection value ± std of the pixel intensities (RGB) averaged over a single facet area.

3.2. Pupil activation in a heterogeneous eye

We have applied the Voronoi tool to study the pupil working range in the satyrine butterfly *Pararge aegeria.* We investigated pupil activation in individual ommatidia by quantifying the reflection at the corneal level, with the question whether there is a difference in the pupil activation range between red and green reflecting ommatidia.

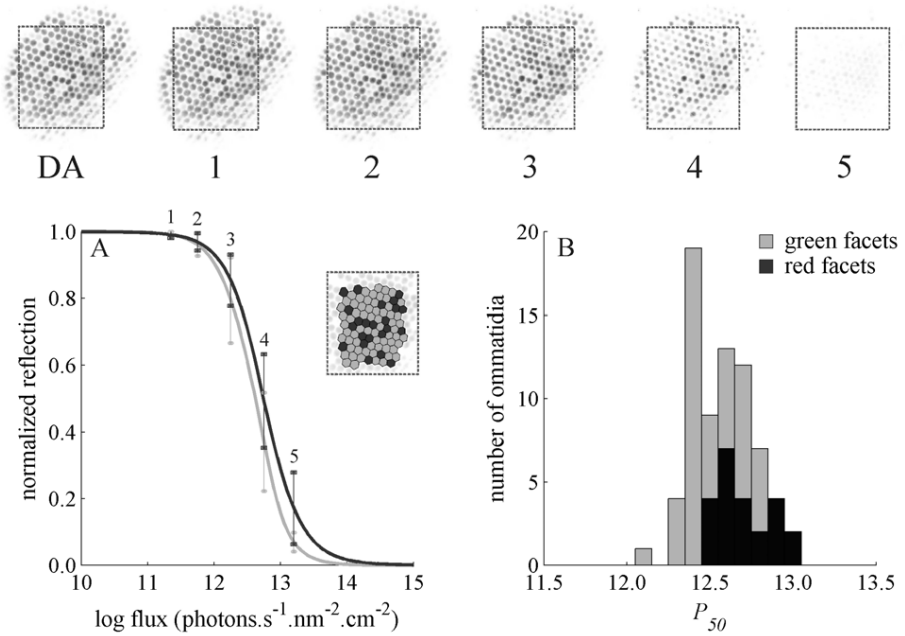

Fig. 5.9: Pupil activation in the ventral area of the satyrine *Pararge aegeria*. Top panel: Immediately after prolonged illumination with monochromatic light (494 nm) the corneal reflection is recorded with a digital camera (shown here as inverted grey images 1-5). Illumination intensity is varied with five density filter combinations covering the dynamic range of pupil activation. Weak light illumination does not trigger pupil migration as the reflection is not different from the control image in the dark adapted (DA) state (picture 1-2 vs DA). **A.** The pupil is gradually activated while increasing the intensity over 1 log-unit and finally results in virtually complete 'pupil closure' (picture 5). We calculated the mean pupil activation curve for 23 red reflecting ommatidia (black line) and 65 green reflecting ommatidia (grey line). The mean curve, together with the standard deviation at the 5 illumination intensities, was calculated after fitting sigmoidal functions through the averaged normalized reflection intensities. Therefore a Voronoi diagram was calculated, based on a selected region in the DA picture (rectangular area). The location of the red/green facets is indicated by black vs grey colored Voronoi cells (inset). The illumination intensity expressed as the photon flux at the focal plane of the objective. **B.** Histogram of the flux intensities which elicit 50% pupil activation (P_{50}). This activation threshold criterion holds for all facets within 0.5 log units. The distributions of both populations partially overlap. Statistically (one sided t-test, $\alpha = 0.05$) the mean P_{50} (12.6 log units) of the green facets is lower than the mean P_{50} (12.8 log units) of the red facets.

The reflection of the ommatidia is maximal in a dark-adapted (DA) eye, and adaptation to increasing light intensities results in a reduced reflection (Fig. 5.9, inverted gray images 1-5). For the estimation of the pupil activation curves of the red and green reflecting ommatidia, we first calculated a Voronoi diagram, based on a selected region in the dark adapted (DA) picture.
The reflection intensities of the Voronoi cells (23 red and 65 green reflecting facets) were then averaged and normalized, using the averaged reflection intensities of the DA image. For each facet the sigmoidal function ,

$$y = \left\{1 + \exp\left[s\,(P - P_{50})\right]\right\}^{-1}$$

where P = log I and I the photon flux, s a slope constant; P_{50}, the 50% pupil activation threshold, was subsequently fitted through the normalized reflection data for the 5 illumination intensities. Finally, for both red and green facets a mean pupil activation curve, the averaged sigmoidal function, was calculated, together with the standard deviation for the 5 illumination intensities. A histogram of the flux intensities which elicit 50% pupil activation (P_{50}), shows that the distribution of the activation threshold criterion for all facets is restricted to 0.5 log units. The distributions of both populations partially overlap and reflect a similar pupil working range in both red and green reflecting facets. Statistically (one sided t-test, $\alpha = 0.05$) the mean P_{50} (12.6 log units) of the green facets is lower than the mean P_{50} (12.8 log units) of the red facets.

4. Discussion

4.1. A new method to quantify single facet reflections

The eye shine of a large number of ommatidia can be photographed with a new optical telescopic set-up (see Chapter 4). The procedure described in the present chapter allows the analysis of the reflected light emerging from individual ommatidia, owing to their regular ordering in a 2-dimensional lattice. First, we use a M.I.P. script, optimized to detect the individual facet centers (Kuipers et al., 2002). Next, after manual corrections with a graphical user-interface, the assembly of facet centers is fitted to a two-dimensional lattice. The lattice is made here of second order polynomial lines fitted through the facet centers, to take into account the slight gradients in the eye. Finally, the coordinates of the lattice points are used to create a Voronoi diagram. The Voronoi algorithm is widely applied in mesh generation problems and partitions space around geometric objects into cells, each of which consists of

points closer to one particular object than to other (Aurenhammer et al., 1991; Okabe et al., 1992). Here the diagram defines interconnected hexagonal areas fully overlapping with the original facet lenses.

4.2. Simultaneous analysis of individual ommatidia

We have demonstrated the 'Voronoi procedure' in two preliminary case studies. First, we investigated bleached ommatidia in the butterfly eye. After superimposing a Voronoi diagram we quantified the averaged RGB intensity values (Figs. 5.6-7) from individual facets. Bleached and unbleached ommatidia are clearly distinguished in the green intensity values, reflecting the decreased absorption in bleached ommatidia, because of depletion of green absorbing visual pigment. It thus appeared that the reflection of the individual ommatidia in both populations is quite variable. Sources of variation may constitute slightly different mode radiation patterns, related to differences in rhabdom size, differences in visual pigment densities, the intrinsic variation of the underlying tapeta and their reflectance spectra (Chapter 6). Further research is required to clarify this point. The result may put into question the reliability of the butterfly eye as a absolute light detector, but it will be more intriguing to analyze how robust contrast sensitivity, the more probable aim of the eye, is to the uncovered optical variability.

As a second example we investigated the pupil working range in the ventral eye region of the satyrine butterfly *Pararge aegeria*. A green-red ommatidial eye shine is observed here in the ventral eye region, similar to the eye shine in the ventral half of the eye of the satyrine butterfly *Bicyclus anynana* (Stavenga 2002b, Chapter 6). In contrast to previous reflectometric recordings in butterfly eyes at the level of the deep pseudopupil (Järemo Jonson et al., 1998), we here analyzed corneal reflection images after different illumination intensities. The integrated signal at the deep pseudopupil neglects the heterogeneous properties of the individual ommatidia, which may cause serious errors, especially in the ventral eye region.

We have found an apparent dynamic range of approximately 2 log-units for the pupil mechanism, corroborating the previous studies (Stavenga et al., 1979; Järemo Jonson et al., 1998). Interestingly, the pupil range of the red and green reflecting ommatidia is rather similar. The ommatidia with green facets seem to have a slightly lower light threshold than the ommatidia with red facets for blue-green light (494 nm). Possibly this is related to the short-wavelength absorbing 'red' screening pigment which presumably borders the rhabdom in red reflecting facets and shifts the light sensitivity towards longer wavelengths (cf. Stavenga, 2002b; single facet reflectance recordings in

Chapter 6). However, the 50% activation criterion values vary over 0.5 log-units in both the green and red reflecting ommatidia (Fig. 5.8B), so further detailed measurements are necessary to substantiate this point.

4.3. Perspectives

Beautiful colorful reflections over a large eye area can be digitally recorded in a specialized optical set-up (Stavenga, 2002b). The challenge is now to set up an automated fast analysis procedure of reflection data from the eyes of butterflies to quantify the spatial properties and to unmask the optical properties of the underlying light regulating machinery. Interesting topics would include the study of pupil activation, visual pigment kinetics, spatial resolution, heterogeneity in the ventral area, development of the eye structure. We have started to explore the spectral sensitivity of the pupil mechanism by pupil activation with selective monochromatic illuminations of variable intensity (unpublished results). In the future the degree of automation, necessary for a workable extensive interspecies exploration, needs to be extended in a number of areas.

Chapter 6

In vivo microspectrophotometry of single butterfly ommatidia in dorsal and ventral eye regions

1. Introduction 76
2. Materials and Methods 76
2.1. Preparation and optical set-up 76
2.2. Spectrophotometric analysis 79
3. Results 79
3.1. A survey of single facet spectral reflectances in dorsal and ventral eye regions 79
3.2. Red pigments in the ventral region of butterfly eyes 82
4. Discussion 83
4.1. Regionalization and heterogeneity of ommatidia in butterfly eyes 85
4.2. Visual pigments, screening pigments and tapetum determine together the ommatidial reflectance spectrum 85

1. Introduction

The eye of butterflies has become an important model system for studying color vision. Using tools from molecular biology (Kitamoto et al., 1998, 2000; Briscoe, 2000; Vanhoutte et al., 2002), optics (Nilsson et al., 1988; Land and Osorio, 1990; Stavenga 2002a,b; Rutowski and Warrant, 2002) and behavioural biology (Kelber and Pfaff, 1999; Kinoshita et al., 1999; Kinoshita and Arikawa, 2000) considerable knowledge has recently been accumulated concerning the visual pigments, their spatial distribution in the eye, and their role in color processing. So far the most detailed investigated system is the eye of the Japanese yellow swallowtail *Papilio xuthus*. It is composed of three classes of ommatidia, each having a set of nine photoreceptors with identified visual and screening pigments (Arikawa and Stavenga, 1997; Arikawa et al., 1999a). Recent work on the small white, *Pieris rapae*, indicated that this butterfly has a similarly complex eye, i.e. also with three classes of ommatidia and different screening pigments (Qiu et al., 2002; Qiu and Arikawa, 2003a). Whereas *Papilio* has no tapetum, *Pieris* ommatidia have a multilayer tapetum proximal to the rhabdom (Ribi, 1979a), further complicating the picture. A tapetum characteristically exists in the ommatidia of all butterfly species except those of the family of Papilionidae (Miller and Bernard, 1968; Ribi, 1979b; Miller, 1979).

The tapetum is most likely of functional significance -presumably the tapetum enhances light sensitivity- but its role has not yet been firmly established. From an experimental point of view, the tapetum is highly functional, because it allows non-invasive, optical probing of the visual processes in the eye (Bernard, 1979a,b, 1983; Bernard and Remington, 1991). This property is further exploited in this chapter, by making an extensive survey of the tapetal reflections in several butterfly species. The survey shows that butterfly eyes quite vary in tapetal properties, not only between species, but also within one and the same eye (Stavenga et al., 2001). It is speculated that these differences are related to the habitat and living conditions of the respective butterflies.

2. Materials and Methods

2.1. Preparation and optical set-up

The majority of the investigated butterflies (Table 6.1) were captured in natural conditions in different locations (Japan, the Netherlands, Uganda). A few species were obtained from laboratory cultures (*Polyommatus icarus*,

	Family	English common name	Dutch common name	Latin name	Reg.	♂/♀	Origin	Habitat
C1	**Charaxinae**	Forest pearl charaxes	(*Charaxes*)	*Charaxes fulvescens*		x	U	
L1	**Lycaenidae**	Holly blue	Boomblauwtje	*Celastrina argiolus*		♀	J	B
L2		Sunbeam	(*Curetis*)	*Curetis acuta*		♀	J	
L3		Small copper	Kleine vuurvlinder	*Lycaena phlaeas*		x	N	Gd
L4		Common blue	Icarusblauwtje	*Polyommatus icarus*		♂	G*	G
L5		Pale grass blue	(*Pseudozizeeria*)	*Pseudozizeeria maha argia*		x	J	
N1	**Nymphalinae**	Small tortoiseshell	Kleine vos	*Aglais urticae*		x	N	
N2		(*Heliconius*)	(*Heliconius*)	*Heliconius melpomene*		♀	N*	
N3		(*Polygonia*)	(*Polygonia*)	*Polygonia c-aureum*		♀	J	
N4		Comma	Gehakkelde aurelia	*Polygonia c-album*		♀	N	B
N5		Variable eggfly	(*Hypolimnas*)	*Hypolimnas anthedon*		x	U	
N7		Red admiral	Atalanta	*Vanessa atalanta*		x	N	T
N8		Painted lady	Distelvlinder	*Vanessa cardui*		♀	J	T
P1	**Pieridae**	(Pieris)	(Pieris)	*Pieris melete*		♀	J	
P2		Green-veined white	Klein geaderd witje	*Pieris napi*		x	N	
P3		Small white	Klein koolwitje	*Pieris rapae*		♂	J	
S1	**Satyrinae**	Squinting bush brown	(*Bicyclus*)	*Bicyclus anyanana*		♂	N*	
S2		Common bush brown	(*Bicyclus*)	*Bicyclus safitza*		x	N*	
S3		Meadow brown	Bruin zandoogje	*Maniola jurtina*		x	N	G
S4		Speckled wood	Bont zandoogje	*Pararge aegeria*		x	N	B

Table 6.1: Single facet reflectances measured in 20 day-light living butterfly species. For each family, the Latin butterfly species name is given in alphabetical order (together with the Dutch and English common name, the sex, land of origin and natural habitat). The eye shine's dorsal-ventral regionalization pattern (Reg.) is indicated with a symbol (see Fig. 6.3). Further abbreviations used for habitat conditions are G: Grassland, Gd: Dry grassland, B: Wood borders, M: migrating, x = sex not determined. The place of origin is indicated with U: Uganda, N: the Netherlands, J: Japan, G*: butterfly culture maintained at Lehrstuhl Tierökologie I, Universität Bayreuth, Germany, N*: butterfly culture maintained at the Department of Evolutionary Biology, Leiden, the Netherlands.

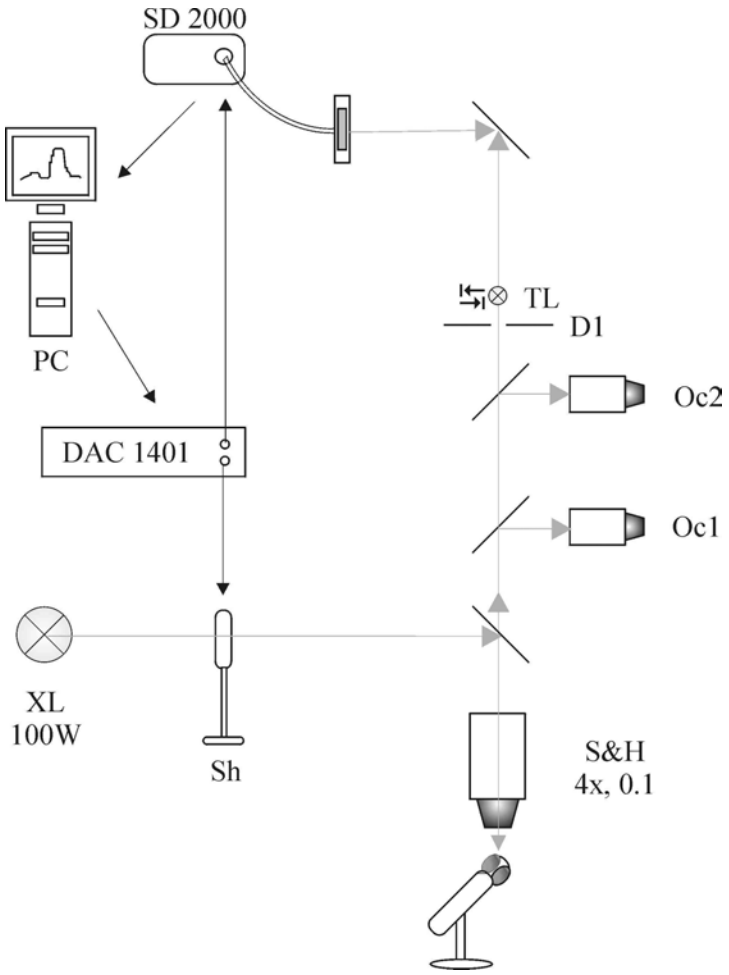

Fig. 6.1: Schematic diagram of the optical set.up used to record the reflection from single facets. Reflection data are acquired by the spectrometer (Avantes, SD2000). Data-acquisition and opening of the shutters (Sh) in the light path can be triggered simultaneously by TTL pulses of DAC's of the CED 1401(Cambridge Electronics Design) under control of Signal2 software (Cambridge Electronic Design, UK) on a Pentium computer (PC). Signals from the DAC and flow of spectral information to the PC are indicated with solid arrows. A half-mirror placed at 45° transmits light from the xenon arc lamp (XL, 150W) and enters the microscope objective (Spindler and Hoyer, 4x, NA 0.1), which is focused on the cornea of an eye of the immobilized butterfly. The animal is adjusted by visual inspection through a pair of oculars (Oc1). A second pair of oculars (Oc2) is used to position a diaphragm around an enlarged image of a single facet. Therefore a displaceable test light (TL) images the adjustable diaphragm (D1) on the corneal image. Finally the light is focussed on the tip of an optical fiber which guides the light to the spectrometer, a 2048 element photodiode array spanning a spectral range of 178 nm to 890 nm.

University of Bayreuth; *Bicyclus* sp. and *Heliconius* sp., University of Leiden). The butterflies were kept in a cage with sugar solution for a couple of weeks at most. For recording the eye reflection, the butterflies were mounted in a plastic tube and positioned on a goniometer in a microspectrophotometric set-up. The head and thorax were sealed to the plastic tube.

Single facet reflection spectra were measured with a SD2000 spectrophotometer (Avantes) connected to a conventional epi-illumination microscope (Leitz Ortholux) equipped with a 4x, 0.1 objective (Spindler and Hoyer). The light source was a 150 W xenon arc lamp. The microscope was focused at the level of the cornea and a small diaphragm, selecting the reflection from a single facet lens, was positioned in the microscope's image plane (Fig. 6.1).

2.2. Spectrophotometric analysis

Raw spectral data from the spectrophotometer were stored on a Pentium PC and subsequently analyzed off-line with Matlab. The reflection spectra were smoothed with a Savitzky-Golay polynomial smoothing filter with polynomial order 2 and a frame size less than 25 nm (75 data points). The recorded spectral data were converted into relative reflectance spectra by dividing the spectra with a spectrum measured from a white reference reflector (MgO) and then normalized by dividing the relative reflectance spectra by the value of maximal (relative) reflectance. Many butterfly species have an eye shine consisting of a few distinctly different colors, revealing a few different classes of ommatidia, and the spectra were thus grouped based on their colored appearance. The shape of the reflectance band was quantified by calculating the peak reflectance, λ_{peak}, and 50% cut-on and cut-off wavelengths, i.e. the λ_{50}-values, where the reflectance is half the maximal value (Table 6.2). The spectral data gained by measuring the reflectance spectra from individual ommatidia in the eyes of various butterfly species are summarized in Fig. 6.2. The reflectance band is characterized by three symbols, indicating the peak wavelength together with the wavelengths where the reflectance is half maximal.

3. Results

3.1. A survey of single facet spectral reflectances in dorsal and ventral eye regions

We recorded reflectance spectra from single facets, i.e. from single ommatidia at the level of the corneal facet lens, in dorsal and ventral eye

			Ventral				Dorsal			
	Latin name	Reg.	Colours	$\lambda_{50,l}$ (nm)	λ_{peak} (nm)	$\lambda_{50,r}$ (nm)	Colours	$\lambda_{50,l}$ (nm)	λ_{peak} (nm)	$\lambda_{50,r}$ (nm)
C1	*Charaxes fulvescens*		Orange (4)	592 ±7	644 ±7	694 ±10	Orange (5)	585 ±5	644 ±13	686 ±12
			Red (3)	614 ±4	679 ±6	722 ±8	Red (4)	615 ±2	679 ±15	726 ±15
L1	*Celastrina argiolus*		Orange (12)	587 ±6	647 ±18	732 ±6	Orange (10)	602 ±15	667 ±30	729 ±39
			Red (3)	620 ±3	685 ±17	749 ±6	Red (2)	618 ±1	682 ±15	748 ±5
L2	*Curetis acuta*		Red (7)	618 ±5	667 ±8	687 ±10	Red (5)	610 ±7	669 ±6	687 ±7
L3	*Lycaena phlaeas*		Yellow (3)	568 ±4	606 ±6	642 ±9	-	-	-	-
			Red (3)	604 ±4	657 ±9	706 ±16				
L4	*Polyommatus icarus*		Pink (5)	591 ±5	636 ±3	679 ±4	Green-Blue (6)	513 ±12	595 ±4	632 ±11
			Y.-Gr. (3)	592 ±3	634 ±2	680 ±4				
			Red (4)	624 ±2	689 ±21	753 ±12				
L5	*Pseudozizeeria maha argia*		Blue (4)	570 ±5	614 ±12	643 ±15	Orange (12)	576 ±7	628 ±10	649 ±11
			Red (5)	652 ±4	706 ±23	751 ±15				
			Orange (6)	572 ±12	623 ±12	662 ±14				
N1	*Aglais urticae*		Orange (5)	567 ±6	597 ±12	624 ±13	Orange (5)	574 ±6	623 ±11	661 ±10
N2	*Heliconius melpomene*		Yellow (5)	576 ±4	612 ±8	646 ±10	Orange (4)	572 ±5	609 ±5	644 ±6
			Red (5)	597 ±7	630 ±9	662 ±11	Red (4)	587 ±14	622 ±11	655 ±9
N3	*Polygonia c-aureum*		Red (13)	616 ±11	661 ±12	688 ±16	Blue (n =1)	556 ±0	576 ±0	587 ±0
							Yellow (7)	563 ±5	583 ±5	596 ±7
							Orange (3)	572 ±2	593 ±4	621 ±7
N4	*Polygonia c-album*		Orange (9)	577 ±3	629 ±20	702 ±18	DA: Orange (5)	575 ±4	638 ±33	683 ±25
							Bl: Yellow(4)	535 ±5	598 ±2	693 ±10
N5	*Hypolimnas anthedon*		Green (6)	556 ±2	585 ±7	596 ±21	-	-	-	-
			Yellow (5)	561 ±3	599 ±8	629 ±5				
N7	*Vanessa atalanta*		Green (4)	559 ±3	578 ±4	594 ±5	Green (3)	539 ±2	571 ±4	603 ±4
			Yellow (4)	568 ±4	596 ±4	620 ±5	Yellow (3)	550 ±1	586 ±3	620 ±3
N8	*Vanessa cardui*		Orange (4)	574 ±8	619 ±12	656 ±14	Orange (5)	570 ±4	610 ±9	649 ±18
			DarkOr. (4)	563 ±10	632 ±34	688 ±17	DarkOr. (1)	562 ±0	616 ±0	692 ±0
P1	*Pieris melete*		Red 1 (5)	614 ±1	638 ±1	661 ±3	-	-	-	-
			Red 2 (4)	647 ±1	677 ±2	704 ±2				
P2	*Pieris napi*		Red 1 (2)	597 ±3	618 ±1	640 ±1	Green (4)	570 ±8	607 ±12	633 ±14
			Red 2 (5)	622 ±6	651 ±8	676 ±8				
			Red 3 (2)	651 ±1	685 ±0	704 ±0				
P3	*Pieris rapae*		Red 1 (4)	609 ±5	633 ±4	655 ±4	-	-	-	-
			Red 2 (4)	644 ±3	672 ±3	698 ±2				
S1	*Bicyclus anyanana*		Green (5)	576 ±3	623 ±6	653 ±7	Green (7)	555 ±6	599 ±6	627 ±10
			Red (6)	604 ±9	707 ±31	756 ±8				
S2	*Bicyclus safitza*		Green (4)	571 ±4	606 ±9	627 ±6	Green (5)	565 ±2	595 ±4	631 ±5
			Red (4)	588 ±3	641 ±21	710 ±8				
S3	*Maniola jurtina*		Green (4)	545 ±1	567 ±1	585 ± 3	Green (4)	540 ±4	564 ±5	579 ±4
S4	*Pararge aegeria*		Yellow (10)	561 ±3	594 ±3	627 ±4	-	-	-	-
			Sienna (5)	617 ±7	663 ±6	704 ±7				

Table 6.2: The main spectral normalized reflectance bandwith is summarized here for the 20 different species (Table 6.1) in ventral and dorsal eye regions. For each apparent spectral class, annotated with a color, the tapetal reflection is given by the peak reflection λ_{peak} and $\lambda_{50,l/r}$-values, where the reflection left (l) and right (r) to the peak is half maximal**.** For all recorded reflections (given by *n*) the mean and standard deviation is calculated. In *Polygonia c-album*, single facet spectra were recorded before (DA, in the dark-adapted state) and after bleaching (bl); the spectra are shown in Fig. 6.7.

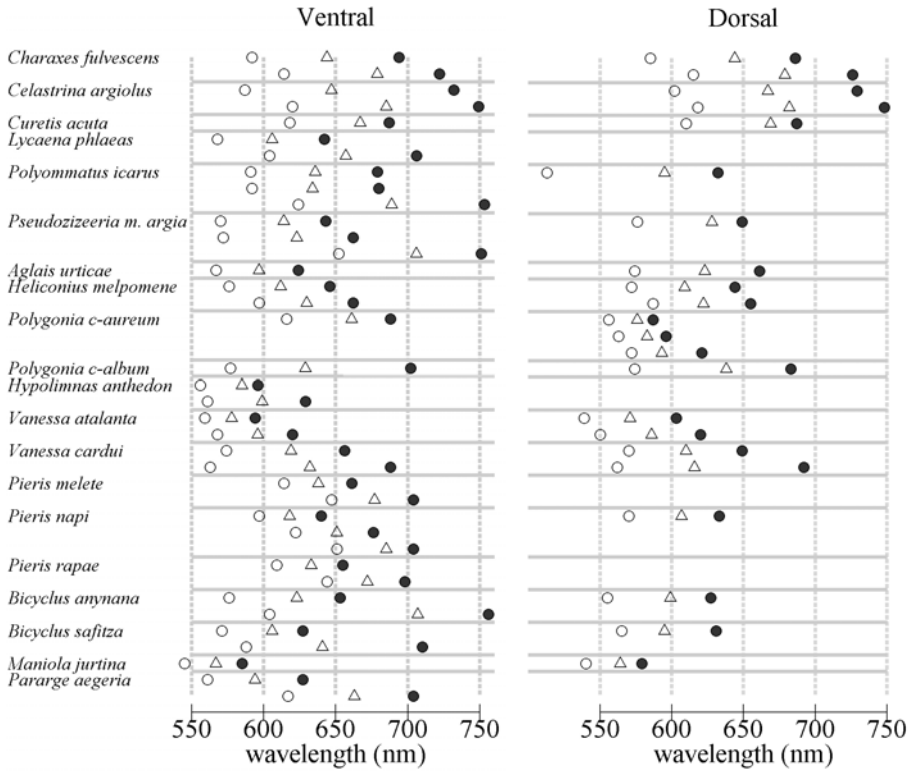

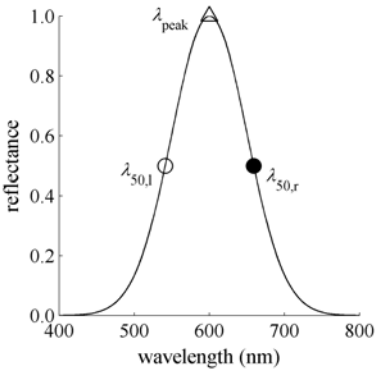

Fig. 6.2: Schematic summary of the main reflectance band in normalized reflectance spectra in 20 butterfly species (Table 6.2). For each spectral class, based on the colored appearance, the wavelength of peak reflection, λ_{peak}, and corresponding λ_{50}-values, where the reflectance is half maximal, on the left ($\lambda_{50,l}$, o) and right from the peak value ($\lambda_{50,r}$, •), are plotted (see schematic plot). The horizontal lines separate the species. For a few species, the reflection spectra in the dorsal region were not recorded. The $\lambda_{50,r}$ cut-off wavelength (•) is in general shifted towards shorter wavelengths in dorsal eye regions, even in completely homogeneous eyes. Ventral regions appear to have mostly two different tapeta. Intrinsic differences in the tapeta and visual pigment (Fig. 6.4) account for the apparent higher diversity in spectral classes, like in *Polyommatus* en *Polygonia c-aureum*.

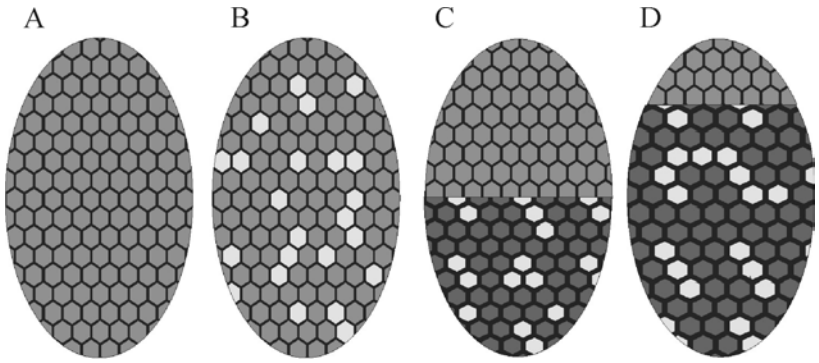

Fig. 6.3: Schematic representation of 4 variations in eye shine pattern. **A.** Uniform homogeneous eye shine, e.g. *Polygonia c-album*; **B.** uniform mixed eye shine, e.g. *Heliconius melpomene*; **C.** clear ventral-dorsal eye with mixed ventral eye shine and a homogeneous dorsal eye region, e.g. *Bicyclus anynana*; **D.** heterogeneous ventral eye region with a small homogeneous dorsal eye region, e.g. *Pieris rapae*.

regions in Charaxidae, Lycaenidae, Nymphalidae (Nymphalinae and Satyrinae), and Pieridae (Table 6.1).

A number of butterfly species have a totally homogeneous eye shine, e.g. the orange-red eye shine in some Nymphalinae (e.g. *Polygonia c-album*; Figs. 6.3A, 6.4, see also chapter 4), yielding very similar reflectance spectra from the different ommatidia in one and the same eye.

Commonly the eye shine is heterogeneous. A mixed yellow-red pattern is encountered in all eye regions of Heliconidae (e.g. *Heliconius melpomene*; Figs. 6.3B, 6.5). Most frequently the heterogeneity is restricted to a certain eye region, resulting in a clear ventral-dorsal regionalization of differently colored reflections, with a transition zone at the equator, in e.g. *Bicyclus anynana* and *B. safitza*, and in *Polyommatus icarus* (Figs. 6.3C, 6.6), or with only a very small distinctly colored eye shine in the upper dorsal region, in e.g. *Pieris* (Figs. 6.3D, 6.7).

The reflectance spectra slightly scatter within each spectral class (Figs. 6.4-7), specifically at the long-wavelength side; in *Polygonia* the wavelength of half-maximum reflectance varies over ca 50 nm (Fig. 6.4B).

3.2. Red pigments in the ventral region of butterfly eyes

The ventral area of many butterfly species exhibit a spectral dichotomy of the ommatidia with respect to the color of the reflected light (Fig. 6.2). In satyrines for example, like *Bicyclus anynana* and *Pararge aegeria*, the eye shine of dark adapted eyes consists of bright green and red reflecting ommatidia. The eye shine of the small white, *Pieris rapae*, reveals also two

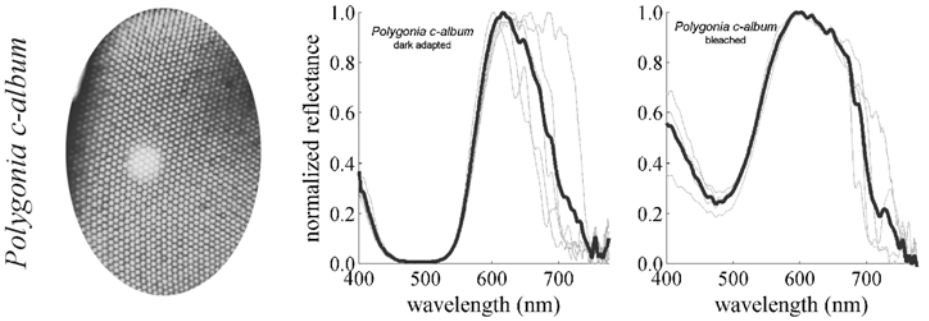

Fig. 6.4: Normalized reflectance spectra of single facets in the uniform, homogeneous eye of *Polygonia c-album* (Fig. 6.2, type A). Thick lines are averages of normalized reflectances of single facets (see Table 6.2). The reflectance spectra in the range 450-550 nm are primarily determined by the absorption of the predominant green rhodopsin. Bleaching green visual pigment (protocol outlined in Chapter 4-5) results in an increased reflectance at 475-520 nm and a corresponding 40 nm shift in reflectance towards shorter wavelengths, i.e., the eye shine color shifts from red to yellow. This is characterized in Table 6.2 by the peak reflection wavelength and the $\lambda_{50,l}$-values, being the wavelengths of 50% reflectance at the short wavelength side of the peak wavelengths. The 50% reflectance values at the long wavelength tail is unaffected.

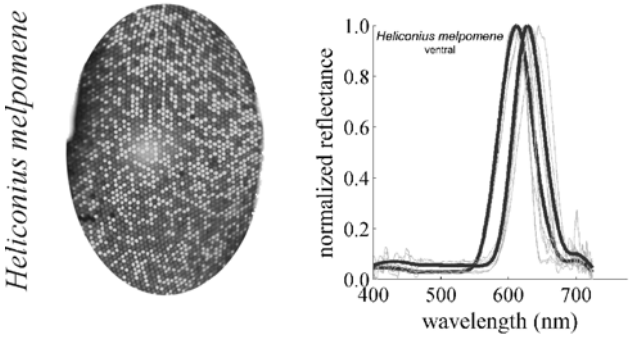

Fig. 6.5: Normalized reflectances of single facets in the eye of *Heliconius melpomene*. The eye has a mixed yellow-red eye shine with heterogeneous ommatidial spectral types (Fig. 6.2, type B). Thick lines are averages of single facet normalized reflectances (see Table 6.2).

different classes of reflecting ommatidia, pale red and deep red, with reflectance spectra peaking at about 635 nm and 675 nm, respectively (Fig. 6.7; see also Qiu et al., 2002). As the long-wavelength limit of the reflectance spectra is determined by the tapetum, it follows that the two ommatidial classes must have different tapeta. The short-wavelength region of the reflectance spectra is determined by the absorbance spectra of the screening pigments in

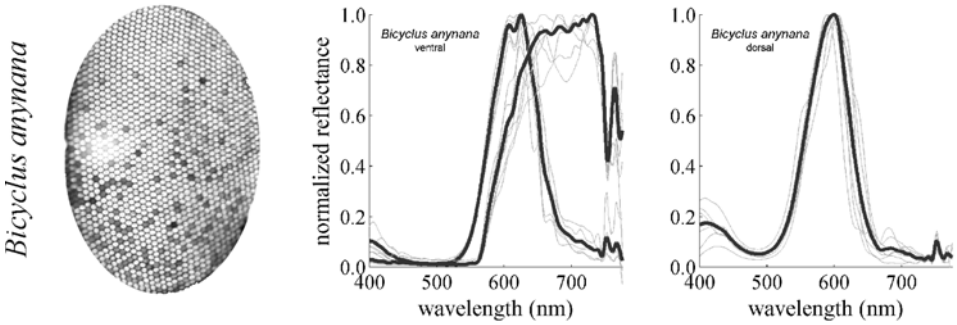

Fig. 6.6: Normalized reflectances of single facets in the eye of *Bicyclus anynana* with distinct ventral and dorsal eye regions (Fig. 6.2, type C). Thick lines are averages of single facet normalized reflectances (thin lines, see Table 6.2).

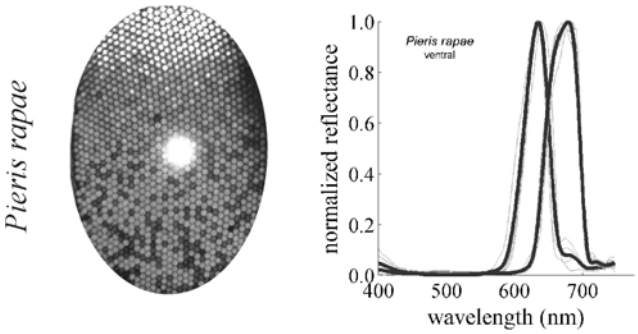

Fig. 6.7: Normalized reflectances of single facets in the ventral eye region of *Pieris rapae.* The eye has a large ventral eye region and a smaller dorsal area (Fig. 6.2, type D). Thick lines are averages of single facet normalized reflectances (see Table 6.2).

the photoreceptors. Therefore, the two classes of ommatidia also must have different screening pigments. Histology corroborates this conclusion: in light-microscopic sections two types of pigmentation were found, i.e. within each ommatidium four clusters of either pale-red or deep-red colored clusters surround the rhabdom (Qiu et al., 2002).

4. Discussion

4.1. Regionalization and heterogeneity of ommatidia in butterfly eyes

In all microspectrophotometric recordings maximally three different classes of ommatidia were found, distributed over the eye. The regionalization of the colored eye shine falls into four classes: a uniform eye with homogeneous or mixed eye-shine, clear dorso-ventral regionalization or disproportional dorso-ventral regionalization with a large ventral area (see Fig. 6.3). In the epi-illumination microsope one observes that frequently the dorsal eye region has a homogeneous eye shine. The eye shine in the dorsal area can be blue-violet, yellow or green (Stavenga, 2002b). One apparent exception is the heterogeneous colored eye shine in *Polygonia c-aureum* (Fig. 6.2). However our recordings shows that the intrinsic variability of the tapetal reflection and differences in the relative amplitude at short wavelengths -due to bleaching and/or variable expression of SW opsins (White et al., 2003)- explains the colorful diversity. The ventral area frequently has heterogeneous types of reflection (Miller and Bernard, 1968; Stavenga et al., 2001). The heterogeneous ommatidia, mostly of two types, are randomly distributed and the ratio between the heterogeneous ommatidia is variable (Stavenga, 2002), with mostly a minority of red reflecting ommitidia. The omnipresent heterogeneity is probably intimately linked to color vision in butterflies (Kinoshita et al., 1999).

4.2. Visual pigments, screening pigments and tapetum determine together the ommatidial reflectance spectrum

The recorded reflection data allow an interpretation of the colored eye shine in terms of the tapetal reflectance spectra, visual pigments and red screening pigments, occasionally surrounding the rhabdom. The bleaching experiments show that the trough in the visible range can be largely modified, thus demonstrating that the low reflectance around 500 nm is due to the abundant green rhodopsin (Fig. 6.4, see also Chapter 4). The long-wavelength side stays unaffected, in agreement with the view that the spectrum there is determined by the reflectance properties of the tapetum (Bernard and Remington, 1991; Briscoe et al., 2003). Here we present the reflectance spectra of 4 different species, representative for the diversity in eye shine pattern.

In the simplest uniform eye type, e.g. *Polygonia* (Fig. 6.4), all ommatidia fall into one class, with often the long-wavelength side distributed over several tens of nm (Fig. 6.4B). This can be understood from the inevitable

variability in the thickness of the layers in the tapetum, which is in the order of 100 nm (Miller and Bernard, 1968).

Often butterfly eyes have two classes of ommatidia with reflectance spectra where both long-wavelength sides differ. *Heliconius melpomene* (Fig. 6.5), has two ommatidial classes, randomly distributed over the whole eye, reflecting yellow and red. The reflection in the short wavelength region is very low. Bleaching experiments and especially histological sections have to confirm the presence of yellow and red screening pigments surrounding the rhabdom, as is the situation in *Papilio* species.

The green-reflecting ommatidia of *Bicyclus anynana* (Fig. 6.6) in the ventral eye region belong to the same class as the ommatidia of the dorsal eye region. The latter ommatidia do not contain a photoreceptor screening pigment, as a bleaching protocol strongly changes the reflectance spectrum; bleaching negligibly changes the reflectance spectra of the red-reflecting ommatidia however (data not shown). The reflectance of the red class is extremely low at wavelengths below 580 nm, most likely due to a red-transmittant screening pigment absorbing strongly in the middle and short wavelength range, which acts as a red filter for the co-localized photoreceptors (Stavenga, 2000). The red class does not have the same reflectance band in *Bicyclus anynana* and *Bicyclus safitza*, which may be related to the different eye size of the *Bicyclus* species and in differences in the number of tapetal layers.

The short-wavelength sides of the reflectance spectra of *Pieris* (Fig. 6.7) can be straightforwardly attributed to the two classes of red photoreceptor screening pigments (Qiu et al., 2002). The differences in the long-wavelength side mean that the tapetum is also different. The screening pigments and tapetum of an ommatidial class appear to be tightly connected. The red pigment clusters function as red-transmittant filters, favouring long-wavelength-shifted sensitivity spectra of the proximal photoreceptors of *Papilio xuthus* (Arikawa et al., 1999a). Presumably therefore, the red reflecting ommatidia in the eyes of other butterflies are due to red photoreceptor pigments, and also act to shift the sensitivity spectrum (Stavenga, 2002b).

Chapter 7

Summary and General Discussion

1. Visual pigments: filters inside the lightguide 88
2. Tapeta: mirrors on the bottom of the lightguide 89
3. Colored screening pigment: filters surrounding the rhabdom..... 90
4. A model of light absorption in the butterfly rhabdom 91
5. Towards modeling photoreceptor spectral sensitivity..... 91
6. Combining photoreceptor sensitivities to provide color vision..... 94
7. Perspectives 95

Most of our daily activities depend on recognizing and discriminating objects in the outside world. Therefore many scientists are intrigued by the mechanisms behind it, and explore vision in experimentally accessible species. Insects are very useful as many experimental techniques can be applied to their eyes, which have an anatomically well-known crystalline structure. In this thesis we investigated spectral processing in the eyes of butterflies with tools from molecular biology, i.e. cloning visual pigments (*Chapter 2*) and optics, especially spectrophotometry (*Chapters 3-6*).

Processing spectral information or color vision is possible with a combination of spectrally different photoreceptors. One of the primary driving questions in this thesis is to understand how the set of spectral photoreceptors are optimized to the photic environments inhabited by butterfly species. In butterflies, tuning might be directed towards the reflected light on wings and leaves. It has been postulated in lycaenids that differential expression of visual pigments is a prime mechanism *(*see *Chapter 2-4*, Bernard and Remington, 1991). However, the spectral properties of screening pigments and tapeta, frequently expressed in heterogeneous sets of ommatidia, should not be neglected (see *Chapter 5-6*, Arikawa et al., 1999a; Qiu et al., 2002; Stavenga 2002a,b).

In this thesis we have started to assess the physical properties of visual pigments, tapeta and screening pigments, all influencing light absorption in the butterfly eye. This will facilitate building quantitative models of light absorption (see also *Chapter 3*) which can explain the reflectance spectra as well as electrophysiologically recorded spectral sensitivities of the photoreceptors.

1. Visual pigments: filters inside the lightguide

The visual pigments of the photoreceptor cells selectively absorb light and therefore primarily determine the light absorption. The most basic description of visual pigments is the primary structure, obtained by molecular cloning. By analyzing the homology of visual pigment sequences one can derive the absorption properties and thus distinguish between short- (UV), middle- (blue) and long-wavelength (green, red) absorbing pigments. Like in bees, a trichromatic color system based on three different opsins absorbing in the UV, blue and green seems to be the rule. Molecular cloning in all investigated lepidopteran species, i.e. *Manduca sexta* (Chase et al., 1997), *Heliconius sp.* (Hsu et al., 2001), *Vanessa cardui* (Briscoe et al., 2003) revealed no more than 3 different opsins. *Papilio* sp. exceptionally has at least five retinal opsins, with three different LW opsins (Kitamoto et al., 1998; Briscoe, 1998). In *Chapter 2*

we described the partial cloning and homology analysis of cDNA sequences of green and UV absorbing rhodopsins in the satyrine *Bicyclus anynana*.

Our knowledge of the spatial distribution of visual pigmens in butterflies is based on extensive histological studies in the small white, *Pieris rapae* (Qiu et al., 2002), the Japanese yellow swallowtail, *Papilio xuthus* (Kitamoto et al., 1998, 2000), the painted lady *Vanessa cardui* (Briscoe et al., 2003) and the moth *Manduca sexta* (White et al., 2003). All these butterfly species have a fused rhabdom with nine photoreceptor cells. The green rhodopsins are expressed in all ommatidia over the whole eye, at least in 6 photoreceptor cells. The short- and middle-wavelength (UV/B) absorbing rhodopsins are expressed in different combinations in the two distal dorso-ventral (dv) oriented photoreceptors in three types of ommatidia, i.e. UV-UV, UV-B and B-B. The ninth cell presumably also expresses a green rhodopsin. In *Papilio* and *Pieris* the dominant layer, taking up about the distal two thirds of the rhabdom, is composed of the rhabdomeres of the four distal cells, Rl-4. The proximal one third consists almost completely of R5-8 rhabdomeres, and a short basal part is due to an R9 rhabdomere. The UV-rhodopsin is predominantly present in the dorsal region; the blue rhodopsin is more present in ventral areas.

Chapter 3 presented a photochemical formalism to model visual pigment processes in the butterfly eye based on reflection microspectrophotometry. Such a model is necessary for a quantitative interpretation of the visual pigment processes, the kinetics and absorption spectra. We illustrated photoconversion of visual pigment under broad-band illumination in a rhabdom with green, blue and UV receptors in a 6:1:1 ratio. In *Chapter 4* we explored visual pigment photochemistry in a group of homogeneous ommatidia with a few experimental protocols, e.g. bleaching (Bernard, 1983) and photochemical conversion of rhodopsin and metarhodosin with adapting monochromatic stimuli. We investigated visual pigment absorbance spectra in the eye of *Polygonia c-album,* a butterfly with a uniform homogeneous eye shine. Our data corroborate the predominant expression of a green opsin.

2. Tapeta: mirrors on the bottom of the light guide

Butterfly eyes, observed with an epi-illumination microscope, may have a highly heterogeneous eye shine especially in ventral regions (Stavenga et al., 2001; Stavenga 2002a,b). In *Chapter 5* we described an image analysis procedure based on Voronoi diagrams to analyze reflections of single ommatidia of the butterfly compound eye with a digital camera. The procedure

allows the investigation of an eye with heterogeneous eye properties. After bleaching green visual pigment in the eye of *Polygonia* we investigated the reflection of bleached and unbleached ommatidia. In the ventral eye region of the satyrine *Pararge aegeria*, we measured the pupil action spectrum in single ommatidia of red and green reflecting ommatidia.

The spectrophotometric recordings on single ommatidia in 20 different butterflies (cf. *Chapter 6*) show that, though the tapeta reflect over a broad range (Ribi, 1979b), there is a variable cut-off in the long-wavelength range of the reflectance spectra between 550 and 750 nm. Below 500 nm a flat tapetal reflectance spectrum may be assumed. The role of tapeta in the dorsal region with a cut-off value within the absorption range of the visual pigment needs to be clarified. It has been speculated that the role of the tapetum may be especially linked to enhance the red sensitivity of the basal R9 cell (next section). The tapeta show a high variability in reflection amplitude (*Chapter 5*) possibly hampering reliable coding of absolute light sensitivities. The intraspecific diversity in retinal properties and color perception may offer a solution to face a challenging range of potential photic environments (Cronin et al., 2002a,b).

3. Colored screening pigment: filters surrounding the rhabdom

Modelling light absorption in the rhabdom of *Papilio xuthus,* taking into account the additional filtering properties of the absorbing substances, i.e. red and yellow screening pigments and an additional fluorescing substance, retinol presumably, could explain the electrophysiologically determined sensitivities of the photoreceptor cells (Arikawa et al., 1999a). The retinol could account for the narrowing of the sensitivity spectrum of a violet receptor. Red sensitivity of photoreceptors expressing green rhodopsins could be explained by red and yellow screening pigments, essentially long-pass filters, shifting the spectral sensitivity of the proximal photoreceptors towards longer wavelengths (Arikawa et al., 1999a).

Recent microspectrophotometric recordings and anatomical studies in *Pieris* (Qiu et al., 2002, *Chapter 6*) revealed two types of red screening pigments together with two tuned types of tapeta. This corroborates behavioural evidence that color discrimination in the red is well developed in this species (Kolb and Scherer, 1982; Scherer and Kolb, 1987).

4. A model of light absorption in the butterfly rhabdom

In *Chapter 3* we presented a formalism to model light absorption and conversion of visual pigment in a fused rhabdom. The model could account for the conversion experiments described in *Chapter 4*. The model also explains the recorded spectral reflectances. For example, with a known rhabdom length of 450 μm (Qiu et al. 2002; Briscoe et al., 2003), visual pigment templates (Govardovskii et al., 2000) and estimated extinction coefficients (*Chapter 3*; Warrant and Nilsson, 1998) of rhodopsins and metarhodopsins with peak wavelengths at 340 nm (UV), 440 nm (B) and 532 nm (G), respectively, the resulting decrease in light flux in the rhabdom can be calculated to explain the reflectance spectra in *Polygonia c-album*. After reflection on the tapetal mirror and a double passage back through the rhabdom, the eye shine reflectance, the product of the tapetal reflectance M (Fig. 7.1A) and squared transmittance, T^2, dependent on absorbance κ and length L(Fig. 7.1B) is plotted in Fig. 7.1C. It is assumed here that the tapetum reflects with a maximal efficiency of 0.8, declining at long wavelengths. The tapetal reflectance spectrum is approximated by a sigmoidal equation $M = M_0\{1+\exp[s(\lambda-\lambda_{50})]\}^{-1}$ with M_0 = 0.8, a slope constant s = 0.1 and λ_{50} = 691 nm. Clearly, the rhabdom-tapetum combination works as a long-pass spectral filter, strongly reducing the reflected light intensity at all but the long wavelengths.

5. Towards modeling photoreceptor spectral sensitivity

Photoreceptors signal the incident light intensity by the number of quanta absorbed by the visual pigment. However, a single photoreceptor can impossibly distinguish between wavelengths: color vision requires at least two photoreceptors with different sensitivity spectra. The sensitivity spectrum of a photoreceptor is its normalized light sensitivity to different wavelengths. Typically the spectral sensitivity is experimentally measured by determining at each wavelength the photon flux that elicits a certain physiological criterion response. The spectral sensitivity, which is the inverse normalized criterion intensity, then is:

$$S(\lambda) = \left[\frac{I(\lambda)}{I(\lambda_{max})}\right]^{-1} \quad (1)$$

A certain criterion response will be reached when the light stimulus causes the

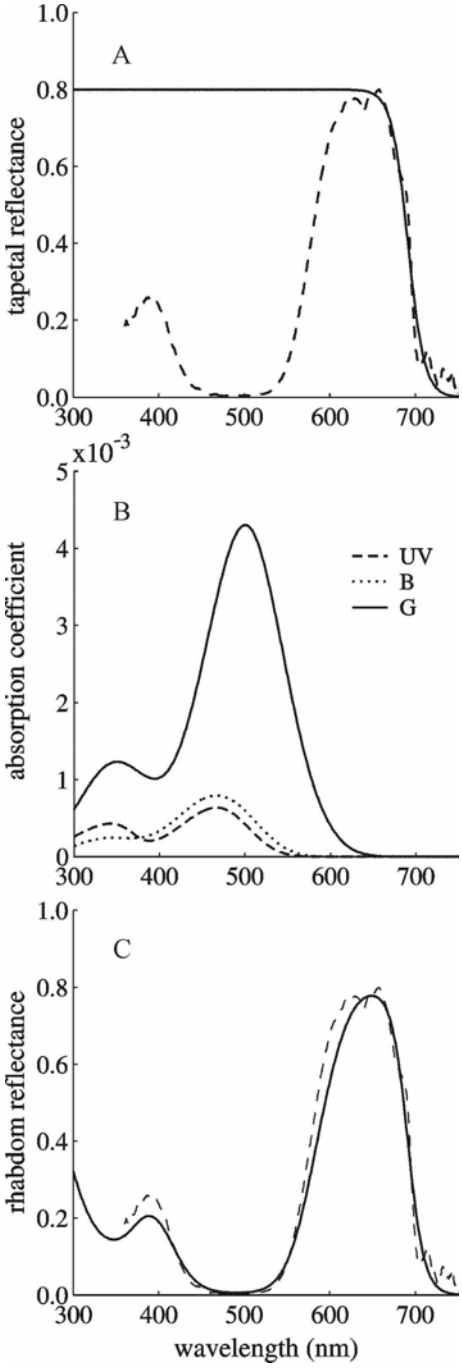

Fig. 7.1: The reflectance spectra of single ommatidia are explained by light absorption in a model where UV, B and G rhodopsins are present in a 1:1:6 ratio **A.** The tapetal reflectance spectrum (solid line) is estimated here with a sigmoidal equation, fitted to the experimental reflectance spectra in *Polygonia c-album* (dashed line),which are normalized here to a maximal tapetal reflection coefficient of 0.8. **B.** The absorbance of the UV, B and G receptors is calculated with absorption spectra of the visual pigments of the comma, *Polygonia c-album* (see Fig. 3.1). The maximal absorbance is 0.005 μm^{-1}. We have taken here the fraction of rhodopsins and metarhodopsins after white light illumination, i.e. approximately 60 and 40% respectively (see Chapter 3). **C.** The reflectance *R,* given by the product of the tapetal reflectance *M* in **A** and the squared transmittance *T* after a double passage through the rhabdom, is primarily determined by the length of the rhabdom *L* and the summed absorbance κ of the UV, B and G photoreceptors in **B.**

creation of a certain number of metarhodopsin. Eq. 1 can be rewritten in terms of the total number of created metarhodopsin molecules per unit-time. If we consider a photoreceptor with pure rhodopsin (f_R = 1, f_M = 0), the sensitivity spectrum S turns out to equal the normalized absorptance spectrum of the visual pigment, $A(\lambda)$ (Goldsmith and Bernard, 1974; Stavenga et al., 2001):

$$S(\lambda) = \frac{A(\lambda)}{A(\lambda_{max})} \tag{2}$$

The sensitivity spectrum of a photoreceptor is affected by lateral filtering (Snyder et al., 1973) or by filtering by photostable screening pigment located near the rhabdom boundary (Arikawa et al., 1999a). When the absorbance is low and due to only one rhodopsin, the spectral sensitivity (Eq. 2) changes as the incident light flux is modified by the transmittance of the filtering pigment $T_f(\lambda)$:

$$S(\lambda) = \frac{T_f(\lambda)A(\lambda)}{T_f(\lambda_{max})A(\lambda_{max})} \tag{3}$$

The consequence is that the sensitivity spectra are narrowed and left/right shifted, with short/long-pass filters, respectively (Arikawa et al., 1999a,b; Fig. 8 of Stavenga, 2002b).

We can estimate the transmitttance spectra T of the screening pigments from the microspectrophotometric recordings of reflections on single ommatidia (*Chapter 6*, Fig. 6.7) by fitting the sigmoidal functions, i.c. $[1 + \exp[1\text{-}c(\lambda - \lambda_{50})]]^{-1}$, to the left-rising flank of the average normalized reflectance spectra. Fig. 7.2 shows as an example the case of *Pieris*, where a green absorbing visual pigment, assumed to peak at 570 nm, is filtered by the experimentally measured red screening pigments with cut-off values, $\lambda_{50,\ typeI}$ = 610 nm and $\lambda_{50,\ typeII}$ = 644 nm (see Chapter 6, Fig. 6.7). The spectral sensitivity is right-shifted by 50 and 80 nm, respectively towards ~620 nm and ~650 nm (Fig. 7.2). Interestingly, the basal retinula cell, R9, of *Pieris rapae* was found to be a narrow-peaked red receptor, peaking at 620 nm (Shimohigashi and Tominaga, 1991). Recently, two types of red receptors were found in the proximal photoreceptors R5-8 in *Pieris rapae* peaking at 620 nm and 640 nm (Qiu and Arikawa, 2003b).

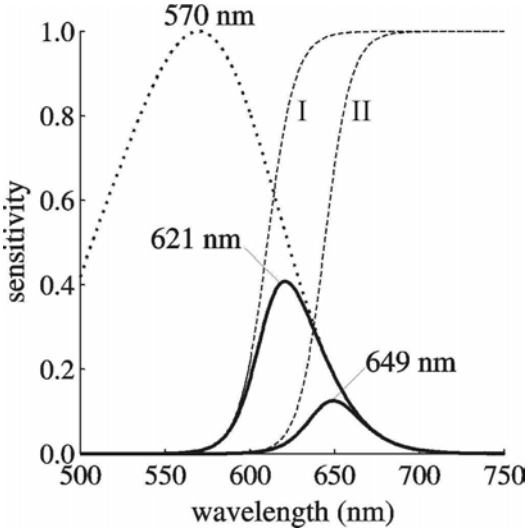

Fig. 7.2: Red shift of the spectral sensitivity with long-pass red filters in *Pieris rapae*. The spectral sensitivity is calculated as the normalized absorbance times the transmittance of the screening pigments (Stavenga, 2002b). Transmittance curves of the pale red (type I) and deep red (type II) screening pigments (Qiu et al., 2002) are derived from fitting a sigmoidal function (dashed lines) to the left side of the averaged normalized reflectance spectra (see Chapter 6, Fig. 6.7). The spectral sensitivity of a green photoreceptor (with $\lambda_{,R,max}$ at 570 nm, dotted line) is shifted ca 50 and 80 nm, in type I and type II ommatidia, respectively.

6. Combining photoreceptor sensitivities to provide color vision

Color vision in insects was first demonstrated in the honeybee, where three photoreceptor classes (UV, B and G) form the standard set of photoreceptors underlying color vision (Menzel and Backhaus, 1989). In butterflies the photoreceptor cells responsible for color vision are not yet identified. It has been argued that especially photoreceptor cells R1, R2 and R9, which project their long axonal fibers towards the medulla constitute the color vision system (Kelber, 1999a). In lycaenids this question has been addressed by calculating the quantum catch Q of the individual receptors, the photon absorption in individual ommatidia with a specific spectral sensitivity (S) after the optical stimulation with light reflected from the wings (R) given the ambient light conditions (Q_o). Hue discrimation is accounted here by the dichromatic ratio of Q values for the different receptor types (Bernard and Remington, 1991).

Color contrast probably also relies on opponent systems deriving signals from several adjacent ommatidia, which are randomly distributed in heterogeneous eyes (Stavenga 2002b, *Chapter 6*; Qiu et al., 2002). A similar organization has been shown in flies, where the photoreceptor cells R7 and R8

mediate color vision by expressing two different combinations of visual pigment (Salcedo et al., 1999).

The ommatidia are not only optimized for color vision. Photoreceptors may be involved in spatial or polarisation vision. In *Papilio xuthus* blue receptors, expressed in dorso-ventrally oriented photorecptor cells are maximally sensitive to vertically polarised light, whereas green receptors are maximally sensitive to horizontal or oblique polarisation angles. Also on the macroscopic level, regionalization of visual function occurs. Many butterflies have specialised dorsal eye regions which presumably express a limited number of rhodopsins. The random spatial distribution of heterogeneous types of ommatidia, mostly in ventral regions is presumably intimately linked to color vision and the detection of colored objects against a green background (Kelber, 1999b).

7. Perspectives

Our research on spectral processing in butterfly rhabdoms under ambient light conditions may be extended in three major directions. First, a biophysical model should incorporate the waveguide properties of the rhabdom and a realistic description of the lens properties, extending recent modelling of the fly facet lens - rhabdomere system (Stavenga, 2003). Second, it is interesting to further investigate the dynamic biochemical regulation of (spectral) light sensitivity by visual pigments and pupillary granules. Third, the exploration of the enormous diversity in eye structures in quantitative detail with diverse experimental techniques will likely be rewarding in view of the behavioural and ecological relevance. Most of the day-light living butterflies at present seem to have experimented with heterogeneous combinations of ommatidia spread over the whole eye, or a variable part of the ventral region. The heterogeneity is mostly dichotomous with respect to the tapetal reflections and probably tuned to color contrast enhancement. In this respect, the environmental objects of interest may be quite different, e.g. wings of mating partners (Bernard and Remington, 1991), green leaves of plants (Kelber, 1999b), and prone to seasonal fluctuations (Brakefield and French, 1999). As such it is interesting to investigate the ommatidial adaptations.

References

Arikawa,K., Inokuma,K., and Eguchi,E. (1987) Pentachromatic visual system in a butterfly. Naturwissenschaften *74*:297-298.

Arikawa,K. and Stavenga,D.G. (1997) Random array of colour filters in the eyes of butterflies. J.Exp.Biol. *200*:2501-2506.

Arikawa,K. (1999) Color vision. In: Eguchi,E. and Tominaga,Y. (eds): Atlas of arthropod sensory receptors. Tokyo Berlin Heidelberg New York: Springer-Verlag, pp. 23-32.

Arikawa,K., Scholten,D.G.W., Kinoshita,M. and Stavenga, D.G. (1999a) Tuning of photoreceptor spectral sensitivities by red and yellow pigments in the butterfly *Papilio xuthus*. Zoological Science *16*:17-23.

Arikawa,K., Mizuno,S., Scholten,D.G., Kinoshita,M., Seki,T., Kitamoto,J. and Stavenga,D.G. (1999b) An ultraviolet absorbing pigment causes a narrow-band violet receptor and a single-peaked green receptor in the eye of the butterfly *Papilio*. Vision Res. *39*:1-8.

Aurenhammer,F. (1991) Voronoi diagrams: a survey of a fundamental geometric data structure. ACM Computing Surveys *23*:345-405.

Bernard,G.D. (1979a) Bleaching of rhabdoms in eyes of intact butterflies. Science *219*:69-71.

Bernard,G.D. (1979b) Red-absorbing visual pigment of butterflies. Science *203*:1125-1127.

Bernard,G.D. (1983) Dark-processes following photoconversion of butterfly rhodopsins. Biophys.Struct.Mech. *9*:227-286.

Bernard,G.D. and Remington,C.L. (1991) Color vision in *Lycaena* butterflies: Spectral tuning of receptor arrays in relation to behavioral ecology. Proc.Natl.Acad.Sci.USA *88*:2783-2787.

Brakefield,P.M. and French,V. (1999) Butterfly wings: the evolution of development of colour patterns. BioEssays *21*:391-401.

Briscoe,A.D. (1998) Molecular diversity of visual pigments in the butterfly *Papilio glaucus*. Naturwissenschaften *85*:33-35.

Briscoe,A.D. (2000) Six opsins from the butterfly *Papilio glaucus*: molecular phylogenetic evidence for paralogous origins of red-sensitive visual pigments in insects. J.Mol.Evol. *51*:110-121.

Briscoe,A.D. and Chittka,L. (2001) The evolution of color vision in insects. Annu.Rev.Entomol. *46*:471-510.

Briscoe,A., Bernard,G.D., Szeto,A.S., Nagy,L.M., and White,R.H. (2003) Not all butterfly eyes are created equal: rhodopsin absorption spectra, molecular identification and localization of UV-,blue-, and green-sensitive rhodopsin-encoding mRNAs in the retina of *Vanessa cardui*. J.Comp.Neurol. *458*:334-349.

Byk, T., Bar-Yaacov, M., Doza, Y. N., Minke, B., and Selinger, Z. (1993) Regulatory arrestin cycle secures the fidelity and maintenance of the fly photoreceptor cell. Proc.Natl.Acad.Sci. *90*:1907-1911.

Chase,M.R., Bennett,R.R., and White,R.H. (1997) Three opsin-encoding cDNAS from the compound eye of *Manduca sexta*. J.Exp.Biol. *200*:2469-2478.

Chyb,S., Raghu,P., and Hardie,R.C. (1999) Polyunsaturated fatty acids activate the *Drosophila* light-sensitive channels TRP and TRPL. Nature *397*:255-259.

Cronin,T.W., Caldwell,R.L., and Erdmann,M.V. (2002a) Tuning of photoreceptor function in three mantis shrimp species that inhabit a range of depths. I. Visual pigments. J.Comp.Physiol.A *188*:179-186.

Cronin,T.W. and Caldwell,R.L. (2002b) Tuning of photoreceptor function in three mantis shrimp species that inhabit a range of depths. II. Filter pigments. J.Comp.Physiol.A *188*:187-197.

Dartnall,H.J.A. (1972) Photosensitivity. In: Dartnall (Ed.): Handbook of Sensory Physiology, Vol VI/I. Berlin-Heidelberg-New York: Springer, pp. 122-145.

Dolph,P. J., Ranganathan, R., Colley, N. J., Hardy, R. W., Socolich, M., and Zuker, C. S. (1993) Arrestin function in inactivation of G protein-coupled receptor rhodopsin *in vivo*. Science *260*:1910-1916.

Eguchi,E., Watanabe,K., Hariyama,T., Yamamoto,K. (1982) A comparison of electrophysiologically determined spectral responses in 35 species of Lepidoptera. J.Insect Physiol. *28*:675-682.

Exner,S. (1891) Die Physiologie der facettierten Augen von Krebsen und Insekten. Leipzig-Wien: Franz Deuticke.

Franceschini,N. and Kirschfeld,K. (1971a) Étude optique *in vivo* des éléments photorécepteurs dans l'oeil composé de *Drosophila*. Kybernetik *8*:1-13.

Franceschini,N. and Kirschfeld,K. (1971b) Les phénomènes de pseudopupille dans l'oeil composé de *Drosophila*. Kybernetik *9*:159-182.

Gärtner,W. (2000) Invertebrate visual pigments. In: Handb.Biol.Phys. Vol. 3, Molecular mechanisms in visual transduction (eds. Stavenga,D.G., DeGrip,W.J. and Pugh, E. N. Jr.). Elsevier, Amsterdam, pp. 297-388.

Goldman,L.J., Barnes, S.N., and Goldsmith,T.H. (1975) Microspectrophotometry of rhodopsin and metarhodopsin in the moth *Galleria*. J.Gen.Physiol. *66*:383-404.

Goldsmith,T.H. (1965) Do flies have a red receptor. J.Gen.Physiol. *49*:265-287.

Goldsmith,T.H. and Bernard,G.D. (1974) The visual system of insects. In: Rockstein, M. (ed.): The physiology of insecta, Vol. 2, 2nd ed. San Francisco: Academic Press, pp. 165-272.

Goodman,O.B. Jr, Krupnick,J.G., Santini,F., Gurevich,V.V., Penn,R.B., Gagnon,A.W., Keen,J.H., and Benovic,J.L. (1996) β-arrestin acts as a clathrin adaptor in endocytosis of the beta2-adrenergic receptor. Nature *383*:447-450.

Goodman,O.B. Jr, Krupnick, J.G., Gurevich, V.V., Benovic, J.L., and Keen, J.H. (1997) Arrestin/clathrin interaction. Localization of the arrestin binding locus to the clathrin terminal domain. J.Biol.Chem. *272*:15017-15022.

Govardovskii,V.I., Fyhrquist,N., Reuter,T., Kuzmin,D.G., and Donner,K. (2000) In search of the visual pigment template. Vis.Neurosci. *17*:509-528.

Hamdorf,K. (1979) The physiology of invertebrate visual pigments. In: Autrum,H. (ed.): Handb.Sens.Physiol. Vol. VII/6A. Berlin-Heidelberg-New York, Springer, pp. 145-224.

Hamdorf,K., Schwemer,J., and Paulsen,R. (1989) Insect photoreception. II. Mechanisms of adaptation and visual pigment renewal. In: Luttgau,H.C. and Necker,R. (eds): Biological signal processing. Weinheim: VCH Publishers, pp. 83-104.

Hardie,R.C. (2001) Phototransduction in *Drosophila melanogaster*. J.Exp.Biol. *204*:3403-3409.

Hateren van,J.H. (1989) Photoreceptor optics, theory and practice. In: Stavenga, D.G. and Hardie, R.C. (eds): Facets of vision. Berlin Heidelberg New York London Paris Tokyo: Springer, pp. 74-89.

Hsu,R., Briscoe,A., Chang,B.S.W., and Pierce ,N.E. (2001) Molecular evolution of a long-wavelength-sensitive opsin in mimetic *Heliconius* butterflies (Lepidoptera: Nymphalidae). Biol.J.Linnean Soc. *72*:435-449.

Huber,A., Smith,D.P., Zuker,C.S., and Paulsen,R. (1990) Opsin of Calliphora peripheral photoreceptors R1-6. Homology with *Drosophila* Rh1 and posttranslational processing. J.Biol.Chem. *265*:17906-17910.

Järemo Jonson,A.C., Land,M.F., Osorio,D.C., and Nillson,D.E. (1998) Relationships between pupil working range and habitat luminance in flies and butterflies. J.Comp.Physiol. A *182*:1-9.

Kelber,A. (1999a) Ovipositing butterflies use a red receptor to see green. J.Exp.Biol. *202*:2619-2630.

Kelber,A. (1999b) Why 'false' colours are seen by butterflies. Nature *402*:251.

Kelber,A., Balkenius,A., and Warrant,E.J. (2003) Scotopic colour vision in nocturnal hawkmoths. Nature *419*:922-925.

Kelber,A. and Pfaff,M. (1999) True colour vision in the orchard butterfly, *Papilio aegeus*. Naturwissenschaften *86*:221-224.

Kinoshita,M., Sato,M., Arikawa,K. (1997) Spectral receptors of nymphalid butterflies. Naturwissenschaften *84*:199-201.

Kinoshita,M., Shimada,N., andArikawa,K. (1999) Colour vision of the foraging swallowtail butterfly *Papilio xuthus*. J.Exp.Biol. *202*:95-102.

Kinoshita,M. and Arikawa,K. (2000) Colour constancy in the swallowtail butterfly *Papilio xuthus*. J.Exp.Biol. *203*:3521-3530.

Kitamoto,J., Sakamoto,K., Ozaki,K., Mishina,Y. and Arikawa,K. (1998) Two visual pigments in a single photoreceptor cell: identification and histological localization of three mRNAs encoding visual pigment opsins in the retina of the butterfly *Papilio xuthus*. J.Exp.Biol *201*:1255-1261.

Kitamoto,J., Ozaki,K., and Arikawa,K. (2000) Ultraviolet and violet receptors express identical mRNA encoding an ultraviolet-absorbing opsin: identification and histological localization of two mRNAs encoding short-wavelength-absorbing opsins in the retina of the butterfly *Papilio xuthus*. J.Exp.Biol. *203*:2887-2894.

Kolb,G. and Scherer,C. (1982) Experiments on wavelength specific behavior of *Pieris brassicae* L. during drumming and egg-laying. J.Comp.Physiol.A *149*:325-332.

Kuipers, E.C., Michielsen, K., and De Raedt, H. (2002) Globale optimalisatie van morfologische beeldverwerking en beeldanalyse. Rijksuniversiteit Groningen. Thesis.

Labhart,T. and Meyer,E.P. (1999) Detectors for polarized skylight in insects: a survey of ommatidial specializations in the dorsal rim area of the compound eye. Microsc.Res.Tech. *47*:368-379.

Land,M.F. (1972) The physics and biology of animal reflectors. Progr.Biophys. *24*:77-105.

Land,M.F. and Osorio,D.C. (1990) Waveguide modes and pupil action in the eyes of butterflies. Proc.R.Soc.Lond.B *241*:93-100.

Lefkowitz,R.J.G. (1998) Protein-coupled receptors. III. New roles for receptor kinases and beta-arrestins in receptor signalling and desensitization. J.Biol.Chem. *273*:18677-186780.

Menzel,R. and Backhaus,W.G.K. (1989) Color vision of honey bees: phenomena and physiological mechanisms. In: Stavenga, D.G. and Hardie, R.C. (eds): Facets of vision. Berlin Heidelberg: Springer, pp. 281-297.

Michielsen, K. and De Raedt, H. (2001) Integral-geometry morphological image analysis. Physics Reports *347*:461-538.

Miller,W.H. and Bernard,G.D. (1968) Butterfly glow. J.Ultrastruct.Res. *24*:286-294.

Miller,W.H. (1979) Ocular optical filtering. In: Autrum,H. (ed) Handbook of sensory physiology, Vol VII/6A, pp. 69-143. Springer, Berlin Heidelberg.

Minke,B. And Hardie,R.C. (2000) Genetic dissection of *Drosophila* phototransduction. In: Handb. Biol. Phys. Vol. 3, Molecular mechanisms in visual transduction (eds. Stavenga, D. G., DeGrip, W. J. and Pugh, E. N. Jr.). Elsevier, Amsterdam, pp. 449-525.

Mollereau,B., Wernet,M.F., Beaufils,P., Killian,D., Pichaud,F., Kuhnlein,R., and Desplan,C. (2000) A green fluorescent protein enhancer trap screen in *Drosophila* photoreceptor cells. Mech.Dev. *93*:151-160.

Nilsson,D.-E., Land,M.F., and Howard,J. (1983) Afocal apposition optics in butterfly eyes. Nature *312*:561-563.

Nilsson,D-E., Land,M. and Howard,J. (1988) Optics of the butterfly eye. J.Comp.Physiol.A *162*:341-366.

Okabe,A., Boots, B. and Sugihara, K. (1992) Spatial tesselations: Concepts and applications of Voronoi diagrams. Wiley, New York.

Paulsen,R. and Schwemer,J. (1983) Biogenesis of blowfly photoreceptor membranes is regulated by 11-cis-retinal. Eur.J.Biochem. *137*:609-614.

Pichaud,F. and Desplan,C. (2001) A new visualization approach for identifying mutations that affect differentiation and organization of the *Drosophila* ommatidia. Development *128*:815-826.

Pichaud,F., Treisman,J., and Desplan,C. (2001) Reinventing a common strategy for patterning the eye. Cell *105*:9-12.

Qiu,X., Vanhoutte,K.J.A., Stavenga,D.G., and Arikawa,K. (2002) Ommatidial heterogeneity in the compound eye of the male small white butterfly, *Pieris rapae crucivora*. Cell Tissue Res. *307*:371-379.

Qiu,X., Arikawa,K. (2003a) The photoreceptor localization confirms the spectral heterogeneity of ommatidia in the male small white butterfly, *Pieris rapae crucivora*. J.Comp.Physiol.A *189*:81-88.

Qiu,X., Arikawa,K. (2003b) Polymorphism of red receptors: sensitivity spectra of proximal photoreceptors in the small white butterfly, *Pieris rapae crucivora*. J.Exp.Biol.A *206*:2787-2793.

Ribi,W.A. (1979a) Coloured screening pigments cause red eye glow hue in pierid butterflies. J.Comp.Physiol.A *132*:1-9.

Ribi,W.A. (1979b) Structural differences in the tracheal tapetum of diurnal butterflies. Z.Naturforsch.C *34*:284-287.

Ribi,W.A. (1980) The phenomenon of eye glow. Endeavour *5*:2-8.

Rutowski,R.L. and Warrant,E. J. (2002) Visual field structure in the Empress Leilia, *Asterocampa leilia* (Lepidoptera, Nymphalidae): dimensions and regional variation in acuity. J.Comp.Physiol.A *188*:1-12.

Salcedo,E., Huber,A., Henrich,S., Chadwell,L.V., Chou,W.H., Paulsen,R., and Britt,S.G. (1999) Blue- and green-absorbing visual pigments of *Drosophila*: ectopic expression and physiological characterization of the R8 photoreceptor cell-specific Rh5 and Rh6 rhodopsins. J.Neurosci. *19*:10716-10726.

Scherer,C. and Kolb,G. (1987) The influence of color stimuli on visually controlled behaviour in *Aglais urticae* L. and *Pararge aegeria* L. (Lepidoptera). J.Comp.Physiol.A *161*:1623-1636.

Schwemer,J. and Paulsen,R. (1973) Three visual pigments in *Deilephila elpenor* (Lepidoptera, Sphingidae). J.Comp.Physiol. *86*:215-229.

Schwemer,J. (1984) Renewal of visual pigment in photoreceptors of the blowfly. J.Comp.Physiol.A *154*:535-547.

Schwemer,J. (1993) Visual pigment renewal and the cycle of the chromophore in the compound eye of the blowfly. In: Wiese, K. et al. (eds.): Sensory systems of arthropods.

Shimizu,I., Yamakawa,Y., Minamoto,T. and Sakamoto,K. (1998) Cloning of genes encoding the visual pigments in the silkworm. Appl.Entomol.Zool. *33*:199-204.

Shimohigashi,M., Tominaga,Y. (1991) Identification of UV, green and red receptors, and their projection to lamina in the cabbage butterfly, *Pieris rapae*. Cell Tissue Res. *247*:49-59.

Snyder,A.W., Menzel,R., Laughlin,S.B. (1973) Structure and function of the fused rhabdom. J.Comp. Physiol. *87*:99-135.

Stavenga,D.G. (1975) Visual adaptation in butterflies. Nature *254*:435-437.

Stavenga,D.G., Numan,J.A.J., Tinbergen,J., and Kuiper,J.W. (1977) Insect pupil mechanisms. II. Pigment migration in retinula cells of butterflies. J.Comp.Physiol.A *113*:73-93.

Stavenga,D.G. (1979) Pseudopupils of compound eyes. In: Autrum, H. (ed): Handbook of Sensory Physiology, Vol VII/6A. Berlin-Heidelberg-New York: Springer, pp. 357-439.

Stavenga,D.G., Schwemer,J. (1984) Visual pigments of invertebrates. In: Photoreception and vision of invertebrates (ed. Ali,M.A.). Plenum, New York, pp. 11-61.

Stavenga, D. G. (1995) Insect retinal pigments: spectral characteristics and physiological functions. Progr.Ret.Eye Res. *15*:231-259.

Stavenga,D.G., Hariyama,T. and Arikawa,K. (2000a) Spectral characteristics and regionalization of the eye of the satyrid *Bicyclus anynana*. Proc.Exper.Appl.Entomol.N.E.V. *11*:77-82.

Stavenga,D.G., Oberwinkler,J., and Postma,M. (2000b) Modeling primary visual processes in insect photoreceptors. In: Stavenga,D.G., Degrip,W.J., and Pugh,E.N. Jr (eds): Molecular mechanisms in visual transduction. Handbook of Biological Physics, Vol. 3. Amsterdam: Elsevier, pp. 527-574.

Stavenga,D.G., Kinoshita,M., Yang,E-C. and Arikawa,K. (2001) Retinal regionalization and heterogeneity of butterfly eyes. Naturwissenschaften *88*:477-481.

Stavenga,D.G. (2002a) Colour in insect eyes. J.Comp.Physiol.A 188:337-348.

Stavenga,D.G. (2002b) Reflections on colourful ommatidia of butterfly eyes. J.Exp.Biol. *205*:1077-1085.

Stavenga,D.G. (2003) Angular and spectral sensitivity of fly photoreceptors. II Dependence on facet lens F-number and rhabdomere type. J.Comp.Physiol.A *189*:189-202.

Suzuki,E., Katayama,E., and Hirosawa,K. (1993) Structure of photoreceptive membranes of *Drosophila* compound eyes as studied by quick-freezing electron microscopy. J.Electron Microsc. *42*:178-184.

Struwe,G. (1971) Spectral sensitivity of the compound eye in three *Heliconius* species. Acta Physiol.Scand. *82*:38A-39A.

Tamura,T., Thibert,C., Royer,C., Kanda,T., Abraham,E., Kamba,M., Komoto,N., Thomas,J.L., Mauchamp,B., Chavancy,G., Shirk,P., Fraser,M., Prudhomme,J.C., Couble,P., Toshiki,T., Chantal,T., Corinne,R., Toshio,K., Eappen,A., Mari,K., Natuo,K., Jean-Luc,T., Bernard,M., Gerard,C., Paul,S., Malcolm,F., Jean-Claude,P., and Pierre,C. (2000) Germline transformation of the silkworm *Bombyx mori* L. using a piggyBac transposon-derived vector. Nat.Biotechnol. *18*:81-84.

Townson,S.M., Chang,B.S., Salcedo,E., Chadwell,L.V., Pierce,N.E., Britt,S.G. (1998) Honeybee blue- and ultraviolet-sensitive opsins: cloning, heterologous expression in *Drosophila*, and physiological characterization. J.Neurosci. *18*:2412-2422

Vanhoutte,K.J.A., Eggen,B.J.L., Janssen,J.J.M., and Stavenga,D.G. (2002) Opsin cDNA sequences of a UV- and green rhodopsin of the satyrine butterfly *Bicyclus anynana*. Insect Bioch.Mol.Biol. *32*:1383-1390.

Warrant,E.J. and Nilsson,D.E. (1998) Absorption of white light in photoreceptors. Vision Res. *38*:195-207.

White,R.H., Xu,H., Münch,T., Bennett,R.R., and Grable,E.A. (2003) The retina of *Manduca sexta*: rhodopsin-expression, the mosaic of blue-green and UV-sensitive photoreceptors. J.Exp.Biol. *submitted*.

Williams,D.S. (2002) Transport to the photoreceptor outer segment by myosin VIIa and kinesin II. Vision Res. *42*:455-462.

Samenvatting

In veel van onze dagelijkse activiteiten gebruiken we ons gezichtsvermogen om objecten in de omgeving te kunnen onderscheiden. De mechanismen die hieraan ten grondslag liggen kunnen bij insekten goed onderzocht worden met behulp van verschillende technieken. De ogen bij insekten zijn goed ontwikkeld en aangepast voor optimale visuele informatieverwerking in hun specifieke ecologische omgeving. Zo hebben bijen en vlinders, specialisten in de herkenning van bloemen, een sterk ontwikkeld kleurenzien. In dit proefschrift willen we een bijdrage leveren aan de opheldering van dit systeem. In het bijzonder willen we begrijpen hoe licht geabsorbeerd wordt in de individuele lichtverwerkende eenheden, de ommatidia van het samengestelde oog. Er worden hierbij technieken toegepast uit zowel de moleculaire biologie als de optica, namelijk het cloneren van visuele pigmenten en spectrofotometrie. In dit proefschrift hebben we bestaande optische lichtreflectiemetingen in vlinderogen verder ontwikkeld en toegepast om in een levend dier, zonder dissectie, de spectrale eigenschappen te kunnen onderzoeken van de componenten die een belangrijke rol spelen in de licht-absorptie, nl. de visuele pigmenten, tapeta en screeningspigmenten. De optische metingen, complementair aan de anatomische en histologische technieken, vormen de experimentele basis voor een kwantitatief model van lichtabsorptie en de interpretatie van spectrale gevoeligheden van fotoreceptorcellen binnen een lichtgeleider, het doel van deze studie. De verschillende onderdelen van het onderzoek met enkele concrete resultaten worden hierna verder kort toegelicht per hoofdstuk.

Hoofdstuk 1 geeft een inleiding in de structurele organisatie van het oog. Het samengestelde vlinderoog is opgebouwd uit enkele duizenden ommatidia, elk met een karakteristieke anatomische structuur. Het omgevingslicht wordt door een lens gefocusseerd op een cylindervormige lichtgeleider, enkele honderden micrometers lang met een diameter van slechts 1 à 2 μm, waar het licht wordt geabsorbeerd door visuele pigmenten. De visuele pigmentmoleculen zitten gepakt in subcompartimenten van negen fotoreceptorcellen die samen het rhabdoom vormen. Ieder ommatidium wordt omgeven door donker gekleurde pigmenten die strooilicht, licht wat niet uit de kijkrichting van het ommatidium komt, absorberen. Door de golfeigenschappen van licht kan de zogenaamde randgolf van het licht, die zich buiten de lichtgeleider bevindt, ook nog eens geabsorbeerd worden door eventueel aanwezige afschermende pigmenten. Dit beïnvloedt dan de spectrale samenstelling van het licht en vormt zo een belangrijke filterende component in het systeem. Ten slotte is er, uniek voor

vlindersoorten, een reflecterende structuur onderaan ieder ommatidium, het tapetum. Al deze componenten van het ommatidium zijn niet allemaal gelijk voor de verschillende vlindersoorten en ook binnen een oog kunnen we op basis van de verschillende optische en anatomische eigenschappen verschillende types aanduiden. Er is dus een duidelijke retinale heterogeniteit, die wellicht functioneel belangrijk is voor het kleurenzien van vlinders (zie ook *Hoofdstuk 6*).
In het inleidend hoofdstuk bespreken we verder in het kort de fototransductie, de biochemische cascade waarbij lichtabsorptie door visuele pigmenten uiteindelijk aanleiding geeft tot een electrisch signaal in een fotoreceptorcel. Een visueel pigment, het rhodopsine, wordt na absorptie van een lichtquantum omgezet in een andere structurele configuratie, het geactiveerd metarhodopsine. Typisch voor invertebraten is dat het metarhodopsine, na inactivatie door fosforylatie en binding van arrestinemoleculen, opnieuw geregenereerd kan worden naar de rhodopsinevorm door absorptie van fotonen in een ander spectraal bereik. De fotochemische experimenten in *Hoofdstuk 4* bouwen hier op voort. We bespreken hier verder ook de dynamische huishouding van het visuele pigment bij de vlieg, de visuele pigmentcyclus, met name metarhopsine-afbraak en *de novo* synthese van rhodopsine in het donker, processen die ook meetbaar zijn in vlinderogen.

In ***Hoofdstuk 2*** beschrijven we de (partiële) clonering en homologie-analyse van cDNA sequenties van groene en UV absorberende rhodopsines van een zandoogje, *Bicyclus anynana*. Door de homologie van cDNA sequenties te onderzoeken kunnen de absorptie-eigenschappen afgeleid worden en kan een onderscheid gemaakt worden tussen kort- (UV), middel- (blauw) en lang-golvig (groen, rood) absorberend visueel pigment. Evenals in het visuele systeem van bijen zijn in de regel bij vlinders drie rhodopsines aanwezig die absorberen in het UV, blauw en groen.

In ***Hoofdstuk 3*** presenteren we een fotochemisch model om de visuele pigmentprocessen in het vlinderoog, die gebaseerd zijn op reflectiespectrofotometrie, te modelleren. Zo'n model is noodzakelijk voor een quantitatieve interpretatie van de visuele pigmenteigenschappen, de absorptiespectra en de kinetiek die experimenteel gemeten worden (zie *Hoofdstuk 4*). We illustreren fotoconversie van visueel pigment onder breed-band belichting in een rhabdoom, waarin zich groen, blauw en UV receptoren bevinden in een verhouding 6:1:1.

In ***Hoofdstuk 4*** verkennen we de fotochemie van visuele pigmenten in een groep homogene ommatidia in het oog van de gehakkelde aurelia, *Polygonia c-album* met een aantal experimentele protocollen, o.a. bleken en fotochemische conversie van rhodopsine en metarhodopsine met adapterende

monochromatische stimuli. De gemeten visuele pigment absorptiespectra bevestigen de dominante expressie van een groen rhodopsine. Na wegbleken van het groene pigment kon ook het UV-absorberend rhodopsine geïsoleerd worden.

In ***Hoofdstuk 5*** beschrijven we een beeldanalyseprocedure gebaseerd op zgn. Voronoi-diagrammen. Met behulp van een digitale camera kunnen de reflecties van enkele ommatidia gequantificeerd worden. Bovendien kunnen we hiermee ook gebieden in het oog met heterogene eigenschappen bestuderen. Dit hebben we geïllustreerd met twee voorbeelden. Na het bleken van groen visueel pigment in het oog van *Polygonia* hebben we gebleekte en ongebleekte ommatidia vergeleken. En, in het ventrale deel van het oog van het bonte zandoogje, *Pararge aegeria*, hebben we met deze procedure de intensiteitsafhankelijke pupilactiviteit gemeten in individuele ommatidia van rode en groen reflecterende ommatidia. De tapeta hebben een sterk variërende reflectie-amplitude, wat een reproduceerbare codering van absolute lichtgevoeligheden zou kunnen beïnvloeden.

In ***Hoofdstuk 6*** tonen we spectrofotometrische metingen aan individuele ommatidia in 20 verschillende vlindersoorten. In de eerste plaats complementeren deze kwantitatieve data de metingen met de digitale camera die de heterogeniteit en regionalisatie van vlinderogen goed in kaart brengt (zie *Hoofdstuk 5*). Deze data illustreren ook dat de tapeta reflecteren over een breed spectraal bereik. De afsnij-golflengte van het tapetum, dit is de golflengte waar de reflectie voor de helft in intensiteit is afgenomen, varieert tussen de 550 en 750 nm. Hoewel de reflectie-eigenschappen van de tapeta nu goed gekarakteriseerd zijn, is de rol van het tapetum nog onduidelijk. Mogelijk speelt het een rol bij het versterken van de roodgevoeligheid in de meest proximale fotoreceptoren. De roodgevoeligheid van fotoreceptoren die groene rhodopsines tot expressie brengen kan verklaard worden door de aanwezigheid van rode screeningspigmenten, die de spectrale gevoeligheid van de proximale fotoreceptoren verschuiven naar langere golflengtes. De aanwezigheid van rode screeningspigmenten blijkt uit de gemeten spectra, waar een sterke absorptie in het kort-golvige gebied onveranderd blijft, ondanks het bleken van de groene visuele pigmenten. Recente anatomische studies in het koolwitje, *Pieris*, konden dit bevestigen.

Hoofdstuk 7 is een algemene discussie en samenvatting van het onderzoek: de studie van de spectrale eigenschappen van visuele pigmenten (*Hoofdstukken 2,4-5*), gecombineerd met additionele filterende componenten, zoals screeningpigmenten en tapeta (*Hoofdstuk 6*), die een realistische beschrijving van lichtabsorptie in het gefuseerde rhabdoom toelaat

(*Hoofdstuk 3*), waardoor de spectrale basis van het kleurenzien van vlinders in belangrijke mate verhelderd is.

Perspectief

Het onderzoek naar de spectrale verwerking in vlinderrhabdomen, ook onder reële omgevingslichtcondities, is nog incompleet. Een vollediger biofysisch model van lichtabsorptie in het vlinderoog zal de optische eigenschappen van de facetlens en het rhabdoom mede in de analyse betrekken. De exploratie van de enorme diversiteit in de optische componenten van vlinderogen met diverse experimentele technieken zal inzicht geven in het visueel georiënteerd gedrag van vlinders.

Nawoord

Iedereen kent het fascinerende verhaal van de monarchvlinder die vanuit Noord-Amerika elk jaar opnieuw duizenden kilometers aflegt om uiteindelijk in Mexico te overwinteren. Of wellicht heb je al eens een vlinder zien ontpoppen. Of misschien ken je het verhaal van de 'plastische vlinderogen' op de vleugels van tropische vlindersoorten. Voor een groot stuk zijn deze fenomenen ondertussen opgehelderd: de genetische programma's en bepalende omgevingsfactoren zijn geïdentificeerd. Men staat dan niet altijd meer stil bij de inzet, de transpiratie, het geduld en de precisie van vele mensen die aan de basis hebben gestaan van deze kennis. Ook de 'vlinderverhalen' in dit proefschrift kwamen mede tot stand door de inzet van velen. Enkelen wil ik hierbij graag bij naam noemen, zonder anderen onrecht aan te doen.

Ik denk dan vooral aan Joyce en mijn ouders, die mijn migratie en verblijf in het noordelijke Groningen altijd enthousiast hebben gesteund.

Directe bron van inspiratie en reflectie bij het tot stand komen van dit proefschrift was vooral mijn promotor en begeleider, Doekele Stavenga.

Ook alle (ex-)medewerkers van het departement Neurobiofysica en Biomedische Technologie hebben bijgedragen aan de concrete invulling van dit proefschrift, o.a. tijdens werkbesprekingen en de toevallige wandelgang- en koffieontmoetingen. Voor het technisch vakmanschap dank ik in het bijzonder Hein Leertouwer, Jannes Land, Wigger Jonker en Ben Pijpker.

De beeldverwerkingsanalyse van reflectiemetingen met de digitale camera is mede mogelijk gemaakt door de computationele ondersteuning van Kristel Michielsen (Materials Science Centre, Groningen).

Erg aangenaam en verrijkend was het, te kunnen rekenen op de gastvrijheid en moleculair biologische kennis van Wim de Grip, Jacques Janssen en Bart Eggen tijdens mijn verblijf op de afdeling Opthalmologie van het St.-Radboud in Nijmegen en Ontwikkelingsgenetica in Haren.

Bij de opstartfase van de cloneringsexperimenten kon ik voortbouwen op de expertise van Kentaro Arikawa en Junko Kitamoto (dept. Neuroethologie, Yokohama, Japan).

Ik dank ten slotte Bas Zwaan en Paul Brakefield (dept. Evolutionaire Biologie, Leiden) voor het 'openstellen' van de *Bicyclus*-vlinderkweek.